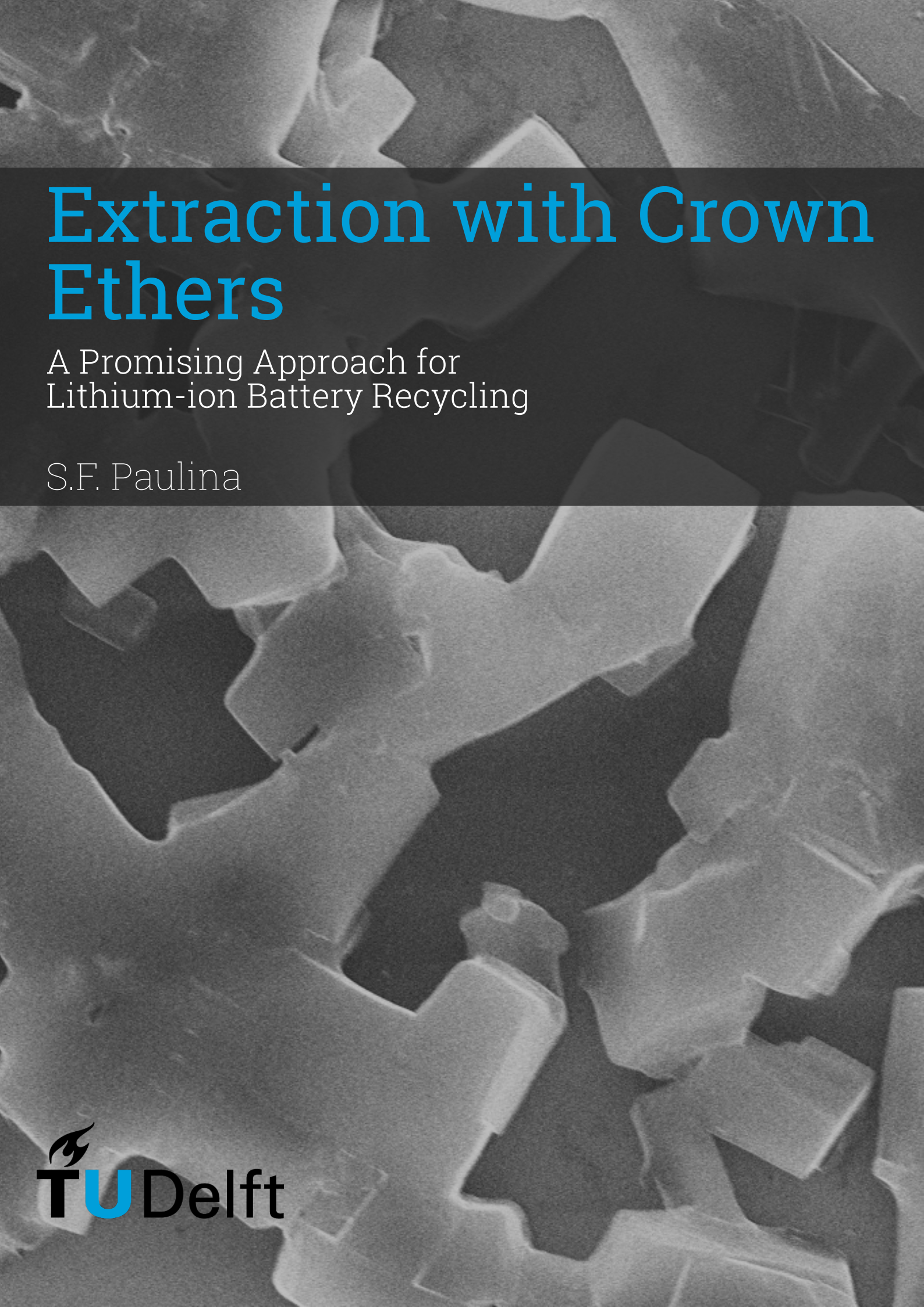

Extraction with Crown Ethers

A Promising Approach for Lithium-ion Battery Recycling

S.F. Paulina

TU Delft

Extraction with Crown Ethers

A Promising Approach for Lithium-ion Battery Recycling

by

Suenley F. Paulina

to obtain the degree of Master of Science
at the Delft University of Technology,
Faculty 3mE - Msc Mechanical Engineering,
Track: Energy, Flow and Process Technology,
to be defended publicly on Tuesday August 29, 2023 at 10:00 AM.

Student number:	5220548	
Project duration:	January 9, 2023 – August 29, 2023	
Thesis committee:	Dr. ir. M. Ramdin,	TU Delft, Supervisor
	Prof. dr. ir. T.J.H. Vlugt,	TU Delft
	Dr. L. Cutz,	TU Delft

TU Delft

Summary

Many of the high-performance portable electronics and electric vehicles (EVs) on the market depend on lithium-ion batteries (LIBs) as their primary energy source. LIBs are popular rechargeable power sources, due to their high capacity, high energy density, light weight, and compact size. If millions of EVs are to be manufactured each year, rigorous resource management for EV battery manufacturing, as well as a material- and energy efficient 3R system (reduce, re-use, recycle), will undoubtedly be required to assure the future sustainability of the automotive industry. The demand for lithium for batteries has rapidly increased over the past years. Due to this, lithium resource reserves have become a critical concern.

Since lithium is only found at a few locations around the world, there is an inherent danger from a geopolitical standpoint when it comes to accessibility. Political turmoil or instability in the nations controlling these lithium stockpiles may have a detrimental impact on world supply. Spent LIBs can be viewed as an alternative source of lithium. Considering that used LIBs contain toxic organic electrolytes and heavy metals, recycling them reduces resource waste and environmental contamination. Due to the difficulty of handling its complex composition and distribution, most recycling efforts and industrial processes focus solely on recycling the cathode and ignore the proper treatment of the aged electrolyte. Recovery of the electrolyte is crucial for achieving the legally mandated recycling efficiency set by the European Commission, as the electrolyte typically comprises of 10-15 wt% of a LIB cell. One of the current techniques used to recycle LIBs is pyrometallurgy. In the pyrometallurgy recycling process, all organic electrolytes are mostly burnt off and the recycling of lithium from the cathode material is impeded by its confinement within the slag of complex materials. On the other hand, the most widely used technique for extracting lithium is hydrometallurgy. However, the numerous processing steps hinder the practical application of this process, which typically reclaim lithium in the final phase, resulting in a low lithium recovery efficiency.

Given the limited emphasis on electrolyte recycling, this investigation takes a specialized direction by focusing precisely on this aspect. The study employs the principles of supramolecular chemistry, a process involving complex formation between specialized host molecules (extractants) and charged guest species (such as metal ions and other charged molecules). Therefore, the study delves into the feasibility of using crown ethers, specifically 12C4 and 15C5, as extractants. These crown ethers are explored for their potential to effectively extract and subsequently recycle the lithium salt ($LiPF_6$) from the electrolyte of spent LIBs. The extraction efficiency of these crown ethers is examined across various extraction conditions (mole ratio, extraction time, and extraction temperature) to identify the most favorable extraction condition. To keep the experiments as simple as possible, the effect of pressure on the extraction yield is not included in this research.

The results and findings obtained from the conducted experiments reveals that the extraction efficiency correlates with the mole ratio between crown ethers and lithium, up to a certain threshold (6:1 for 12C4 and 12:1 for 15C5) where further increase in mole ratio does not significantly enhance the extraction yield. The extraction yield displays an inverse relationship with temperature, indicating an exothermic extraction process that favors lower temperatures. Remarkably, varying the extraction time within the 5 to 30 min range exhibits negligible influence on extraction yield, suggesting rapid kinetics in the formation of the crown ether-lithium

complex. Between the two crown ethers tested, 12C4 emerges as the more suitable option, achieving extraction yields of up to 60 %. In contrast, the use of 15C5 necessitates larger quantities compared to 12C4 to achieve equivalent extraction yields. Consequently, using 15C5 not only increases the cost but also diminishes the overall process efficiency.

Previous literature has demonstrated the application of crown ethers in lithium extraction from sources like leaching solutions and lithium-rich brines. This study extends this concept by showcasing crown ethers' potential to extract lithium from the electrolyte of LIBs. These findings propose an alternative way, reducing the necessity to intensively extract lithium from the Earth's crust at the current rate to keep up with demand. Moreover, it offers a promising means to alleviate the ecological burden associated with extracting lithium from brines, which often entails significant land use and water consumption, diverting both toward more sustainable uses. The findings further indicate progress towards achieving the recycling goals outlined by the European Commission for the complete recycling of all collected batteries.

Nonetheless, this study is only a stepping stone. Further research is proposed to conduct experiments for the extraction of the organic solvents in the electrolyte using CO_2 and to develop innovative methods for separating the extracted lithium from the crown ether without compromising the integrity of the crown ether, allowing for its reuse in subsequent extraction processes.

Acknowledgements

I want to express my heartfelt gratitude to a few remarkable individuals who have been a major part of my thesis journey: First and foremost, I want to give a big thanks to my supervisor, Dr. Mahinder Ramdin, whose guidance and support were invaluable throughout my 7-month thesis journey. His exceptional mentorship, regular discussions, and collaborative approach significantly enriched the quality of this work. I am also thankful to Prof. Dr. Thijs Vlugt for his insightful advice and suggestions, which greatly contributed to shaping my research direction. My profound appreciation goes to Michel van den Brick, whose assistance in the laboratory played an indispensable role in the realization of this work. His expertise and willingness to help with ICP-OES, played a pivotal role in the success of these experiments. A special thank go to Prasad Gonugunta, whose collaboration in conducting essential analyses, such as XPS and SEM, was indispensable.

Furthermore, I want to thank my friends at TU Delft, especially Hamza, Rahul, and Dimitrios, for your laughter, support and companionship. Your presence turned the challenging times into memorable experiences. I would also like to acknowledge Raimbard Merkies for his readiness to help and provide valuable feedback. To my parents, your constant encouragement and belief in my potential have been a driving force. Your support means the world. Last but not least, a special mention to my partner, Gheylla. Your positivity and uplifting presence never failed to brighten my days. I am truly fortunate to have you by my side.

To all of you, I couldn't have done it without your amazing support. This thesis is yours as much as it is mine. Cheers to the incredible journey we've shared!

Contents

1 Introduction

In order to reach the goals set to lower greenhouse gas emissions, to enhance the quality of air in urban areas, and to satisfy the demands of consumers who are becoming more and more interested in alternatives to fossil fuel driven vehicles, the demand for electric vehicles (EV) has increased substantially and the market for these vehicles needs to grow even rapidly. The number of electric cars sold globally exceeded a million for the first time in 2017. If tens of millions of EV are to be manufactured each year, rigorous resource management for EV battery manufacturing, as well as a material- and energy efficient 3R system (reduce, re-use, recycle), will undoubtedly be required to assure the future sustainability of the automotive industry [1]. In this regard, batteries will be crucial to the switch from fossil fuels to renewable energy sources. Many of the high-performance portable electronics, EVs, and stationary energy storage systems of today depend on lithium-ion batteries (LIBs) as their primary energy storage source [2]. They are popularly employed as rechargeable power sources due to their high capacity, high energy density, light weight, and compact size [3]. With a potential of 3.045 V (compared to the standard hydrogen electrode, SHE), lithium is the most electropositive metal. It also has the lowest density and lowest weight. As seen by its widespread use in batteries, all these characteristics make lithium the most important element for energy storage today when compared to other metals [4].

1.1. Lithium Ion Batteries

LIBs are reversible devices that convert their chemical energy during their discharge phase into electrical energy to power an external circuit. The electrode processes are switched around during the charge phase, which involves connecting the cell to an external energy source. Each cell is made up of four major components: an anode, a cathode, a separator, and an electrolyte [4]. Lithium-ions travel from the anode (negative electrode) through the electrolyte towards the cathode (positive electrode), inside the cell during the spontaneous redox reaction (discharge). During the charge process, the direction of lithium-ion transport is reversed, with the ions moving from the cathode to the anode. To maintain electroneutrality, electrons go through the external circuit in the same direction as lithium ions do inside the cell.
During the first charge/ discharge of the LIB, a layer called solid electrolyte interface (SEI) is formed. The SEI is crucial for performance and safety because it protects the electrolyte from further reductive decomposition at the anode surface. The separator, a thin, microporous membrane positioned between the anode and the cathode, prevents the electrodes from short-circuiting. Ionic conductivity and mobility are made possible by the electrolyte that fills the separator and comes into contact with the electrodes. This electrolyte also maintains ionic mobility within the electrodes.

The electrolyte in LIBs consists of three components [4–6]:

- **High-grade Lithium Salts**

  such as: lithium hexafluorophosphate ($LiPF_6$), lithium tetrafluoroborate ($LiBF_4$), lithium bis(trifluoromethanesulfonyl)imide (LiTFSI) and lithium perchlorate ($LiClO_4$).

- **Carbonate Solvents**

  The salts are dissolved in organic carbonate solvents such as: ethyl methyl carbonate (EMC), ethylene carbonate (EC), and dimethyl carbontae (DMC) in varying volume ratios

- **Additives**

  Different additives may be included to modify various properties of the electrolyte. For example, dimethyl methylphosphonate ($C_3H_9O_3P$) can function as a flame retardant, cyclohexylbenzene ($C_{12}H_{16}$) can provide overcharge protection, and vinylene carbonate (VC) can act as a film-forming additive to control the formation of the solid electrolyte interphase (SEI) [7].

Typically, a combination of three components in contact with a current collector foil makes up the electrodes, which are often porous composites. The three components are an active material (AM), a conductive material (CM), and a binder solution (BS). Due to their electronic conductivity and stability, copper and aluminium are typical materials for, respectively, anode and cathode current collectors. Lithium intercalation, which is the process of reversibly incorporating a mobile lithium ion into vacancies in a crystal lattice, is made possible by the active material [8]. The most common cathode active materials are lithium cobalt oxide ($LiCoO_2$ - LCO), lithium iron phosphate ($LiFePO_4$ - LFP), lithium manganese oxide ($LiMn_2O_4$ - LMO), lithium nickel manganese cobalt oxide ($LiNiMnCoO_2$ - NMC), and lithium nickel cobalt aluminium oxide ($LiNiCoAlO_2$ - NCA). The cathode active material can be classified in three different crystal structures [9, 10]:

(a) Phosphates ($LiMPO_4$ with M= Fe, Mn, Co, Ni)

(b) Layered oxides ($LiMO_2$ with M= Co, Ni, Mn, Al)

(c) Spinels (LiM_2O_4 with M= Mn, Ni)

Graphite and silicon are the most often used anode active materials. The most common conductive material utilized in LIBs is carbon black. The conductive material maintains the electrical connection between the current collector and the particles of the active material. Finally, the binder material gives mechanical support to the electrode structure by bonding the AM and CM to the current collectors. The binder must also allow for ionic conduction and be electrochemically inert. The most widely utilized binders in the production of LIBs are polyvinylidene fluoride (PVDF), co-polymers, and polypropylene (PP) [4].

One of the key factors that affect the performance of LIBs is aging, which causes capacity loss, higher resistance, power and energy loss, and ultimately a shorter lifetime. Many aging processes take place and influence each other, such as the interactions between the electrolyte and the anode, SEI growth, the degradation of the cathode and the anode, or the deposition of lithium metal on the anode. The focus of LIB recycling is on damaged batteries or batteries that have reached their end of life (EoL), i.e., strongly aged batteries [6]. Effective recycling of EoL LIBs has become crucial due to the enormous and growing amount of LIBs, environmental and safety concerns, as well as the limited supply of important metals. EoL LIBs can serve as a secondary source of metals such as lithium (Li), nickel (Ni), manganese (Mn), and cobalt (Co) [11].

1.2. Motivation for the study

Compared to vehicles powered by internal combustion engines, EVs are typically regarded as ”zero emission” vehicles. EVs do not emit any gas during operation, however numerous aspects connected to LIBs, the EVs' power source, do have a substantial impact on the environment. With the growth of the EV market, the production of LIBs has significantly increased, posing environmental challenges such as resource use, energy consumption, and waste emission (including gaseous, liquid and solid wastes). Since the demand for lithium for batteries has rapidly increased over the past years, lithium resource reserves have become a critical concern [12].

Lithium is a common element that is widely distributed over the world. In nature, lithium never appears as a pure metal; instead, it is found in various salts and minerals. However, it can only be found in sufficiently high concentrations in two kinds of materials: silicate minerals and mineral-rich brines. Lithium production from a brine source requires less capital investment than lithium production from a mineral source. However, the higher costs associated with the lithium production from mineral sources can be offset by the high concentration of lithium in these mineral. The most abundant source of lithium-rich brine is located in the high-altitude continental brine aquifers of the Andean mountain in South America. Lithium can only be profitably extracted from a few number of minerals, such as spodumene, petalite, and lepidolite. The most common economically available lithium-bearing mineral is spodumene [10]. Three spodumene operations in Australia and two brine operations in Argentina and Chile account for the majority of the world's lithium production [13]. Since lithium is only found in a few locations, there is an inherent danger from a geopolitical standpoint when it comes to accessibility. As a result, political turmoil or instability in these nations' governments may have a detrimental impact on the supply, drive up the price of batteries, and ultimately increase the cost of EVs [14]. Furthermore, the extraction of lithium out of brine, which involves significant evaporation processes, is harshly criticized by environmental stakeholders. The negative effects on the local environment, including groundwater pollution, gas and dust emissions, degrading ecosystems and human sanity, are a major source of concern [13].

In addition to concerns with primary resources, spent LIBs also pose serious environmental and safety risks. Heavy metals like Co, Ni, and Mn would contaminate land and groundwater if a spent LIB is just thrown away without being properly treated. Lithium batteries include reactive chemicals, organic and inorganic compounds that can explode at high temperatures or can pollute the environment [14]. There is a need to prevent the contamination brought on by the hydrolysis of the toxic electrolyte mixture that endangers both human and animal life as well as the soil and water [15]. Hazardous gases like hydrogen fluoride (HF) are easily released when the electrolyte reacts with water [16]. Costa et al. [4] concluded that, electrolyte recovery is a crucial environmental issue. On top of that, several of these organic and inorganic substances are carcinogenic [14]. So, in the interest of protecting the environment and the health of human beings, it is important to recover these materials [12].

Eventhough electrolytes are an essential part of LIBs, numerous recycling techniques for spent LIBs focuses primarily on recovering valuable metals (e.g. Co & Ni), while the electrolyte and other parts of the battery are viewed as worthless and are disposed of in any way feasible [15]. Lithium is wasted when the used electrolyte is disposed of improperly [17]. Therefore, the focus of recycling technology should shift to full LIB recovery [12]. However, according to Liu et al. [17], lithium recovery from the electrolyte is hampered by high recycling costs. Although additional research is required in this area, Liu et al. [17] states that the supercritical carbon dioxide approach appears to be a promising one for recovering lithium from the electrolyte.

Recycling spent LIBs has received a lot of attention in recent years [17]. Nevertheless, in 2019 the global LIB recycling rate was only 5-7 %, which is significantly below the capacity needed for sustainable LIB production [13]. Less than 5 % of LIBs are recycled in the European Union (EU), and for lithium it is less than 1 %, according to a report by the United Nations Environment Program (UNEP) [18]. As reported by Liu et al. [17], lithium is much more concentrated in spent LIBs (5-7 wt%) than it is in the natural resource. Thus, spent LIBs can be regarded as a vast lithium reservoir. Economically speaking, the interest in recycling LIBs is influenced by the price of metal on the market as well as the electrode technology utilized in LIBs. Currently, recycling lithium from batteries in used electronic devices is not economically viable since they only contain a small amount of lithium carbonate, which is less expensive than cobalt or nickel [14]. However, in light of the rising cost of lithium carbonate in recent years, the selective extraction of lithium is becoming a very important area of research [16]. Even if recycling is not sufficiently advantageous economically, government regulations regarding the requirement to recycle lithium-ion batteries may become more stringent in order to address sustainability issues and the safety risks associated with the disposal of spent lithium batteries [14].

In December 2020, the European Commission proposed to update EU legislation on batteries, delivering its first initiative among the actions announced in the new Circular Economy Action Plan. The Commission suggested establishing new requirements and targets on the collection, treatment, and recycling of all types of batteries at the end of their life in order to close the loop and maintain valuable materials used in batteries for as long as possible in the European economy. The present collection rate of 45 % should increase to 65 % in 2025 and 70 % in 2030 in order to considerably improve the collecting and recycling of portable batteries. Other batteries, including those used in automobiles (incl. EVs) and industrial applications, must be fully collected. All batteries that are collected must be recycled and high levels of recovery must be attained, especially for valuable materials like cobalt, lithium, nickel, and lead [19].

1.3. Research Objective

The research proposal is to recycle the electrolyte and to extract lithium ions from LIBs using crown ethers. Therefore, the objective of this study is answering the main research question and sub-questions, defined below:

Can lithium be recycled from lithium ion batteries using crown ethers?

1. What is the current state of Lithium Ion Battery recycling?
2. What is the best operating condition (extraction time, temperature and amount of crown ether) to extract the lithium salt from the electrolyte?
3. Can the same process be used to extract lithium from the cathode?

1.4. Thesis Outline

The research in this report consists of three main sections: a literature review, extraction experiments, and modeling exercise. Chapter 2 provides an in-depth description of current Lithium-ion Battery (LIBs) recycling methods, focusing particularly on the recycling of electrolytes. It also explores the potential role of supramolecular chemistry in facilitating lithium extraction. In Chapter 3, the detailed experimental and modeling methodologies employed in this research are explained. The outcomes of the research are presented and thoroughly discussed in Chapter 4. This chapter covers the detailed analysis of the experimental and modeling results and their implications. Finally, Chapter 5 addresses the primary and secondary research questions, drawing conclusive insights and offering valuable recommendations based on the research findings.

2
Literature Review

This literature review investigate the current LIB recycling methods along with the role that crown ethers can play in LIB recycling, with an emphasis on the recycling of the electrolyte (including the lithium salt) and the lithium ions in the cathode material. The following questions were formulated:

1. What are the current LIB recycling methods and how are they recycling lithium?
2. How is the electrolyte (including the lithium salt) of LIBs being recycled?
3. Are the current LIB recycling methods using crown ethers to recycle lithium?

2.1. Current Recycling Methods

Since spent LIBs still contain some residual energy, recycling them could result in an explosion or fire. Due to this, spent LIBs are typically deactivated before beginning the recycling process [12]. Batteries can be deactivated through discharge, electrolyte evaporation, or cryogenic treatment [2]. To discharge spent LIBs, it is a standard practice to use salt-saturated solutions like Sodium Chlorine (NaCl) and Sodium Sulphate (Na_2SO_4). The key drawback of this approach is the emission of Hydrogen Fluoride (HF) that is immediately brought on by electrolyte leakage into water. In addition to the release of HF, lithium that was included in the electrolyte is wasted since it is lost in the solution [16]. Batteries can also be discharged using an electrical circuit in laboratory-scale operations. An additional way to effectively discharge batteries is to place them in a stainless-steel container with stainless-steel chips. Besides the above mentioned methods, charged LIB cells can also be rendered inactive by heating the entire cell above 150 °C in an inert environment, which causes the electrolyte to evaporate. When the electrolyte evaporates at a high temperature, highly poisonous and combustible gaseous compounds are produced, which requires off-gas treatment [2].

Due to the complex assembly of LIBs or battery packs and the variety of electrode materials, a complete recycling process for LIBs often requires two common operations: physical processes and chemical processes. Pretreatments are generally used to separate materials and parts of spent LIBs based on their form, density, conductivity, and magnetic characteristics. Pretreatments such as disassembly, crushing, screening, magnetic separation, washing and thermal pretreatment are examples of physical procedures. There are also some physical techniques that enable the direct recovery of electrode materials from spent LIBs without chemical treatment (which will be covered in Section 2.1.3) [12]. The main difficulties in the physical process are the various designs and connections of the battery pack enclosure in EVs, the non-uniform size and shape of the battery module, and the various battery management systems. Chemical processes are divided into pyrometallurgical processes and hydrometallurgical processes. The following are the primary issues in the chemical process: energy consumption, the comprehensiveness and

variety of recovery methods, environmental consequences in terms of pollutant emissions, investments and costs impacted by economies of scale, and recycling efficiency [20]. In the following sections, the three recycling methods for LIBs (pyrometallurgy, hydrometallurgy, and direct recycling), as illustrated in Figure 2.1, will be discussed.

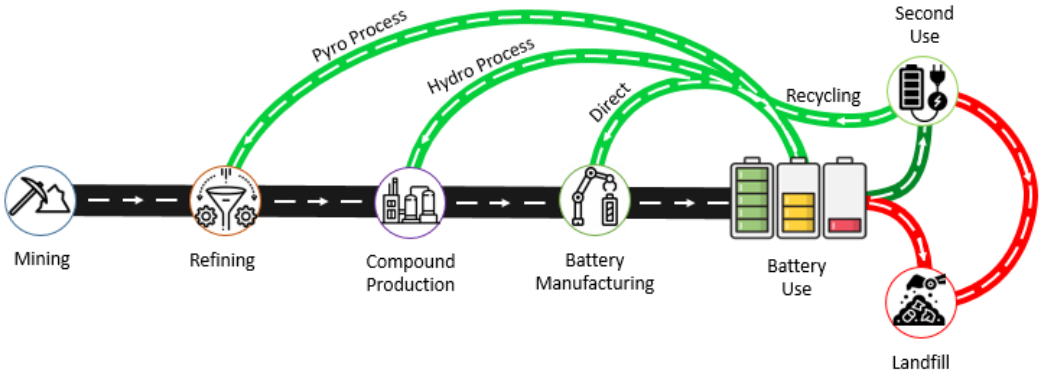

Figure 2.1: Li-ion Batteries Recycling Routes: Pyrometallurgical process, uses thermal processing to decompose the constituent parts of spent LIBs. Hydrometallurgical process comprises of leaching, separation, extraction, and chemical/ electrochemical precipitation to recover the material from spent LIBs. Direct process aims to recover materials from spent LIBs without complex chemical processes.

2.1.1. Pyrometallurgy

Pyrometallurgy uses thermal processing to decompose the constituent parts of spent LIBs. In this process, high temperature is used to enhance the physicochemical transformation to separate valuable metals [20]. A traditional pyrometallurgical dominating route for recycling spent LIBs is often quick and simple to scale up. Additionally, it can accept a variety of LIBs [17]. The only pretreatment step in this process is the straightforward separation of large battery packs into individual cells. The battery cells are then fed into a furnace with a shaft that has three temperature zones: a pre-heating zone, a plastics pyrolizing zone, and a smelting and reduction zone. Spent LIBs are heated at a temperature lower than 300 °C in the pre-heating zone to release the electrolyte vapor without causing an explosion. In order to lower the energy required for the smelting process and incinerate the plastic components of the spent LIB, the plastics pyrolizing zone is run at a temperature of about 700 °C. The elements are then smelt in the last zone, where an alloy consisting of copper, cobalt, nickel, and iron is formed, along with a slag that includes lithium, aluminum, silica, calcium, and some iron. This slag can be utilized as a useful aggregate in concrete [12]. As can be seen in Figure 2.2, the alloy, which is made up of cobalt, nickel, copper, and iron, can be processed further utilizing hydro- and bio-metallurgical methods which produce alloys that are purified [20].

The main drawback of this technique is energy consumption brought on by the high temperature operation and the additional devices needed to control harmful gases. Additionally, all organic electrolytes, binders, acetylene black, and other substances are mostly burnt off. Due to their entrapment in the slag of complex materials, manganese and lithium cannot be directly recycled [20]. However, according to Pinegar and Smith [13], lithium can be recovered from slag and flue dust as lithium carbonate through leaching and precipitation after being crushed into small (e.g., 100 µm) particles. But unless the price of lithium is high enough to cover the operating costs, a second lithium recovery process is not rational. The major LIB recycling technology of pyrometallurgy may be in jeopardy as a result of recent developments in LIB chemistry that aim to reduce cobalt and nickel [13]. As a result, such a typical pyrometallurgical process runs the risk of becoming unprofitable in the future [12].

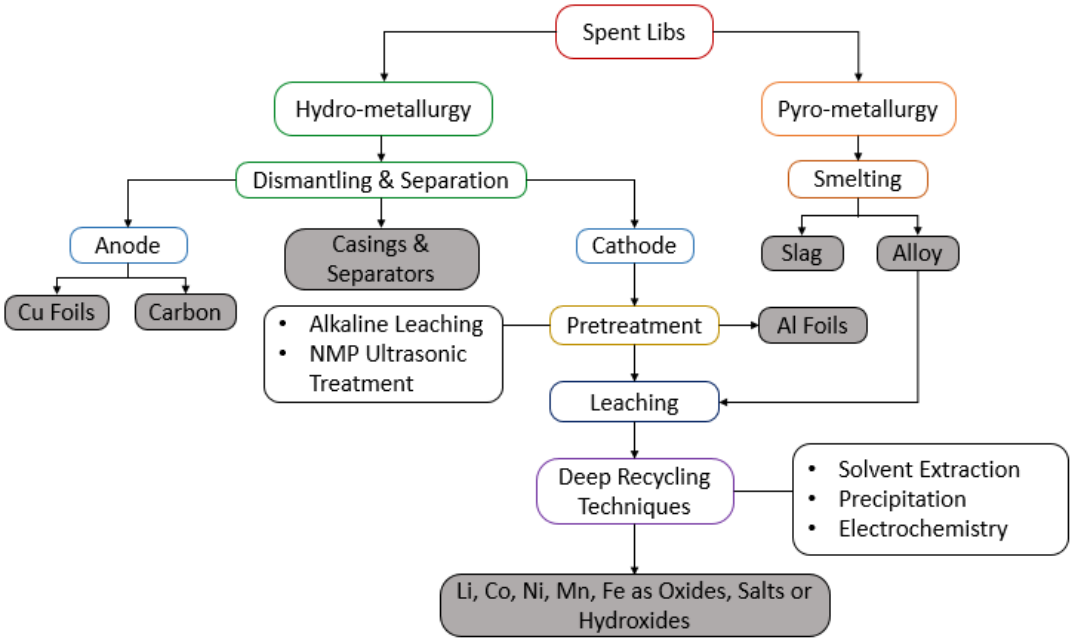

Figure 2.2: Flowchart of Typical Metallurgy Processes: This is the flowchart of hydro- and pyrometallurgical processes. Hydrometallurgy dismantles the LIb into anode, casings, and cathode. The cathode is then subjected to leaching and deep recycling techniques to recover valuable metals. Pyrometallurgy smelt the whole LIB to form a slag and alloy containing valuable metals. This alloy is then subjected to leaching and deep recycling techniques.

2.1.2. Hydrometallurgy

A hydrometallurgical process comprises of mostly leaching, separation, extraction, and chemical/ electrochemical precipitation. By combining mechanical pretreatment with hydrometallurgical processes, it is possible to recover lithium and valuable metals from lithium-based batteries, along with other battery components. Initially, the waste batteries undergo mechanical processing, which involves shredding and sieving them, and using physical methods to separate their various components. The leaching process is used to treat the fine electrode materials (black mass) that have been recovered after the mechanical pretreatment [13]. In contrast to the pyrometallurgical process, hydrometallurgy offers numerous advantages, including high extraction yield, low energy consumption, low hazardous gas emissions, and low capital cost. Furthermore, in hydrometallurgical methods, the electrolyte can be recovered by utilizing an organic or supercritical solvent [16]. In general, the hydrometallurgy process ensures good recovery rates and doesn't require extra equipment, making it very well-liked in the laboratory. However, this process can result in additional chemical costs due to the high amount of acid and base needed for leaching. In addition, the costs associated with discarding these solutions can be significant [18].

The most widely used technique for extracting lithium is hydrometallurgy. Lithium in the pretreated active materials is ionized using acids and bases, and then lithium can be recovered from the Li^+ solutions by leaching. Although inorganic acid reagents like Hydrochloric Acid (HCl), Nitric Acid (HNO_3), and Sulfuric Acid (H_2SO_4) are commonly utilized as leaching agents and demonstrated their effectiveness, they also display certain drawbacks, such as the release of additional pollutants and the complexity of the separation and purification procedures. Unless Hydrogen Peroxide (H_2O_2) or other reductants are introduced, the leaching efficiency of Cobalt (Co) using most reagents would be insufficient. The reason that reductants such as H_2O_2 or Ascorbic Acid ($C_6H_8O_6$) can aid in leaching is because they can convert Co^{3+} to Co^{2+}. Although Co^{2+} is significantly easier to dissolve at ambient temperature than Co^{3+}, Co^{3+} is primarily rich

in wasted materials. As a result, when Co^{3+} is transformed to Co^{2+}, the leaching efficiency and reaction kinetics are clearly improved. With rising reductant concentrations, leaching efficiency and reaction rate would first increase and then reach a plateau where leaching efficiency and reaction rate would not change significantly [16].

Aside from strong inorganic acids, some mild organic acids have received a lot of attention in recent years. Due to the simultaneous leaching and precipitation (creation of Cocaltous Oxalate CoC_2O_4) that takes place during the leaching process, oxalic acid can facilitate quick recovery of cobalt and lithium from used Lithium Cobalt Oxide ($LiCoO_2$) cathode materials. In this instance, cobalt and lithium can be separated without additional processing like chemical precipitation or solvent extraction. Furthermore, because the oxalic acid solution is reductive, no extra reduction agent is needed. It has also been shown that the mild inorganic Orthophosporic Acid (H_3PO_4) may simultaneously separate and leach cobalt and lithium. Cobalt can be recovered directly during the H_3PO_4 leaching process as Cobalt Phosphate ($Co_3(PO_4)_2$) precipitation, leaving lithium in the leach liquid. Due to the high solubility of cathode materials in acidic solutions, acid leaching is able to achieve greater recovery efficiency than pyrometallurgical method [12]. To recycle spent LIBs using the hydrometallurgy method, the cathode components are typically dissolved in leaching reagents, followed by separation and extraction [16].

According to Bae and Kim [18], lithium compounds can be produced by leaching with acids or bases, followed by precipitation, solvent extraction, or selective adsorption:

- **Precipitation**

  The most used technique for removing lithium from leached solutions is precipitation. The different solubilities of metal compounds, which vary according to pH and temperature, are used in this approach. Precipitants such as Sodium Hydroxide (NaOH), Trisodium Phosphate (Na_3PO_4), and Sodium Carbonate Na_2CO_3 are primarily employed to precipitate other dissolved metals, followed by lithium extraction in the form of Lithium Carbonate (Li_2CO_3) or Lithium Phosphate (Li_3PO_4) by the reaction of Li^+ and precipitants.

- **Solvent Extraction**

  Another method to separate lithium from leached solution is solvent extraction. Solvent extraction is a liquid-liquid extraction method for extracting metals from leach liquor [12]. Nonpolar extractants are usually employed to separate precious metals (Co, Ni, Mn), and lithium is extracted from the stratified solution. Although solvent extraction takes less time than precipitation, it requires more expensive solvents and additional extractant chemicals like cyanex272 and PC88A.

- **Selective adsorption**

  The last method, which is selective adsorption, separates lithium by utilizing a lithium-ion sieve to absorb the dissolved lithium. Lithium-ion sieves are inorganic adsorbents that are incredibly selective for lithium in a lithium-containing fluid. Because lithium is the smallest metal ion, lithium-ion sieves use a vacancy to allow only lithium ions. Among the inorganic solvents, lithium manganese oxide offers the highest selectivity, capacity, and stability. It is also the most often utilized substance due to its low toxicity. Low contamination is possible with this simple technique utilizing lithium-ion selective sieves; however, spinel-structured manganese-type lithium-ion sieves are expensive and call for an extra leaching procedure to separate the lithium combined with MnO_2.

Leaching time, agitation speed, solid-to-liquid ratio, temperature, and leachant and reductant concentration are considered to be the most influential determinants on leaching performance. The leaching process would be improved by increasing the temperature, leaching time, agitation

speed, and concentrations of leachant and reductant, however the leaching efficiency and rate would drop as the solid-liquid ratio is increased [16]. The hydro metallurgical process demands a large quantity of acid and various other reagents, leading to a substantial amount of waste acid sludge. Before disposing of the waste, heavy metals and hazardous organic compounds present in the sludge must be removed and the acid must be recycled or neutralized. As a result of this, the hydro metallurgical process is not frequently utilized in industrial recycling operations [12]. Besides that, the numerous processing steps hinder the practical application of hydrometallurgy-dominant technologies, which typically reclaim lithium in the final phase, resulting in a low lithium recovery efficiency, due to its low concentration in the leaching solution. Oxalic acid has been employed as the leaching agent to target the selective leaching of lithium from the cathode active materials in spent lithium-ion batteries (LIBs). Meanwhile, H_3PO_4 has been used both as a leaching agent and precipitant for treating $LiCoO_2$ and $LiFePO_4$. However, due to the diverse array of LIB types, all of these techniques can generate precipitates with complex compositions, which complicates subsequent processing. As a result, the selective separation of lithium through the leaching of spent LIBs remains a challenging task [17, 21]. Various research and development projects aim to extract lithium from the black mass earlier due to the challenges previously discussed. These projects include the use of ion-selective membranes and the selective carbonation of lithium [9].

Companies such as Umicore, Sumitomo-sony, DK recycling und Roheisen, and SNAM recycle batteries on a global scale using pyrometallurgy and hydrometallurgy processes. Most of these companies focus on recycling cobalt and nickel more than lithium. However, Li-Cycle, Accurec and Retriev (TOXCO) use the same processes to also retrieve lithium compounds from spent LIBs [18].

2.1.3. Direct Recycling

The direct physical recycling process aims to recover materials from spent LIBs without complex chemical processes. This involves discharging the LIBs and treating it to extract the electrolyte, so that it can be reused in new battery production (electrolyte extraction is covered in the next section). After removing the electrolyte, the LIB cells are disassembled and crushed, and physical methods are used to separate the cell components. The cathode materials are then gathered and likely reused in new batteries, possibly with the addition of lithium (relithiation). The direct physical recycling process is advantageous as it has a short recycling route, consumes low energy, is environmentally friendly, and has a high recovery rate. If the direct recycling process is successfully implemented, it could significantly reduce the energy consumption required for LIB production (for example, $LiCoO_2$ cathode could save up to 40 % energy). However, the process is currently in the development stage and the quality of the recycled battery materials remains a key challenge. It is uncertain if the performance of the recycled materials will be equivalent to that of fresh materials in the long run [12, 13].

2.2. Electrolyte Extraction

Improper disposal of waste materials from spent LIBs presents a significant challenge, particularly with regard to the electrolyte. This is due to the presence of lithium salts and volatile organic compounds, which can have harmful effects on both human health and the environment. Given the toxic, flammable, volatile, and hazardous nature of these compounds, it is crucial that research also focuses on electrolyte extraction in order to prevent severe threats [22]. Currently, a few studies have focused on recovering the electrolyte from spent LIBs, while various methods have been developed to recycle the valuable metals [23]. The electrolyte in spent LIBs tends to diffuse throughout the electrode structure and solidify over time. Due to the difficulty of handling its complex composition and distribution, most recycling efforts and industrial processes focus solely on recycling the cathode and ignore the proper treatment of the aged electrolyte.

This results in significant environmental damage and material loss. In traditional recycling processes, the common approach for handling the aged organic electrolyte is the direct sampling method. This involves removing the aged electrolytes through calcination or evaporation during pretreatment steps of the recycling process. The lithium salts are left in the active materials and are recovered along with other metal components using a hydrometallurgical method. Improper handling of the aged electrolyte using this method could result in significant waste and pose potential environmental risks in the long term. However, solvent extraction methods such as organic solvent extraction and supercritical extraction can avoid these issues [5]. The subsequent subsections will cover the discussion of organic solvent extraction and supercritical extraction.

2.2.1. Organic Solvent Extraction

One of the most promising techniques for recycling the organic electrolyte in spent LIBs is organic solvent extraction. The aged electrolyte is typically dispersed throughout the electrode materials and separator pores. To remove the electrolyte, the electrode and separator components are soaked in appropriate organic solvents, allowing the electrolyte to transfer into the solvent. Following dissolution, the electrolyte is separated from the extraction solvents through distillation, which is based on their different boiling points. To extract the electrolyte, the solvents need to have a boiling point below the lithium salt decomposition temperature and they should be in an anhydrous state [5]. One of the earliest reports in the field of solvent extraction methods is the patent of Schmidt et al. [24]. The top and bottom of each individual cell are drilled or sawed open. The electrolyte solution is then pressed, suctioned, or washed out using a suitable solvent that dissolves the conductive salt while preventing moisture from the casing from entering. The method of organic solvent extraction allows for the recovery of aged electrolyte from spent LIBs, but the yield of reclaimed electrolyte is low and a significant quantity of organic solvents are consumed. Moreover, the reclaimed electrolyte is likely to have small amounts of impurities from the extraction solvents, which results in additional purification costs and decreased performance of the recovered electrolyte when used in new LIBs [5]. Supercritical fluid extraction is an alternative process as it does not leave solvent residue in the product and provides considerable extraction yields [23].

2.2.2. Supercritical Extraction

Super critical fluid extraction (SCFE) is a separation technology that makes use of the density-to-dissolving-capacity relationship of supercritical fluid. The supercritical phase refers to a substance state between gas and liquid with gas-like viscosity and liquid-like density. Carbon dioxide (CO_2) is a suitable extraction medium for recycling the electrolyte in spent LIBs due to the fact that it is easily available in high purity form, its easy-to-reach critical point, dissolving power, and non-toxic nature. The temperature and pressure needed to reach the super critical region for CO_2 is 31 °C and 74 bar. CO_2 has a high dissolving capacity for low and non-polar compounds in the supercritical state. Given its high volatility, CO_2 is easily removed from the extract and can be entirely recovered and reused without emitting toxic solvent wastes. Despite the significant advancements made in laboratory-scale supercritical CO_2 ($scCO_2$) extraction for recycling electrolytes, there are still crucial challenges that prevent its widespread use in industrial-scale applications, primarily due to its high inherent cost [5, 6, 15, 25].

In general, the solubility of solutes in supercritical fluids (SCF) increases as temperature is raised while pressure is held constant. However, the impact of temperature on pressurized systems is intricate because it is influenced by two factors: first, temperature rise results in higher vapor pressure of the solute, thus increasing its solubility in SCF; second, temperature rise leads to lower solvent density, which in turn reduces the solubility of the solute in the solvent. Other factors that influence the solubility of a solute in SCF are the mass molecular and polarity of the solute, the position of functional groups in the molecule, and the type of SCF employed

[25]. CO_2 has been used in many works for extracting LIB electrolytes because of its mature extraction and separation technology. The first mention of CO_2 as an extraction medium was made in 2003 in a patent by Sloop [26]. As is customary for patents, the specific operating conditions and parameters were not revealed.

Grützke et al. [27] published the first report on the use of $scCO_2$ for the extraction of LIB electrolytes. They investigated the extraction behavior with supercritical helium head pressure carbon dioxide ($scHHPCO_2$) of a poly ethylene fleece (Freudenberg 2190) and a porous glass fiber (Whatman GF/D) separator soaked with LP30 (DMC/ EC, 1:1; 1 mol/L $LiPF_6$) and LP50 (EMC/ EC, 1:1; 1 mol/L $LiPF_6$) electrolytes. A typical $scCO_2$ extraction setup uses liquid CO_2 that has been super critically adjusted with a compressor and a heating unit. The use of a traditional autoclave with Helium Head Pressure CO_2 ($HHPCO_2$) is the less expensive option because the pressure for supercritical conditions can be obtained by the helium pressure, eliminating the need for a compressor. Unfortunately, the extraction properties of $scHHPCO_2$ can differ from those of $scCO_2$. However, because the experiments were intended to be application-oriented proof of principle tests, $scHHPCO_2$ was selected as the appropriate system. Non-flow-through one chamber autoclave tests with $scHHPCO_2$ were carried out to keep the proof of concept investigations as simple as possible.

It was possible to recover 73.5 ± 3.6 wt% of electrolyte from the polyethylene fleece and 36.7 ± 1.6 wt% from the porous glass fiber separator. There was a slightly higher EC concentration in the extract from the polyethylene fleece separator, compared to the small amounts of EC recovered from the porous glass fiber separator. This observation can be explained by the fact that EC is more polar than linear organic carbonates resulting in a better adsorption on the polar surface of the glass fiber separator. Furthermore, the polyethylene fleece separator allowed for the recovery of $LiPF_6$. Utilizing ion chromatography (IC), the lithium salt's concentration in the extract was determined to be 1.15 ± 0.04 mol/L. The salt concentration is slightly over the reference (1 mol/L), because a small amount of the organic carbonate solvents evaporated when the pressure was released. Because salts are polar, $LiPF_6$ stayed adsorbed and could not be recovered from the polar surface of the glass fiber separator. This study demonstrated the possibility of extracting LIB electrolytes using $scHHCO_2$ and that the extract composition strongly depends on the separator's adsorption characteristics and perhaps also on other battery components, such as the electrodes. Further extraction experiments conducted on commercial 18650 cells using only $scHHCO_2$ have revealed that only small amounts of $LiPF_6$ could be obtained from the electrolyte. The low polarity of CO_2 makes it unsuitable as a super critical fluid for extracting polar compounds such as $LiPF_6$. However, the addition of a polar solvent or co-solvent can modify the process and increase the likelihood of extracting polar compounds. This can optimize the extraction process and expand the potential uses of CO_2 as a fluid for extracting polar compounds [25].

To address the limitation of only being able to extract the organic solvent and not the lithium salt, Grützke et al. [7] developed and optimized a flow-through technique to achieve quantitative extraction of the electrolyte from commercial $LiNi_{1/3}Co_{1/3}Mn_{1/3}O_2$ (NMC)/graphite 18650 cells using $scCO_2$ and liquid carbon dioxide (liq CO_2) with the addition of various solvents. A fixed amount of LIB electrolyte adsorbed in a polyethylene fleece separator was placed into the extraction chamber of the extraction equipment. The results of the study indicated that altering the pressure under supercritical extraction conditions (40 °C, 80 bar vs. 300 bar) led to only minimal differences in recovery rates at a constant flow of CO_2. However, modifying the flow at the same pressure resulted in significantly higher recovery rates (measured by weight) within the same time frame. A comparison was made between two different CO_2 extraction conditions: liq CO_2 (25 °C, 60 bar) and $scCO_2$ (40 °C, 300 bar). It was found that at the same extraction

time and volumetric flow, a higher amount of electrolyte was extracted using liq CO_2. This may be due to differences in flow behavior, with liq CO_2 being laminar and $scCO_2$ being turbulent. The majority of the extracted electrolyte was obtained in the first few minutes of extraction, and the recovery with liq CO_2 was better from the beginning. Interestingly, the results showed that the amount of linear carbonates (DMC and EMC) extracted was higher with liq CO_2 than with $scCO_2$. However, $scCO_2$ was found to be more effective in extracting EC compared to liq CO_2. This can be attributed to CO_2 being a nonpolar extraction medium, resulting in the lower extraction yield of the more polar EC. The low polarity of CO_2 is also responsible for the limited extraction of the lithium salt, which could only be obtained in trace amounts.

To address the challenges of low EC concentration in the extract and inability to extract the lithium salt, additional solvents were introduced to the liq CO_2 extraction process. Anhydrous acetonitrile (ACN), diethyl carbonate (DEC), and propylene carbonate (PC) were added to the CO_2 extraction experiments (see Figure 2.3). The experiments using ACN and DEC exhibited comparable trends, with high recovery rates in the initial minutes, while the ACN/PC mixture showed slow extraction initially, but ultimately yielded the best overall result. The experiment with only PC as the added solvent resulted in a much lower extract yield compared to the scenarios where ACN, DEC, or ACN/PC were used. Moreover, a substantial amount of PC remained in the solid battery material during the extraction process. Therefore, it can be inferred that the addition of highly polar solvents such as PC is only effective when combined with solvents of moderate polarity, which serve as a "moderator" between the highly polar solvent and the less polar CO_2. The ACN/PC mixture resulted in the highest overall recovery rate of (89.1 ± 3.4 wt%) and also yielded the highest concentrations of EC and $LiPF_6$ [7].

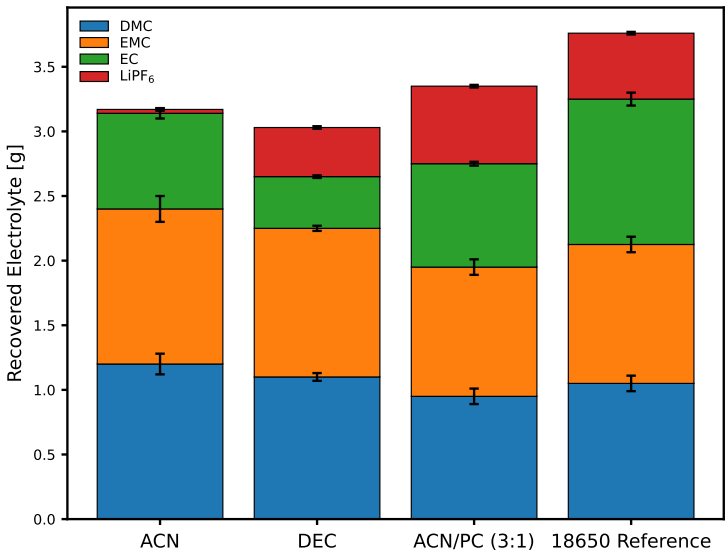

Figure 2.3: Compositions and amounts of the recovered electrolytes from commercial 18 650 cells after formation extracted with liquid CO_2 and additional solvents (ACN, DEC, and ACN/PC). Red, top: $LiPF_6$; green, below: EC; orange, middle: EMC; blue, bottom: DMC.

Liu et al. [15] used $scCO_2$ to extract organic carbonate-based electrolytes from the LIBs in a manner that was similar to the extraction of electrolytes from a depleted lithium-ion battery. After being adsorbed in a LIB separator, the electrolytes were contained in an extraction vessel within an argon-filled glove box. A series of experiments were conducted at pressures ranging from 15 to 35 MPa, temperatures ranging from 40 to 50 °C, and static extraction times ranging

from 45 to 75 minutes, with each variable set at three levels. There were a total of 15 experiments, including triplicate runs for the center points. To prevent potential degradation of the unstable electrolyte salt $LiPF_6$, the temperature was maintained below 60 °C in this study, in accordance with the recommendation of the patent Lain [28] to conduct electrolyte dissolution at temperatures below 60 °C. Zhang et al. [29] showed that a sample of $LiPF_6$ under flowing nitrogen at 70 °C for 200 minutes, lost 60 % of its mass. Upon further heating to 150 °C, the sample's mass reached a final value of 17 %. The result of the thermal gravimetric analysis (TGA) indicate that $LiPF_6$ is highly unstable, as it produces LiF and PF_5 gas at temperatures significantly lower than its decomposition temperature of 175 °C [30, 31].

The study of Liu et al. [15] showed that, during a certain extraction interval, raising the pressure significantly increased the extraction yield. An increase in extraction pressure results in higher fluid density, which enhance the solubility of the electrolyte composition. While the SCF density decreases as the temperature rises, the volatilities of the electrolyte composition continue to rise. Because the composition of the electrolytes is more volatile in the temperature range used in this study, raising the temperature gradually increases the extraction yield of the electrolyte. Liu et al. [15] concluded that, the mildest experimental conditions with a considerable extraction yield were at 23.4 MPa, 40 °C, and 45 min. The extraction yield under these conditions was 85.07 %. Inductively Coupled Plasma - Optical Emission Spectrometry (ICP-OES) was utilized to determine the quantity of $LiPF_6$ present in the extracts. The results show that while the extract only contains 0.0636 mol/L of Li^+, the electrolyte solution has 0.9038 mol/L of Li^+. This means that the lithium salt was not extracted. Besides that, after an analysis, it was concluded that $LiPF_6$ was hydrolyzed during the $scCO_2$ extraction process.

Rothermel et al. [32] investigated the viability of anode recycling in conjunction with three various electrolyte extraction techniques. After discharge, the battery packs were disassembled into their component cells before being safely shredded in an inert environment. At this stage, the electrolyte that has partially evaporated was collected by condensation, and three strategies were studied to extract the electrolyte that was still present in the shredded material:

1. Thermal drying renouncing the recovery of the conductive salt.

2. A flow-through sub critical CO_2 - assisted electrolyte extraction with a co-addition of the solvent acetonitrile, intended to extract the conductive salt.

3. Static super critical carbon dioxide - assisted electrolyte extraction without co-solvents.

Based on the findings, Rothermel et al. [32] showed that electrolyte extraction utilizing sub critical CO_2 results in the best performance of recovered graphite anodes. It can be said that $scCO_2$ has such a damaging effect on graphite crystallinity that the discharge capacity decreases. When employed as an anode material, graphite's crystallinity is thought to be of utmost significance because it affects the electrochemical performance. High pressure carbon dioxide has the ability to affect this parameter since, in addition to being used as an extracting agent, it has also been used in targeted intercalation and exfoliation of layered graphite. Electrolyte and SEI remnants may be intercalated between the graphite layers as a result of the high pressure of the extraction agent. These intercalated compounds evaporate or degrade as a result of the subsequent thermal treatment on the extracted graphite, which could increase graphite exfoliation. Rothermel et al. [32] concluded that graphite from a commercial cell that had previously undergone electrochemical aging and had been subjected to sub critical CO_2-assisted electrolyte extraction along with thermal treatment generally proved to have the best electrochemical properties, outperforming the benchmark commercial synthetic graphite TIMREX SLP50.

2.3. Supramolecular Extraction

As mentioned before, the addition of a polar co-solvent can modify the liquid or supercritical CO_2 extraction process and increase the likelihood of extracting polar compounds such as $LiPF_6$ [25]. One technique that can be utilized to extract these polar compounds is supramolecular extraction [21, 33–35].

Traditional extraction methods have typically utilized the varying solubilities of the desired compound in two immiscible phases, often involving co-solvent systems, and have found extensive use in separating uncharged molecules. However, such approaches are often inadequate in separating charged species, such as metal ions. On the other hand, supramolecular extraction is a process that use complex formation between the host molecules (extractants) and charged guest species (metal ions and other charged molecules). A "complex" is a molecule or ion formed by the coordination of metal ions with ligands. Ligands are molecules or ions that can donate electron pairs to the metal center, forming coordination bonds. These complexes enable an efficient phase transfer of the target molecule, allowing for selective extraction from a mixture [33].

The host molecule needs to be created to match the guest molecule in terms of their size, shape, and chemical characteristics, including their charge, hardness, acidity, and other relevant properties. In designing the host, it is also important to consider the medium in which the binding will occur, as well as any other molecules that may compete for binding sites. Solvent molecules have a significant influence on the association dynamics and energetics due to their greater abundance compared to the host and guest molecules. Polar solvents can form electrostatic interactions with the host molecules, which can hinder the binding of charged species. The solvent dipole can strongly interact with the charged centers, making it difficult to break the solvent-host or solvent-guest interactions. Since most supramolecular interactions are electrostatic, polar solvents tend to decrease the observed binding. Thus, it is common practice to conduct experiments in the least polar solvent possible to reduce competition for the host [35]. Crown ethers are cyclic molecules with alternating carbon and oxygen atoms that contain structural units of [-CH_2-CH_2-O-] as can be seen in Figure 2.4. Their name "crown" comes from the resemblance of their structure to a crown or a ring with a central cavity, which allows them to act as "molecular hosts" for specific guest ions or molecules. They exhibit a high degree of selectivity in the extraction of metal ions, particularly alkali and alkaline earth metals, due to their ability to form ion-dipole interactions [21]. Crown ether and its derivatives have been widely utilized in the separation and recovery of metals due to their established principles of host-guest recognition. They are popular for metal separation and recovery due to several advantages, including easy preparation and modification, well-defined cavity sizes and binding sites for specificity control, strong binding affinity and selectivity towards metal ions, inherent stability even under extreme conditions, and simple regeneration [33].

The optimal size of the macrocyclic ring must be carefully designed to match the size of the target molecule. If the ring is too small or too large, the ligand will interact poorly with the target molecule, leading to a reduced binding constant. According to the patent of Gluckman, Kraft, and Southard [34], lithium tends to favor four planar coordination sites, which makes it suitable for different versions of the 12-crown-4, 13-crown-4, 14-crown-4, 15-crown-4, and 16-crown-4 ethers. One of the preferred choices for extracting lithium ions is the 12-crown-4 ether. The 14-crown-4 ether, on the other hand, is even more preferable as its cavity is specifically designed to optimize the ionic radius of lithium. While some progress has been made in the application of supramolecular extraction, there are still various challenges that need to be addressed. For instance, there are limited systems with adequate efficiency and selectivity to satisfy the demands of real-world and industrial situations. Hence, there is a need to develop novel macrocycles that offer high efficiency and selectivity to specific targets or to enhance the existing systems [33].

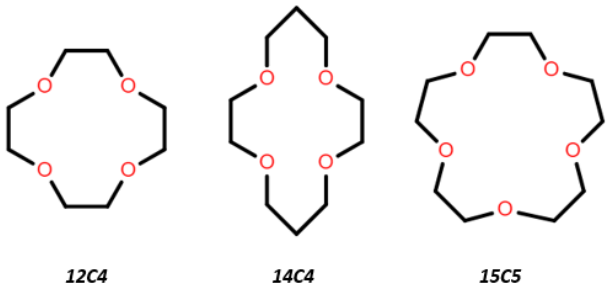

Figure 2.4: Skeletal Structure of Crown Ethers: 12C4, 14C4, and 15C5. The skeletal structures show the molecular arrangement of the crown ethers. Carbon atoms are denoted by lines, representing the backbone of the molecule. Hydrogen atoms are omitted for clarity. The ring of oxygen atoms (O), forms the "crown" shape that gives the molecule its name. These oxygen atoms possess unshared electron pairs, contributing to the molecule's ability to form complexation with metal ions and other species. Keep in mind that this representation does not account for the three-dimensional nature of the molecule and the spatial orientations of atoms in a real-world scenario.

In a recent study by Pálsdóttir, Alabi, and Tester [36], two extractants for lithium recovery were synthesized and tested for suitability in a supercritical carbon dioxide fluid extraction process from natural brines. Although previous studies have indicated the effectiveness of 14-crown-4 ethers as lithium extractants, their solubility in supercritical carbon dioxide has been found to be poor, rendering the development of an effective supercritical fluid extraction process unfeasible. Two 14-crown-4 ethers, namely 3-methylene-14-crown-4 (M14C4) and a newly developed fluorinated 14-crown-4 (F14C4), were chosen for this study based on their favorable structural features and significant solubility in supercritical carbon dioxide. The primary finding of this research is the high solubility of the synthesized crown ethers in supercritical carbon dioxide. At a temperature of 60 °C and a pressure of 205 bar, the highest solubility of M14C4 was measured to be 0.30 mol/L, while the highest solubility of F14C4 was 0.27 mol/L at 60 °C and 285 bar. These solubilities were significantly higher than those of other previously solubilized crown ethers in $scCO_2$ under similar conditions, by two or three orders of magnitude [36].

Sun et al. [21] conducted a study on the extraction properties to lithium ion of Benzo-15-Crown-5 (B15C5) in a solution containing Li^+, Co^{2+}, Ni^{2+}, and Mn^{2+}. Under the experimental condition of pH of 6.0 and 30 °C for 2 hours, B15C5 extractant showed 37 % extraction rate for Li^+ and only 5.18 % for Ni^{2+}, while Co^{2+} and Mn^{2+} were not extracted significantly. The experimentally obtained free energy changes were in accordance with the calculated values. Therefore, using B15C5 as an extractant could be considered a promising method for recovering Lithium from spent lithium-ion batteries leaching solution. Eventhough the feasibility of using B15C5 as an extractant for selective Li^+ extraction was confirmed by Density Functional Theory (DFT) calculations and preliminary experiments, two issues need improvement. Firstly, the single extraction rate of Li+ (37 %) in this study is lower than the reported recovery rate (around 80 %) in conventional hydrometallurgy. Secondly, the solubility of B15C5 in organic solvents is insufficient for use in the extraction of solutions with higher concentrations of Li^+ [21].

2.4. Summary

When it comes to LIB recycling, there are two major methods: Pyrometallurgy and Hydrometallurgy. The pyrometallurgy recycling process does not recycle the electrolyte, and the lithium from the cathode material ends up in the slag making it harder to be recovered. Pinegar and Smith [13] stated that lithium can be recovered from the slag and flue dust as lithium carbonate through leaching and precipitation. But unless the price of lithium is high enough to cover the operating costs, a second lithium recovery process is not rational. The hydrometallurgical recycling process deals with this challenge, however the numerous processing steps hinder the practical application of hydrometallurgy-dominant technologies, which typically reclaim lithium in the final phase, resulting in a low lithium recovery efficiency, due to its low concentration in the leaching solution. In comparison to the pyrometallurgical process, it offers numerous advantages, including high extraction yield, low energy consumption, low hazardous gas emissions, and low capital cost [13, 20].

In traditional recycling processes, the common approach for handling the aged organic electrolyte involves removing the aged electrolytes through calcination or evaporation during pretreatment steps of the recycling process. The lithium salts are left in the active materials and are recovered along with other metal components using a hydrometallurgical method. The use of CO_2 as an extraction medium displays great potential for future applications like LIB electrolyte extraction. During use, aged LIBs often appear "dry" due to the partial decomposition of the liquid electrolyte into solid and gaseous byproducts. The electrolyte becomes immobilized in the electrode's deeper layers and the solid electrolyte decomposition products, making it challenging to recover. Subcritical and supercritical CO_2 extraction techniques are attractive solutions for overcoming this challenge. Hence, more attention must be paid to recycling electrolytes from spent LIBs [5, 6, 37].

Several papers ([7, 15, 32]) have reached a consensus that CO_2 alone is insufficient for extracting the electrolyte and the lithium salt from LIBs, necessitating the use of a co-solvent. Despite the claim made by Grützke et al. [27] that sc$HHCO_2$ can effectively extract the electrolyte and $LiPF_6$ from a polyethylene fleece separator, subsequent extraction experiments on commercial 18650 cells have shown that only minimal amounts of $LiPF_6$ can be obtained. Crown ethers are a promising class of compounds that can be explored as potential co-solvents due to their high selectivity in metal ion extraction, with 12-crown-4 and 14-crown-4 ethers being among the preferred choices for lithium ion extraction according to Gluckman, Kraft, and Southard [34]. Sun et al. [21] demonstrated that Benzo 15-crown-5 ether can also selectively extract lithium ions. Pálsdóttir, Alabi, and Tester [36] synthesized and tested two extractants for lithium recovery for suitability in a supercritical CO_2 fluid extraction process from natural brines.

It is important to note that the existing literature on current LIB recycling processes excludes the utilization of crown ether. Furthermore, the review highlights a limited amount of research focused on recycling the electrolyte, particularly the lithium salt. Therefore, this study explores the possibility of recycling lithium from the electrolyte, with the utilization of crown ethers.

3
Methodology

Now that the potential gap has been identified, the next step involves exploring and conducting a series of investigations to provide valuable insights to bridge this gap. The focus of the first section of this chapter is on the experimental methodology of the study. This includes the measurement methods, experiments design, practical considerations, experimental procedure (including the safety measures), and last but not least an estimation of the uncertainties in the obtained results. The second section of this chapter provides a detailed description of the modeling methodology employed in this study.

3.1. Experimental Methodology

In order to investigate whether it is possible to recycle lithium out of LIBs by utilizing crown ethers, two distinct sets of experiments are proposed. In the first set, the interaction between the electrolyte, specifically the lithium salt, and crown ether is investigated. It is important to also investigate the suitability of this proposed method for extracting lithium from the cathode material. Therefore, the second set of experiments will investigate whether crown ether can be used to also extract lithium from the cathode material. The main focus of these experiments is to determine the extraction yield of the crown ether with regards to lithium.

3.1.1. Measurement Methods

To establish the measurement methods for this study, it is crucial to define the approach for determining the extraction yield of the proposed extraction process. By defining the specific parameters and calculations involved in determining the extraction yield, suitable measurement methods can be selected.

Extraction Yield: The extraction yield ($\eta_{\text{c.e.}}$) is defined in equation 3.1, where $C_{i,\text{Li}}$ and $C_{f,\text{Li}}$ denotes the initial and final concentration of lithium in the electrolyte-crown ether or cathode-crown ether mixture, respectively.

$$\eta_{\texttt{c.e.}} = \frac{C_{i,\text{Li}} - C_{f,\text{Li}}}{C_{i,\text{Li}}} \tag{3.1}$$

The extraction yield can also be based on mass instead of concentration, as can be seen in equation 3.2, where $m_{i,\text{Li}}$ and $m_{f,\text{Li}}$ denotes the initial and final mass of lithium in the electrolyte-crown ether or cathode-crown ether mixture, respectively.

$$\eta_{\texttt{c.e.}} = \frac{m_{i,\text{Li}} - m_{f,\text{Li}}}{m_{i,\text{Li}}} \tag{3.2}$$

The outcomes obtained from equation 3.1 and 3.2 may vary due to change in the mixture's volume (and subsequently, the mass of lithium in the mixture) caused by complex formation and precipitation.

The key parameters that needs to be measured in this study includes the volume and mass of the added electrolyte solution and crown ethers, and the concentration of $LiPF_6$ and crown ether in the electrolyte-crown ether mixture before and after the experiments. Besides that, the formed complex is also analyzed in order to determine its composition. These parameters are significant in determining the extraction yield of the process.

Mass and Volume Measurements: The volume of the electrolyte solutions and crown ether is determined using calibrated 1000 µL pipettes. The mass of the added electrolyte solution, added crown ether, samples, formed complex, and remaining electrolyte-crown ether mixture is determined using an electronic precision balance.

Inductively Coupled Plasma - Optical Emission Spectrometry (ICP-OES): Inductively Coupled Plasma - Optical Emission Spectrometry (ICP-OES, Spectro, Acros-eop), equipped with Modified Lichte Nebulizer is used to determine the concentration of $LiPF_6$ in:

1. The electrolyte solution,
2. The remaining mixture of electrolyte and crown ether after the experiments.

The concentration of $LiPF_6$ in the electrolyte solution is initially provided by the supplier. To ensure the accuracy of the measurements, the electrolyte solution is used as control samples in each batch of experiments. Standard ICP-OES instruments are primarily designed for the analysis of metals and metalloids, making them unsuitable for direct measurement of fluorine (F) due to its low ionization potential and difficulty to excite in plasma source. Similarly, direct measurement of phosphorus (P) is not typically performed by ICP-OES. However, in the scenario where the sample contains phosphate (the lithium salt contains hexafluorophosphate anions (PF_6^-)), ICP-OES can be used to indirectly determine the P content. While alternative techniques specifically designed for the direct measurement of P may offer better sensitivity and accuracy for phosphorus analysis, ICP-OES is still selected as the preferred method for this study due to its ability to accurately measure the concentration of lithium cations, which is the primary objective of this study. This choice also serves the purpose of minimizing the number of measurements required, thus streamlining the experimental process.

Gas Chromatography (GC): To quantify the concentration of crown ethers in the mixture after the completion of the experiments, Gas Chromatography (GC) is employed. GC analysis is conducted using an Agilent 7890A instrument with a split injector set at a ratio of 25. A Flame Ionization Detector (FID) is employed in conjunction with an RTX-1 column measuring 60 m in length, an internal diameter of 0.25 mm and a film thickness of 0.25 µm. The temperature program for the analysis starts at 200 °C, followed by a gradual increase of 10 °C/min to reach 300 °C, resulting in a total analysis duration of 10 min. The calibration is done with external standardization and it involves analyzing pure samples of the specific crown ethers (12C4 and 15C5) that are of interest in the study. The calibration procedure ensures that the GC instrument is properly calibrated and provides accurate measurements of the crown ether concentrations in the mixture.

Field Emission Scanning Electron Microscopy (FESEM): To visualize the structure of the formed complex, field emission scanning electron microscopy (FESEM, JEOL, JSM-6500F) is used. It is a powerful imaging technique used to obtain high-resolution, three-dimensional images of the surface of a sample. Around 1 to 5 mg of 12C4-$LiPF_6$ and 15C5-$LiPF_6$ complex sample is taken in isopropanol solution and sonicated for 20 minutes. A droplet of this solution is deposited onto a silicon wafer and allowed to dry. Following this, the silicon wafer is introduced into the FESEM instrument for analysis.

Energy Dispersive X-ray Spectroscopy (EDX): In combination with SEM, Energy Dispersive X-ray Spectroscopy (EDX, JEOL, JSM-6500F) allows for the simultaneous imaging and elemental analysis of a sample, providing valuable insights into its composition and structure. EDX utilizes the interaction between the primary electron beam and the sample to generate characteristic X-rays. When the primary electron beam strikes the atoms in the sample, it causes the inner-shell electrons to be displaced. As the displaced electrons return to their original positions, they release energy in the form of X-rays. The detected X-rays are then processed to generate a spectrum, known as an EDX spectrum. The EDX spectrum displays peaks at specific energy values corresponding to the characteristic X-rays emitted by the elements in the sample. The intensity of the peaks provides information about the relative abundance of each element. By comparing the peak positions and intensities with known reference spectra, it is possible to identify the elements present in the sample. This technique is used to analyze the composition of the formed complex.

X-ray Photoelectron Spectroscopy (XPS): To gain insight into the composition between the 12C4-$LiPF_6$ and 15C5-$LiPF_6$ complexes, x-ray photoelectron spectroscopy (XPS) is employed. XPS is a surface analysis technique used to determine the elemental composition and chemical states of elements present on the surface of a sample. The sample is placed onto an Indium foil and gently pressed to ensure a flat surface. Subsequently, This prepared sample, along with the Indium foil, is positioned onto the XPS sample holder and loaded into the XPS chamber. The XPS measurements are performed by exposing the sample, which contains the crown ethers and lithium salt, to X-ray radiation. The X-rays cause the ejection of photoelectrons from the surface of the sample, and their kinetic energy and intensity are then measured by the XPS instrument. Analysis is carried out using a PHI-TFA XPS spectrometer (Physical Electronic Inc.) featuring an X-ray A1 K X-ray monochromatic source (energy: 1486.7 eV). The obtained spectra undergo processing using MultiPak v.8.0 (Physical Electronics Inc.) software for tasks such as curve fitting and the determination of atomic concentrations.

3.1.2. Design of Experiments

In this section, the experimental design employed for conducting the experiments is described in detail. The main goal of these experiments is to investigate the lithium extraction yield of crown ether. These experiments are a proof of concept, therefore the experimental setup and procedure is as simple as possible.

Type of Crown Ether, Electrolyte and Cathode Material

First, the type of crown ether, electrolyte, and cathode material that are used in this study are chosen.

Crown Ether: According to Gluckman, Kraft, and Southard [34], 12C4, 14C4 and 15C5 are the best options to extract lithium. This is mainly due to the cavity size of the crown ether ring. If the ring is too small or too large, the crown ether will interact poorly with the target molecule, leading to a reduced binding constant. Table 3.1 shows the diameter of the different crown ethers in relation to the diameter of the lithium- (Li^+), sodium- (Na^+) and potassium ion (K^+).
The observed diameter of Li^+ fits just right in the cavity size of 12C4 and 14C4, while the cavity of 15C5 and 18C6 is larger than the diameter ofLi^+. However, since 14C4 is not readily available and needs to be synthesized, it would require additional time and expertise. Given these constraints, this study will proceed with the readily available 12C4 and 15C5 for the experimental runs.

Table 3.1: Diameters of Crown Ether Cavities and Metal Ions [38].

Compound	Cavity Diameter (Å)	Ion	Ionic Diameter (Å)
12C4	1.2 - 1.5	Li^+	1.36
14C4	1.2 - 1.5	Li^+	1.36
15C5	1.7 - 2.2	Na^+	1.90
18C6	2.6 - 3.2	K^+	2.66

Electrolyte: As already mentioned in Section 1.1, the electrolyte in LIBs consists of high-grade lithium salt which is dissolved in organic carbonate solvents. Lithium hexafluorophosphate ($LiPF_6$) is the most common lithium salt used in commercialized lithium-ion batteries. Solvent mixtures commonly involve a combination of two or more of the following organic carbonates: ethylene carbonate (EC), ethyl methyl carbonate (EMC), dimethyl carbonate (DMC), diethyl carbonate (DEC), and propylene carbonate (PC) [39]. The electrolyte that is used in this study consists of a 1 M concentration of $LiPF_6$ dissolved in a solvent mixture of EC, DMC, and DEC. The selection of this electrolyte formulation is motivated by its previous usage in a prior bachelor end project, which makes it a convenient choice for this research.

Cathode Material: The cathode is the electrode where lithium ions move to during discharge, creating an electron flow through the external circuit. While the electrolyte contains lithium ions in solution, the cathode material holds lithium ions within its crystalline structure. The most common cathode active materials used in commercial LIBs, can be classified in three different crystal structures: layered oxides, spinels or phosphates [9, 10]. The crystal structure can influence the ability to extract lithium from the cathode material. Therefore, cathode active materials from of each class are used in this study:

- Layered Oxides: Lithium Cobalt Oxide ($LiCoO_2$),
- Spinels: Lithium Manganese Oxide ($LiMn_2O_4$),
- Phosphates: Lithium Iron Phosphate ($LiFePO_4$).

Properties: Different batches of electrolyte and crown ethers are used for the experiments. Specifically, 2 batches of electrolyte are employed, along with 6 of 12C4, and 2 of 15C5. The relevant properties of the compounds used in this study are compiled in Table 3.2.

Table 3.2: Molar mass and density of different compounds

Compound	Molar Mass (g/mol) [40]	Density (g/mL) [31]
Electrolyte	-	1.2067
$LiPF_6$	151.91	-
Li^+	6.941	-
P	30.974	-
12C4	176.21	1.089
15C5	220.26	1.113
$LiCoO_2$	97.87	-
$LiMn_2O_4$	180.81	-
$LiFePO_4$	157.76	-

Interaction between Electrolyte and Crown Ether

This series of experiments aims to explore the interactions between the electrolyte and crown ether. Specifically, the extraction yield of crown ether in relation to the lithium salt present in the electrolyte. To determine the most favorable extraction conditions, three distinct parameters are systematically varied:

1. Ratio of Crown Ether to Lithium Salt,
2. Operating Temperature,
3. Extraction Time.

To keep the experiments as simple as possible, the effect of pressure on the extraction yield is not included in this research.

Ratio: To establish an optimal range for the crown ether to lithium salt ratio, valuable insights were obtained from a prior Bachelor End Project (BEP). This project focused on the extraction of lithium from the electrolyte using 12C4 as the selected crown ether. It was observed that for mole ratios up to 1:1 (1 mole of 12C4 to 1 mole of $LiPF_6$), the extraction yield was remarkably low, reaching a maximum of 20 %. Therefore, a ratio of 2:1 is chosen as the lower limit of the range. By considering the maximum ratio between solvent and feed in commercial liquid-liquid extraction processes, which typically is around 5:1 based on mass, an upper limit of the range can be determined [41]. Applying the same ratio in this context, would require 5 kg of crown ether for every 1 kg of electrolyte. Using the given properties in Table 3.2, 5 kg of 12C4 and 15C5 can be converted to mole with equation 3.3, where $\text{Mol}_{\text{c.e.}}$ represents the mole of crown ether, $m_{\text{c.e.}}$ denotes the mass of the respective crown ether and $M_{\text{c.e.}}$ the molar mass of the respective crown ether.

$$\text{Mol}_{\text{c.e.}} = \frac{m_{\text{c.e.}}}{M_{\text{c.e.}}} \tag{3.3}$$

$$\text{Mol}_{12C4} = \frac{5000\,\text{g}}{176.21\,\text{g/mol}} = 28.375\,\text{mol}$$

$$\text{Mol}_{15C5} = \frac{5000\,\text{g}}{220.26\,\text{g/mol}} = 22.7\,\text{mol}$$

To determine the amount of mole of $LiPF_6$ in the electrolyte, first the volume (V_e) of 1 kg electrolyte needs to be calculated using equation 3.4, where m_e denotes the mass of the electrolyte solution and ρ_e the density of the electrolyte solution.

$$V_e = \frac{m_e}{\rho_e} = \frac{1000\,\text{g}}{1.2067\,\text{g/mL}} = 828.71\,\text{mL} \tag{3.4}$$

According to the supplier, the molarity of $LiPF_6$ in the electrolyte solution (c_{LiPF_6}) is 1M (1 mole of $LiPF_6$ in 1 L of electrolyte). Therefore, the amount of mole of $LiPF_6$ in the electrolyte can be calculated with equation 3.5.

$$\text{Mol}_{LiPF_6} = c_{LiPF_6} \times V_e = 0.001\,\text{mol/mL} \times 828.71\,\text{mL} = 0.828\,71\,\text{mol} \tag{3.5}$$

Finally, the mole ratio between crown ether and $LiPF_6$ (MR), based on a 5:1 mass ratio between crown ether and electrolyte solution, can be calculated with equation 3.6.

$$MR = \frac{\text{Mol}_{\text{c.e.}}}{\text{Mol}_{LiPF_6}} \tag{3.6}$$

$$MR_{12C4} = \frac{28.375\,\text{mol}}{0.828\,71\,\text{mol}} = 34:1$$

$$MR_{15C5} = \frac{22.7\,\text{mol}}{0.828\,71\,\text{mol}} = 27:1$$

Despite the possibility of using higher mole ratios such as 34:1 for 12C4 and 27:1 for 15C5, this study will limit the experiments to a maximum mole ratio of 20:1. This decision is made to minimize the quantity of crown ethers required for the experiments. As a result, the mole ratios selected for both 12C4 and 15C5 sre 2:1, 4:1, 6:1, 8:1, 10:1, 12:1, and 20:1. All parameters that are not under investigation are kept constant throughout the experiments to isolate the specific effects of variation in mole ratios. The pressure is maintained at 1 atmosphere, the temperature is set at 30 °C, and the extraction time is fixed at 30 minutes throughout the experiments. In order to ensure the reliability of the results, each experiment is conducted in triplicate.

Temperature: The next parameter to be examined is the influence of temperature on the extraction of lithium from the electrolyte. To keep the experiments simple, the temperature lower bound of the range is chosen to be room temperature, which is around 20 °C. According to [28], $LiPF_6$ is not stable at elevated temperature and will decompose if it is heated above 60 °C. Therefore, a conservative approach is taken, and the upper limit of the temperature range for this study is set at 50 °C. Three temperature levels are chosen from this range: room temperature (approximately 20 °C), 30 °C, and 50 °C. In this set of experiments, the pressure is maintained at 1 atmosphere, the mole ratio is set at 8:1 for 12C4 and 20:1 for 15C5, and the extraction time is fixed at 30 minutes. In order to ensure the reliability and repeatability of the results, each experiment is conducted three times.

Extraction Time: The extraction time is the final parameter to be investigated. Initially, the extraction time is reduced from 30 minutes to 5 minutes. If the extraction yield decreases, it suggests that the complex formation kinetics are slow, indicating the need for a longer extraction time. In such a case, the extraction time is increased to 90 minutes or longer, depending on the requirements, to observe any improvements or a potential plateau in the extraction yield.

Interaction between Cathode and Crown Ether

Even though the focus of this project is on the extraction of lithium salt from the electrolyte, it is valuable to explore the feasibility of applying the same method for extracting lithium from the cathode material. Extracting lithium from the cathode material would involve recovering lithium ions directly from its solid crystalline structure. Consequently, the interactions between these ions and the extraction method can vary in comparison to the lithium salt present in the electrolyte, due to the inherent differences in their chemical contexts. Given this, a second set of experiments is designed to investigate the interactions between the cathode material and crown ether. The purpose of this set of experiments is only to check whether the same extraction method used for electrolyte is viable for the cathode material. Therefore, a single mole ratio between the crown ether and the lithium in the cathode material, operating temperature, and extraction time is investigated. This set of experiments is also conducted at atmospheric pressure to keep the experiments as simple as possible.

Ratio: The determination of the mole ratio between the crown ether and the lithium in the cathode material is based on the conventional ratio observed in liquid-solid extraction. Previous studies, have reported a solid/liquid ratio (S/L ratio) ranging from 0.05 g/mL to 0.2 g/mL in leaching studies of spent LIBs [42]. Therefore, a favorable ratio of 0.1 g/mL is selected for this study. By utilizing this ratio, the mole ratio between the crown ether and lithium in the cathode material can be determine. If the S/L ratio and the mass of the cathode material ($m_{\text{c.m.}}$) is known, the volume of needed crown ether ($V_{\text{c.e.}}$) can be calculated with equation 3.7.

$$V_{\text{c.e.}} = \frac{m_{\text{c.m.}}}{\text{S/L ratio}} \tag{3.7}$$

Subsequently, the mass of the crown ether ($m_{\text{c.e.}}$) can be determined with equation 3.8, where $V_{\text{c.e.}}$ and $\rho_{\text{c.e.}}$ denotes the volume and the density of the crown ether, respectively.

$$m_{\text{c.e.}} = V_{\text{c.e.}} \times \rho_{\text{c.e.}} \tag{3.8}$$

The mole of crown ether ($\text{Mol}_{\text{c.e.}}$) can then be calculated with equation 3.9 where $m_{\text{c.e.}}$ is the mass of the crown ether and $M_{\text{c.e.}}$ the molar mass of the crown ether.

$$\text{Mol}_{\text{c.e.}} = \frac{m_{\text{c.e.}}}{M_{\text{c.e.}}} \tag{3.9}$$

Looking at composition of the cathode materials ($LiMn_2O_4$, $LiCoO_2$ and $LiFePO_4$), 1 mole of cathode material is equal to 1 mole of lithium. Therefore, the mole of lithium (Mol_{Li}) can be calculated using equation 3.10 where $m_{\text{c.m.}}$ represents the mass of the added cathode material and $M_{\text{c.m.}}$ is the molar mass of the cathode material.

$$\text{Mol}_{\text{Li}} = \text{Mol}_{\text{c.m.}} = \frac{m_{\text{c.m.}}}{M_{\text{c.m.}}} \tag{3.10}$$

The mole ratio (MR) can now be calculated with equation 3.11 where $\text{Mol}_{\text{c.e.}}$ and Mol_{Li} represent the mole of crown ether and lithium in the cathode material, respectively.

$$MR = \frac{\text{Mol}_{\text{c.e.}}}{\text{Mol}_{\text{Li}}} \tag{3.11}$$

By combining equation 3.7, 3.8, 3.9, 3.10 and 3.11, a general equation for the mole ratio between crown ether and lithium in the cathode material can be derived. As can be seen in equation

3.12, the mole ratio can be calculated, if the S/L ratio, crown ether density, and the molar mass of the crown ether and cathode material is provided.

$$MR = \frac{\rho_{\text{c.e.}} \times M_{\text{c.m.}}}{\text{S/L Ratio} \times M_{\text{c.e.}}} \tag{3.12}$$

The mole ratio (MR_{12C4}) between 12C4 and lithium in $LiCoO_2$ for an S/L ratio of 0.1 g/mL is calculated in equation 3.13, using the properties given in Table 3.2.

$$MR_{12C4} = \frac{\rho_{12C4} \times M_{LiCoO_2}}{\text{S/L Ratio} \times M_{12C4}} = \frac{1.098\,\text{g/mL} \times 97.87\,\text{g/mol}}{0.1\,\text{g/mL} \times 176.21\,\text{g/mol}} = 6.1:1 \tag{3.13}$$

This calculation has been done for the 12C4 and 15C5 in combination with each of the three cathode materials. The results are compiled in Table 3.3.

Table 3.3: Mole ratio of crown ether (12C4 and 15C5) to lithium in each cathode material ($LiCoO_2$, $LiMn_2O_4$, $LiFePO_4$)

	12C4	**15C5**
$LiCoO_2$	6.1 : 1	4.95 : 1
$LiMn_2O_4$	11.27 : 1	9.14 : 1
$LiFePO_4$	9.83 : 1	7.97 : 1

Temperature and Extraction Time: From preliminary results of a bachelor end project, $LiMn_2O_4$ appeared to be poorly soluble in crown ether. However, these experiments were conducted at room temperature. Therefore, the choice is made to increase the temperature to 60 °C to help increase the solubility of the cathode material in the crown ether solution. Since the cathode material appeared to be poorly soluble in crown ether, the extraction time is extended to 1 hour. Depending on the results, the extraction time can be adjusted accordingly.

3.1.3. Practical Considerations and Limitations

During the course of this study, a few practical considerations and limitations were encountered that are worth mentioning. These factors have an influence on the execution of the experiments and may have implications for the interpretation of the results.

Firstly, $LiPF_6$ is prone to hydrolysis upon contact with moisture or water, leading to the degradation of $LiPF_6$ and potential detrimental effects on the environment and the health of individuals involved in its handling [43]. To prevent this, the electrolyte container should be opened in a moisture-free and inert environment, such as a glove box. To minimize the risk of hydrolysis of $LiPF_6$, the duration of electrolyte exposure with air is minimized, and necessary safety precautions are taken by opening the bottle in a fume hood. Despite these preventive measures, there remains a possibility of hydrolysis occurring during the experiments, which could have potentially influence on the obtained results. Additionally, it should be noted that the electrolyte and crown ether used in the initial experiments have already been opened in a prior study, potentially affecting their composition due to prior hydrolysis.

Secondly, there is a constraint on the amount of chemicals available for the experiments, particularly the limited amount of crown ethers. As a result, a plan is presented to use these resources efficiently by using smaller amounts, thereby ensuring enough resource to run all the experiments. However, this approach introduces the challenges of measuring smaller quantities, which can lead to higher level of uncertainty in the experimental outcomes. Hence, this factor

should be considered during the interpretation and analysis of the results. Besides this, some of the experiments are conducted under ambient conditions, posing challenges in maintaining precise and consistent temperature control throughout the duration of the experiments.

Moreover, the project encountered notable time constraints, which had an impact on the number of experiments conducted. The P&E department is experiencing a shortage of staff, which in the case of this study, resulted in longer-than-anticipated result analysis time. Consequently, insufficient time remained to carry out all planned experiments. A decision is made to prioritize and delve deeply into the investigation of the interaction between the electrolyte and crown ether while postponing the investigation of the interaction between the cathode material and the crown ether. Section 3.1.2 provides an explanation of the experimental design, while the necessary materials to run the second set of experiments are readily available in the laboratory. Therefore, a subsequent study can proceed with the execution of these experiments.

Despite these practical considerations and limitations, this study provides valuable insights into the examined extraction method and establishes a foundation for further research in this area. Addressing these limitations and building upon this work will contribute to a more comprehensive understanding of the.

3.1.4. Experimental Procedure

This section outlines the step-by-step procedures for the experimental process, including the preparation of the electrolyte solution, the setup of the extraction experiments, the analytical techniques for analysis, and any additional considerations for ensuring accuracy and reproducibility. The scope of this section is limited to the discussion of the experimental procedures for the investigation of the interaction between the electrolyte solution and the crown ether.

Preparation

The electrolyte solution (purchased commercially from Merck) consists of $LiPF_6$ (purity >99 %) dissolved in a solvent mixture of Ethylene Carbonate (EC), Di-Methyl Carbonate (DMC) and Di-Ethyl Carbonate (DEC) (volume ratio 1:1:1) with a concentration of 1 M. The crown ethers, 12C4 and 15C5, (obtained commercially from Merck), have purities specified by the supplier to be >98 %. The electrolyte solution and the crown ethers are used as received without further purification. However, the electrolyte solution is analyzed using ICP-OES to determine the exact concentration of $LiPF_6$ present in the electrolyte solution prior to the experiments.

The extraction experiments are conducted using plastic vials with screw caps. Each vial is filled with a specific volume of the electrolyte solution using a pipette, followed by the addition of a predetermined volume of the crown ether (depending on the ratio). The mass of the electrolyte solution, crown ether, and final mixture is also measured using a precision electronic balance. Prior to each measurement, the tare weight of the empty vial is determined to account for its mass. The electrolyte solution is then carefully added to the vial, and the combined mass of the vial and electrolyte solution is measured. The difference between the combined mass and the tare weight provides the mass of the electrolyte solution. Following that, the crown ether is added to the vial containing the electrolyte solution. The combined mass of the vial, electrolyte solution, and added crown ether is measured, and the difference between this combined mass and the combined mass of the electrolyte solution and the empty vial provides the mass of the added crown ether. Finally, to determine the mass of the resulting mixture, the mass of the empty vial is subtracted from the new combined mass.

The vials containing the mixture of electrolyte solution and crown ether, are then tightly closed with a screw cap to prevent any leakage or evaporation. In order to facilitate thorough mixing and enhance the extraction yield, the vials, securely sealed with the mixture inside, are subjected to controlled mechanical agitation during the extraction period.

Ratio Variation

The experiments investigating the impact of various ratios between the crown ether and the electrolyte solution are performed at a constant temperature of 30 °C. To ensure consistent and controlled conditions, the vial containing the mixture, along with the mechanical shaker, are placed inside an oven set at 30 °C. The mixture is mechanically agitated during the entire 30-minute extraction period.

Table 3.4 and Table 3.5 present the mole ratios of crown ether to $LiPF_6$, the corresponding mass ratios between the crown ether and the electrolyte solution, as well as the required mass of the electrolyte solution and crown ether for the experiments.

Table 3.4: Mole ratio, mass ratio and required resources for the experiments with 12C4.

Mol Ratio	Mass Ratio	Mass Crown Ether (g)	Mass Electrolyte (g)
2:1	0.292:1	0.705	2.413
4:1	0.584:1	1.410	2.413
6:1	0.877:1	2.115	2.413
8:1	1.169:1	2.115	1.810
10:1	1.46:1	1.762	1.207
12:1	1.752:1	2.115	1.207
20:1	2.919:1	1.410	0.483

Table 3.5: Mole ratio, mass ratio and required resources for the experiments with 15C5.

Mol Ratio	Mass Ratio	Mass Crown Ether (g)	Mass Electrolyte (g)
2:1	0.365:1	0.881	2.413
4:1	0.73:1	1.322	1.810
6:1	1.095:1	1.322	1.207
8:1	1.46:1	1.762	1.207
10:1	1.825:1	2.203	1.207
12:1	2.19:1	2.114	0.965
20:1	3.648:1	1.762	0.483

Temperature Variation

This study investigates the impact of different temperatures, specifically 20 °C, 30 °C, and 50 °C. For experiments conducted at 20 °C, the vials with the mixture are kept at room temperature in a laboratory and subjected to mechanical agitation for 30 minutes. Similarly, for experiments conducted at 30 °C and 50 °C, the vials with the mixture are placed in an oven to maintain the desired temperature and shaken for 30 minutes. To ensure the reliability and reproducibility of the results, each experiment is repeated three times. Table 3.6 provides an overview of the mole ratios and the corresponding mass of electrolyte and crown ether required for each experiment.

Table 3.6: Mole ratio and amount of resources needed for each experiments with 12C4 and 15C5.

	12C4	**15C5**
Mole Ratio	8:1	20:1
Electrolyte Solution (g)	0.905	0.483
Crown Ether (g)	1.057	1.762

Extraction Time Variation

The experiments examining the effect of various extraction times, on the extraction yield of crown ether, are performed at a constant temperature of 30 °C. The vial containing the mixture, along with the mechanical shaker, is placed inside an oven set at 30 °C. Three distinct extraction times are investigated: 5 minutes, 15 minutes, and 30 minutes. Detailed information on the mole ratio, and the corresponding mass of the electrolyte solution and crown ether required for each experiment can be found in Table 3.6.

Sample Collection

After the completion of the extraction experiments detailed above, samples are collected to analyze and determine the extraction yield of the crown ether. Since the complex formed by the lithium salt and crown ether is in a solid state, it remains suspended in the liquid phase after agitation. To ensure accurate sampling of the residual mixture without inadvertently collecting the complex, the vials containing the electrolyte-crown ether mixture are allowed to settle at the same temperature as the extraction experiment for a period of 30 minutes before sampling. This settling time allows for the separation of the complex from the liquid phase, enabling accurate sampling of the remaining electrolyte-crown ether mixture. Figure 3.1 shows the difference before and after settling.

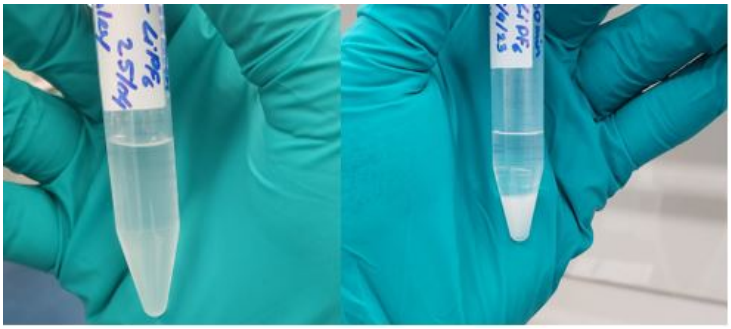

Figure 3.1: Difference in the suspension of the complex prior to and after the settling period. This technique aims to separate the mixture from the formed complex, in order to get a representative sample from the mixture for further analysis.

The sample is extracted using a syringe and needle, ensuring that only the electrolyte-crown ether mixture is collected. The collected sample is then transferred into a sample tube. To determine the mass of the sample, the tare weight of the empty tube is measured, the collected sample is added to the tube, and the combined mass of the sample tube and sample is measured. The mass of the collected sample is determined by subtracting the tare weight of the empty sample tube from the combined mass. The collected samples are analyzed using both ICP-OES and GC techniques. ICP-OES analysis is performed to determine the concentration of $LiPF_6$ remaining in the mixture, while GC analysis is utilized to measure the concentration of the crown ether in the remaining electrolyte-crown ether mixture. These analyses provides valuable insights into the residual amounts of $LiPF_6$ and crown ether present in the remaining liquid mixture. These analysis provides crucial data for evaluating the effectiveness of the extraction process.

Following this, the complex is separated from the remaining electrolyte-crown ether mixture using vacuum filtration, as illustrated in Figure 3.2. A glass fiber filter paper is placed at the bottom of the Buchner funnel. The electrolyte-crown ether mixture, along with the complex, are carefully poured onto the filter paper in the funnel. The vacuum created by the vacuum pump causes the electrolyte-crown ether mixture to pass through the filter paper and collect in the flask, while the complex remains on the filter. The mass of the liquid collected in the filter flask is subsequently determined employing the same weighing method described earlier.

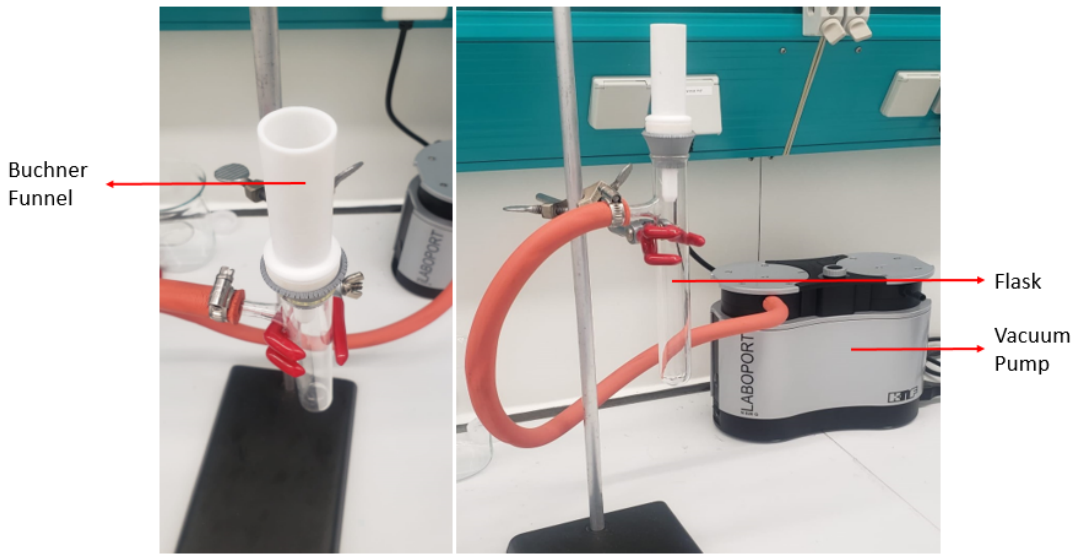

Figure 3.2: Vacuum filtration Setup: The mixture and formed complex are poured into the Buchner funnel, with a glass fiber filter paper positioned at its base. Application of vacuum using a vacuum pump drives the electrolyte-crown ether mixture through the filter paper, collecting it in a flask, while retaining the complex on the filter.

The complex, once separated, is collected and its initial wet mass is determined. To remove any moisture, the complex undergoes vacuum drying in an oven for 24 hours. The final dry mass of the complex is measured, and the difference between the wet and dry masses is added to the mass of the sample and the mass of the separated electrolyte-crown ether mixture. This calculation enables the determination of the total mass of the remaining electrolyte-crown ether mixture following the extraction process. The dry complex obtained is subjected to analysis using X-ray Photoelectron Spectroscopy (XPS)to determine its content and composition. Additionally, Scanning Electron Microscopy (SEM) is conducted to visualize the crystal structure of the complex. A summary of the different measurement methods that is employed is illustrated in Figure 3.3.

Safety Measures

The experiments are conducted in a separation laboratory. Personal protective equipment, including lab coats, gloves, and safety goggles, are worn during the handling and manipulation of chemicals and equipment. To ensure a safe working environment, the experimental area is equipped with a fume hood to provide adequate ventilation.

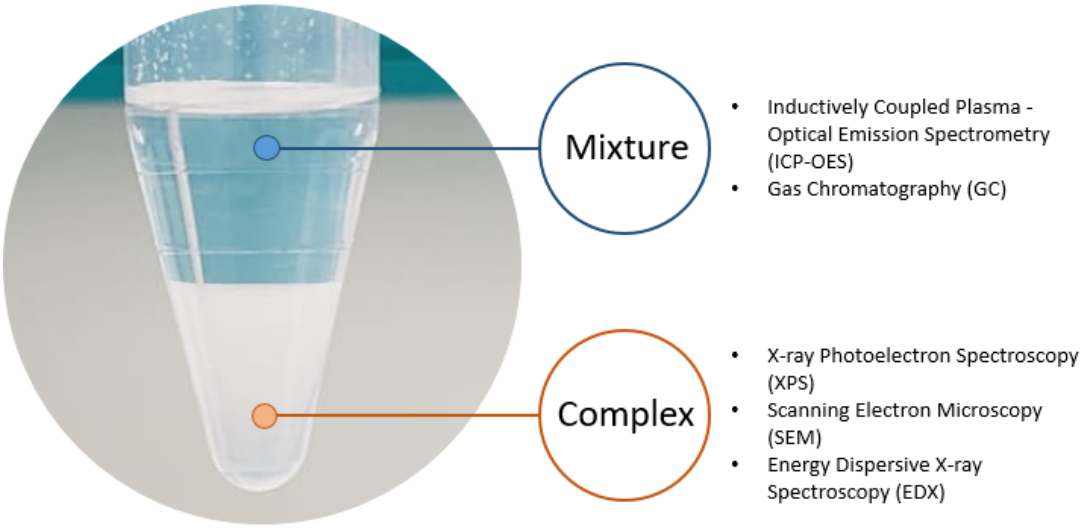

Figure 3.3: Summary of the analysis employed on the remaining electrolyte-crown ether mixture and the formed crown ether-$LiPF_6$ complex.

3.1.5. Error and Uncertainty

In order to ensure the accuracy and reliability of the experimental findings, the error and uncertainty associated with the obtained data is evaluated. The experiments are conducted in triplicate to capture and account for any random fluctuations or systematic errors that might impact the results. The first step in the analysis involves calculating the mean value of the measured quantities ($\bar{x}$), using equation 3.14, by summing up the replicate measurements (x_i) and dividing by the total number of replicates (n).

$$\bar{x} = \frac{1}{n}\sum_{i=1}^{n} x_i \tag{3.14}$$

In addition to assessing the mean of the data, it is essential to quantify the spread of the measurements. To achieve this, the standard deviation (s) is computed, using equation 3.15. The standard deviation measures the average deviation of each data point from the mean and provides insight into the variability within the data set.

$$s = \sqrt{\frac{1}{n-1}\sum_{i=1}^{n}(x_i - \bar{x})^2} \tag{3.15}$$

To further evaluate the precision of the mean estimation, the standard error (SE) is calculated. The standard error is determined to assess the precision of the mean estimation. The standard error represents the standard deviation of the sample mean and is calculated, using equation 3.16, by dividing the standard deviation by the square root of the number of replicates.

$$SE = \frac{s}{\sqrt{n}} \tag{3.16}$$

To establish the uncertainty associated with the measurements (U), a 95 % confidence level is chosen, indicating a high level of confidence in the reported values. The resulting product of the standard error and the critical value (CV) provides an estimation of the uncertainty associated with the measured values. The CV is approximately 2 at a 95 % confidence level.

$$U = SE \times CV = SE \times 2 \tag{3.17}$$

The mean, standard deviation, standard error, and uncertainty analysis provide valuable insights into the reliability and accuracy of the obtained results.

3.2. Modeling Methodology

Several studies in literature [15, 27, 32] have highlighted the potential of supercritical CO_2 for extracting the organic solvent component in electrolyte. To gain deeper insights into this extraction process, the objective is to conduct experimental studies to quantitatively evaluate its efficiency and performance. Prior to conducting the experimental investigations, it is important to characterize the phase equilibrium between CO_2 and the solvent components through thermodynamic modeling. This modeling exercise is essential for identifying the optimal CO_2 quantity and the associated operating conditions needed to facilitate the extraction process effectively. Understanding the thermodynamic behavior of the CO_2-solvent system lays the foundation for designing and optimizing subsequent experimental studies to further develop the extraction process.

3.2.1. Modeling Procedure

This section outlines the step-by-step procedures followed during the thermodynamic modeling exercise to determine the phase equilibrium between CO_2 and the electrolyte solvents.

In this study, the phase equilibrium between CO_2 and the electrolyte solvents is determined using a thermodynamic model. This model incorporates Matlab computer programs specifically designed for calculating phase equilibrium and thermodynamic properties of fluid mixtures. The specific Matlab codes utilized in this study are obtained from the supplementary data provided by Martín et al. [44]. For applications at moderate or high pressures, cubic equations of state (EOS) such as Soave-Redlich-Kwong or Peng-Robinson are commonly utilized. Given the objective of reaching supercritical CO_2, which requires high pressures (above 74 bar), the Peng-Robinson EOS is selected as the model for this study. The program uses the Peng-Robinson equation of state (EoS) coupled with Van der Waals quadratic mixing rules to calculate and plot a pressure-composition ($P-xy$) diagram for a binary system at a fixed temperature T. The Peng-Robinson EoS for a binary mixture is shown in equation 3.18 [45]:

$$P = \frac{RT}{V - b_m} - \frac{a_m}{V^2 + 2Vb_m - b_m^2} \tag{3.18}$$

where R is the gas constant, T is temperature (K), P is the pressure (MPa) and V is the molar volume. a_m is the attraction parameter and b_m is the repulsion parameter for the mixture and can be calculated with equation 3.19 and 3.20 respectively, where x is the component mole fraction, k_{ij} is the binary interaction parameter, and a_i and b_i are respectively the attraction and repulsion parameters for a pure component.

$$a_m = \sum_{i=1}^{2}\sum_{j=1}^{2} x_i x_j (1 - k_{ij})\sqrt{a_i a_j} \tag{3.19}$$

$$b_m = \sum_{i=1}^{2} x_i b_i \tag{3.20}$$

The attraction and repulsion parameters for a pure component can be calculated with equation 3.21 and 3.22, respectively, where T_c is the critical temperature (K) and P_c is the critical pressure (MPa) of the pure component.

$$a_i = 0.45724\frac{R^2 T_c^2}{P_c}\left(1 + \kappa\left(1 - \sqrt{T/T_c}\right)\right)^2 \tag{3.21}$$

$$b_i = 0.0778\frac{RT_c}{P_c} \tag{3.22}$$

The simplification term κ can be determine with equation 3.23, where ω is the acentric factor for a pure component.

$$\kappa = -0.26992\omega^2 + 1.54226\omega + 0.37464 \tag{3.23}$$

To simplify the modeling process, the complex mixture of CO_2 and the electrolyte solvents, consisting of four components, are treated as individual binary mixtures. This approach allows for a more focused analysis of the interactions between CO_2 and each solvent component: CO_2 with DMC, CO_2 with DEC, and CO_2 with EC. The thermodynamic model based on the Peng-Robinson EoS utilizes the following input parameters for the components:

- M: molecular weight (g/mol)
- T_c: Critical Temperature (K)
- P_c: Critical Pressure (Pa)
- ω: Acentric Factor

These properties are shown in Table 3.7. The properties for CO_2, DMC and DEC are obtained from the NIST ThermoData Engine (103b) in Aspen Plus v12 [46] and the properties for EC are obtained from Yaws and Narasimhan [47].

Table 3.7: Properties of Carbon Dioxide (CO_2), Dimethyl Carbonate (DMC), Diethyl Carbonate (DEC), and Ethylene Carbonate (EC): Molar Mass (M), Critical Temperature (T_c), Critical Pressure (P_c), and Acentric Factor (ω).

	M (g/mol)	T_c (K)	P_c (Pa)	ω (-)
CO_2	44.01	304.2	7380000	0.2252
DMC	90.084	557	4800000	0.336
DEC	118.13	576	3146410	0.4434
EC	88.062	613	6141842	0.442

In order to calculate and visualize the $P-xy$ diagram of the binary mixture, it is necessary to determine the binary interaction parameter (k_{ij}) between the two components. This parameter captures the non-ideal mixing behavior and quantifies deviations from ideality within the mixture. To accomplish this, a dedicated MATLAB script, as developed by Martín et al. [44], is employed. This MATLAB script is specifically designed to fit the Peng-Robinson equation of state to experimental data, enabling the determination of the binary interaction parameter for the binary mixture under investigation. It iteratively adjusts the value of the 'par' parameter, which represents k_{ij}, and calculates the pressures using the Peng-Robinson equation of state. The calculated pressures are compared to the experimental pressures, and the objective function (average percentage error) is calculated. By minimizing the objective function through the optimization process, the script aims to find the optimal value of the k_{ij} parameter that best fits the experimental data. The experimental data for the phase equilibrium at different temperatures between CO_2 and DMC, CO_2 and DEC, and CO_2 and EC obtained from Aspen Plus v12 are displayed in Appendix A [46]. It must be noted that the lack of experimental data for the CO_2 and EC mixture restricts the possibility of conducting modeling for this specific system. As a result, the $P-xy$ diagram for the CO_2 and EC mixture are not pursued in this study.

After obtaining the binary interaction parameter (k_{ij}) for the three distinct binary mixtures, the corresponding $P-xy$ diagram is constructed. By doing this, the operating conditions for this process can be determined.

The script is structured in the following sections:

- First all components present in the mixture and their properties are defined.
- The second step consists of defining the mixture formed by these components, as well as mixture parameters. In this case, the binary interaction parameter k_{ij}.
- Then the equation of state to be used is specified (in this case, the standard Peng–Robinson equation).
- Finally, the calculations required for the $P - xy$ diagram are performed.

3.2.2. High Pressure Setup

To investigate the extraction of electrolyte solvents using supercritical CO_2, a high-pressure setup capable of withstanding elevated pressures is required.

Sapphire Visualization Cell

For the high-pressure setup, a sapphire visualization cell (SVC) is utilized (Figure 3.4). The cell is made of a high-purity single sapphire crystal, which is transparent and durable material. Its transparent nature enables the visual observation and monitoring of reactions, phase transitions, and fluid flow occurring within the cell. The SVC has a total cell volume of 56 mL, an internal diameter of 24.5 mm, a temperature range of 0 °C to +150 °C, and its maximum allowable pressure is 340 bar (design pressure is 365 bar).

Figure 3.4: Sapphire Visualization Cell: A transparent and durable setup for visual observation of dynamic phenomena in closed systems. The SVC including housing has a diameter of 10 cm and height of 15 cm.

It is possible to equip the cell with various instrumentation for enhanced functionality. Figure 3.5 illustrates the configuration of the SVC, showcasing the inclusion of a stirrer, temperature sensor, and pressure sensor. Two electrical cabinets have been supplied: one for displaying the pressure and temperature, and another for controlling the stirrer. Additionally, the SVC is equipped with a double-jacket option. By connecting the outer jacket to a julabo heater, the desired temperature of the cell can be reached. Water up to 90 °C can be connected on the jacket ports, shown in Figure 3.5, with 6 mm 100 °C resistant plastic tubes.

Using a protective screen or a shield to catch potential projectiles or shrapnel is a good safety measure when working with systems or equipment that involve high pressures or potential hazards. Therefore, the SVC is placed behind a shield . The system is also protected by a rupture disc installed on the cell, which has a burst pressure of 359.68 bar. The SVC is placed in a fume hood to prevent the accumulation of any hazardous gases or vapors that may be released during the experimental process.

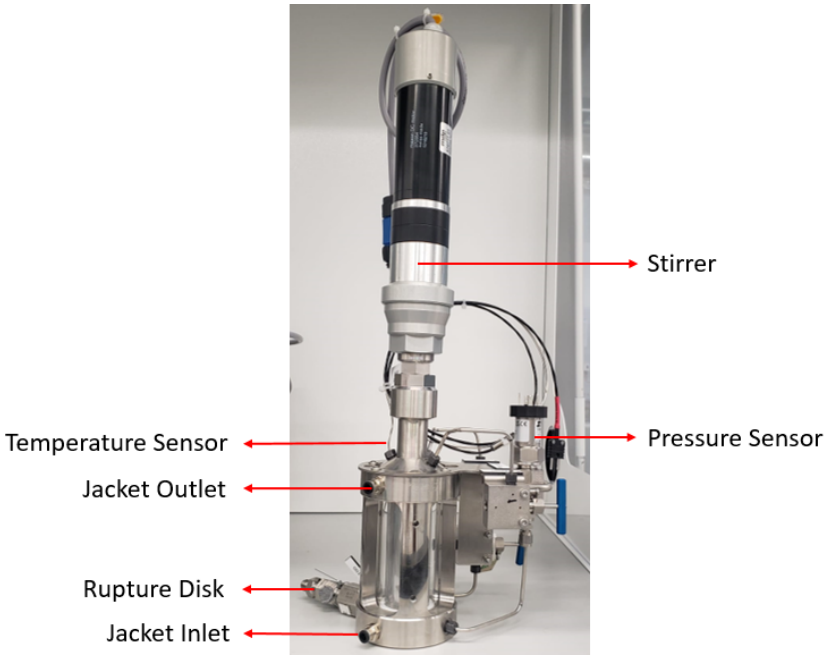

Figure 3.5: Sapphire Visualization Cell (SVC) Equipped with Various Instruments for Enhanced Control and Monitoring of Experimental Parameters: A stirrer to mix the contents in the SVC, sensors to monitor the temperature and pressure within the SVC, jacket inlet and outlet to keep the SVC on a certain temperature using a cooling or heating medium, and rupture disk with a burst pressure of 359.68 bar. The total height of the SVC is 50 cm.

Pump

In order to reach the critical pressure of CO_2, a volumetric type pump (Piston Pump) is used. The pump, shown in Figure 3.6, works with liquid and liquefied gas, has dual inlet and outlet check valves, cooled pump heads, and Modbus TCP/IP communications for external control and status monitoring.

Figure 3.6: Volumetric CO_2 Pump Used to Attain Critical CO_2 Pressure for the Experiments. The pump is 50 cm x 45 cm x 25 cm.

To ensure optimal operation of the piston pump, it is critical to supply liquid CO_2 rather than its gas form. This requires the CO_2 bottle to be equipped with a dip tube that extends to the bottom, enabling the extraction of liquid CO_2. The CO_2 feed should maintain a pressure within the range of 50 to 60 bar and a temperature between 0 °C and 5 °C. To monitor the remaining pressure, a pressure gauge is positioned at the outlet of the CO_2 bottle. To avoid the formation

of CO_2 gas during operation, the pump is outfitted with a cold jacket. This cold jacket serves to maintain the CO_2 in its liquid state, promoting smooth pumping and preventing the formation of gas bubbles that could disrupt the pump's performance. The cold jacket of the pump is connected to a Julabo chiller using a 12 mm plastic tube. The chiller is filled with a mixture of de-ionized water and glycol in an 80/20 ratio. The overall setup is can be seen in Figure 3.7.

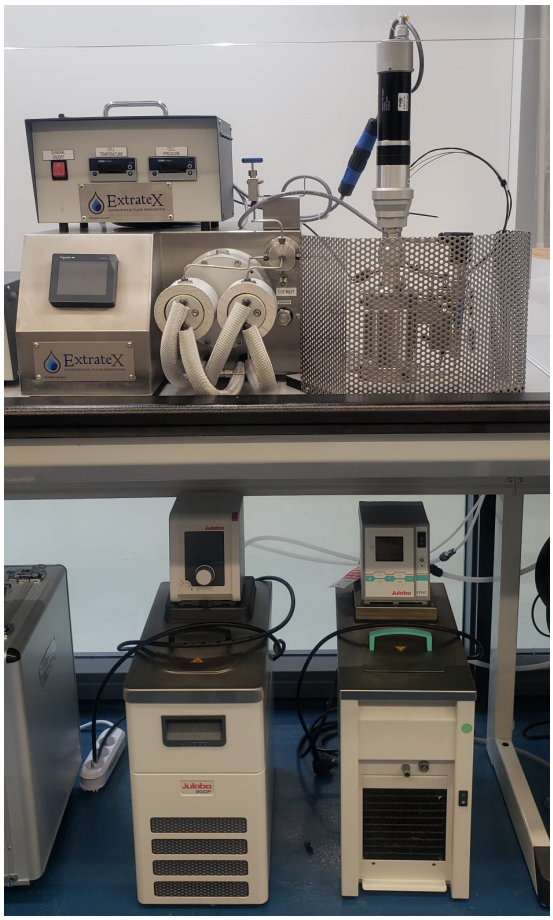

Figure 3.7: Experimental Setup Featuring the Sapphire Visualization Cell, Volumetric CO_2 Pump, Chiller, and Heater: Essential components for the experiments. The CO_2 tank, not shown in this image, completes the setup for the extraction studies.

3.2.3. Practical Considerations and Limitations

The SVC requires modifications to enable quantitative research. Since the experiments involve high pressures, it is essential to take samples at these elevated pressures. However, the SVC lacks a suitable sampling device for high-pressure conditions. Unfortunately, the delivery time for such a device exceeds the available time for this project. As a result, experiments to evaluate the performance and efficiency of CO_2 to extract the organic solvent components in the electrolyte can not be conducted in this project.

4

Results and Discussion

The results and discussion section of this report provides a detailed analysis and interpretation of the data obtained from the conducted experiments and modeling exercise. It delves into the key findings of the experiments and modeling, discuss their implications, and provide insights into the underlying mechanisms and phenomena observed. Additionally, any limitations or unexpected observations are also addressed, offering opportunities for further investigation. Overall, this chapter aims to provide a comprehensive and insightful discussion of the results.

4.1. Experimental Results

The results and findings obtained from the conducted experiments are presented in this section. First, the calculations employed to obtain the relevant results are outlined and after that, the obtained results are presented. This section will only discuss the results of the investigation of the interaction between the lithium salt in the electrolyte solution and the crown ether. The objective of these experiments is to investigate the impact of different mole ratios, temperatures, and extraction times on the extraction yield of the process. The extraction yield is quantified based on the initial and final concentrations of Lithium and Phosphorus. For the calculation example, the 2:1 mole ratio of 12C4 at 30 °C is chosen.

As mentioned previously in section 3.1.1, the concentration of Li and P in the electrolyte solution is determined using ICP-OES analysis. The obtained results indicate that the electrolyte contains 7.259 mg/g of Li-ions and 25.354 mg/g of P-ions. The initial mass of the added Li- and P-ions ($m_{i,\text{ Li or P}}$) can be calculated by multiplying the initial concentration of the Li- and P-ions ($C_{e,\text{ Li or P}}$) with the mass of the added electrolyte solution (m_e), which in this case is 2.48 g, as shown in equation 4.1.

$$m_{i,\text{Li or P}} = C_{e,\text{Li or P}} \times m_\text{e} \tag{4.1}$$

$$m_{i,\text{Li}} = 7.354\,\text{mg/g} \times 2.48\,\text{g} = 18\,\text{mg}$$

$$m_{i,\text{P}} = 25.354\,\text{mg/g} \times 2.48\,\text{g} = 62.88\,\text{mg}$$

Afterwards, the mass of the mixture ($m_{i,\text{m}}$) is determined, by adding the mass of the electrolyte solution (m_e) to the mass of the crown ether ($m_\text{c.e.}$), as can be seen in equation 4.2.

$$m_{i,\text{m}} = m_\text{c.e.} + m_\text{e} = 0.74\,\text{g} + 2.48\,\text{g} = 3.22\,\text{g} \tag{4.2}$$

Finally, the initial concentration of Li and P-ions ($C_{i,\text{ Li or P}}$) can be obtained through equation 4.3.

$$C_{i,\text{Li or P}} = \frac{m_{i,\text{Li or P}}}{m_{i,\text{m}}} \tag{4.3}$$

$$C_{i,\text{Li}} = \frac{18\,\text{mg}}{3.22\,\text{g}} = 5.590\,\text{mg/g}$$

$$C_{i,\text{P}} = \frac{62.88\,\text{mg}}{3.22\,\text{g}} = 19.528\,\text{mg/g}$$

Following the experiments, samples of the remaining solution are taken and subjected to ICP-OES analysis. The results indicated a final concentration ($C_{f,\text{ Li or P}}$) of 4.212 mg/g for Li-ions and 13.739 mg/g for P-ions in the remaining mixture. Subsequently, the extraction yields of 12C4, based on concentration, are determined using equation 4.4. The extraction yields presented in the following sections are determined using this calculation method.

$$\eta_{\texttt{c.e.}} = \frac{C_{i,\text{Li or P}} - C_{f,\text{Li or P}}}{C_{i,\text{Li or P}}} \times 100\% \tag{4.4}$$

$$\eta_{\texttt{12C4,Li}} = \frac{5.590\,\text{mg/g} - 4.212\,\text{mg/g}}{5.590\,\text{mg/g}} \times 100\% = 24.65\,\%$$

$$\eta_{\texttt{12C4,P}} = \frac{19.528\,\text{mg/g} - 13.739\,\text{mg/g}}{19.528\,\text{mg/g}} \times 100\% = 29.64\,\%$$

4.1.1. Effect of Ratio

In this section, the results of the experiments investigating the impact of varying the mole ratio between the crown ether and the lithium in the electrolyte on the extraction yield are presented and discussed. The experiments involve different mole ratios (2:1, 4:1, 6:1, 8:1, 10:1, 12:1 and 20:1) of crown ether to lithium in the electrolyte. For each case, the mean extraction yield (for Li and P) and its corresponding uncertainty are calculated. The results for 12C4 and 15C5 are summarized in Table B.1, and B.1 in Appendix B, respectively, and visually represented in Figure 4.1.

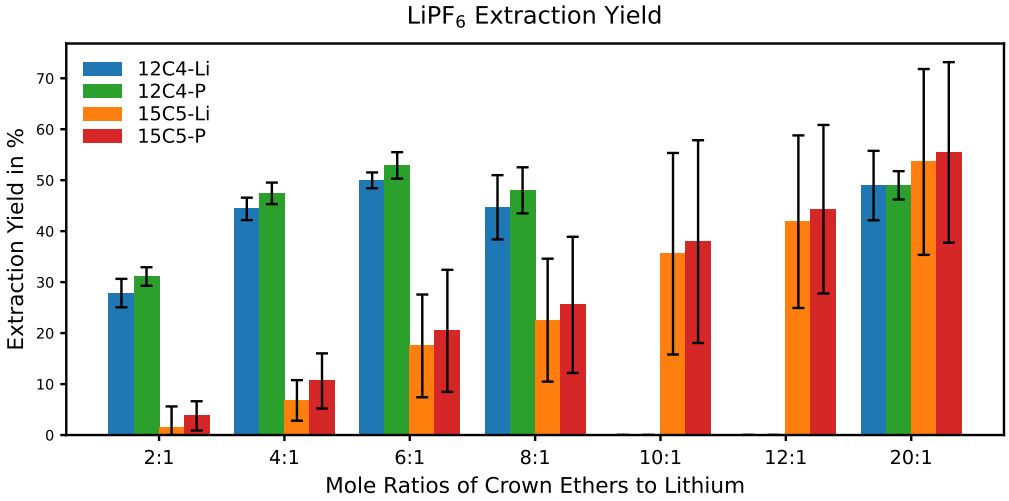

Figure 4.1: Effect of Mole Ratio on Extraction Yield: This graph showcases the mean extraction yield for lithium (Li) and phosphorus (P) at different mole ratios, along with corresponding uncertainties for both 12C4 and 15C5 crown ethers, shedding light on their distinct performances in the extraction process. The extraction yield increases with increasing mole ratios, until it reaches a plateau around 6:1 for 12C4 and beyond 12:1 for 15C5.

Figure 4.1 clearly illustrates the significant impact of the mol ratio on the extraction yield of the process. A lower mol ratio corresponds to a lower extraction yield, while an increase in the mol ratio leads to higher extraction efficiency. However, it is worth noting that the extraction yield tends to plateau at a mol ratio of approximately 6:1 to 8:1, as observed in the case of 12C4. To minimize resource consumption while assessing the plateau for 12C4, the decision is taken to omit the 10:1 and 12:1 ratios and investigate the 20:1 ratio. Interestingly, the extraction yield of 12C4 at 20:1 did not show any substantial increase compared to the 8:1 ratio. Hence, it can be reasonably assumed that the extraction yields for the 10:1 and 12:1 ratios would likely exhibit a similar trend to that of 8:1 and 20:1. Thus, the extraction yield of 12C4 reaches a plateau at approximately 50 %. By examining the uncertainties of the experiments in Table B.1b, it becomes evident that the largest uncertainty is 6.81 % and it occurs at the mole ratio of 20:1, suggesting that the results are relatively accurate, and the experiments can be repeated with consistent outcomes.

Considering the case of 15C5, it shows a contrasting pattern. The extraction yield displays a consistent linear growth as the mol ratio increases, reaching around 53 % at a mol ratio of 20:1. The observed trend indicates that 15C5 has not yet reached its plateau, and the linear relationship may continue even at higher mol ratios. However, it is important to consider the x-axis intervals, which range from 2 to 12 in steps of 2, and goes from 12 to 20 in one single step, creating a gap of 8, rather than the usual 2-step increments. Considering this, it can be inferred that the extraction yield of 15C5 has likely reached or is approaching its plateau for mol ratios beyond 12:1. The experimental results for 15C5 exhibited a higher level of uncertainty when compared to those of 12C4. This suggests that replicating the outcomes of the experiments is notably challenging. The data points for 15C5 are more scattered and less consistent, making it difficult to precisely determine the extraction yield. Further investigations or analysis of the experimental setup and procedure might be required to understand and address the factors contributing to this variability.

For example, two batches of 15C5 are utilized due to insufficient quantity of a single batch (25 g) to accommodate all the required experiments. The initial three runs are conducted using the first batch, while the last run is performed with the second batch. Notably, as can be seen in Table B.2a in Appendix B, the third run of the first batch exhibited distinctively better outcomes compared to the previous two runs. Surprisingly, the run with the second batch deviated significantly from the outcomes obtained with the first batch (yielding inferior results). At present, the precise cause behind this discrepancy remains unidentified. It is plausible that 15C5 is more sensitive to certain factors or impurities compared to 12C4. Crown ethers have distinct structural characteristics, which can influence their interactions with specific ions and the formation of stable complexes. Even minor variations in temperature, pressure, or other factors might have a more pronounced impact on 15C5 ability to efficiently extract the lithium salt. In contrast, 12C4 may exhibit a more stable and reliable performance due to its different structural properties. Further investigations may be necessary to determine the exact reasons behind the observed differences and ensure the reliability and reproducibility of the experimental results.

Comparing the performance of the two crown ethers reveals that 12C4 stands out as the superior option. Despite both crown ethers achieving similar maximum extraction yields, the critical difference lies in the mol ratio required to reach this point. 12C4 accomplishes this at a much lower mol ratio of 6:1, while 15C5 necessitates a significantly higher mol ratio of 20:1. Consequently, the use of 15C5 demands a larger quantity compared to 12C4 to attain the same extraction yield. As a result, using 15C5 not only increases the cost but also diminishes the overall process efficiency.

4.1.2. Effect of Temperature

This section shows and discuss the results of the effect that a variation in temperature has on the extraction yield. Mole ratios of 8:1 and 20:1 are used for 12C4 and 15C5 respectively. The results for the extraction yield, while varying the temperature(20 °C, 30 °C, and 50 °C), are shown in Figure 4.2.

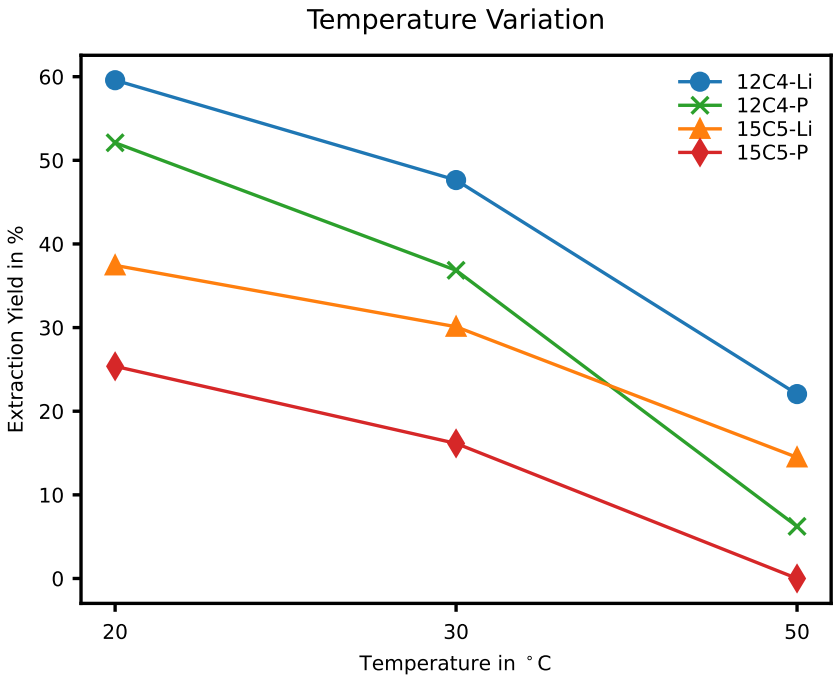

Figure 4.2: Effect of Temperature on Extraction Yield: The graph illustrates the extraction yields of 12C4 and 15C5 crown ethers at various temperatures (20 °C, 30 °C, and 50 °C) using mole ratios of 8:1 and 20:1. The extraction yield decreases with increasing temperatures.

The extraction yield of both 12C4 and 15C5 shows a remarkable dependence on temperature. As the temperature rises, the extraction yield declines, implying an exothermic nature of the complex formation process (heat is released during its formation). This indicates that lower temperatures are more favorable for complex formation, as they promote higher extraction yield. Figure 4.3 shows the difference in formed complex for 12C4 as the temperature is increased from 20 to 50 °C.

Figure 4.3: Effect of temperature on 12C4 Complex Formation: The figure displays the variations in the formed complex as temperature increases, with the left, middle, and right vials representing 20 °C, 30 °C, and 50 °C, respectively. The amount of formed complex decreases with increasing temperature, meaning that lower temperatures are more favorable for this extraction process.

The intriguing question that arises is whether further lowering the temperature will lead to a continuous increase in the extraction yield or if it will eventually reach a plateau, similar to the observations made during the crown ether-to-electrolyte ratio investigations. This investigation is essential because a substantial increase in the extraction yield may result in a trade-off between achieving higher extraction yield and incurring higher energy consumption. When considering the option of lowering the extraction temperature, further than room temperature, to enhance the yield, it is crucial to acknowledge that such a reduction would necessitate increased energy input, often in the form of cooling systems or refrigeration. Consequently, this energy-intensive operation would likely escalate the overall costs associated with the extraction process.

In an effort to explore the potential advantages of lower temperatures (below 20 °C) on the extraction process, additional experiments are conducted. Their purpose is to visually confirm the possible influence of lower temperatures on the extraction yield. Several vials, previously utilized for experiments at room temperature, containing the electrolyte-crown ether mixture along with the formed crown ether-$LiPF_6$ complex, as depicted in Figure 4.3, are subjected to an ice-bath and then agitated. Visual inspections are carried out to observe if additional complex formation occurs. Given the greater reliability of the results with 12C4, it is chosen for these experiments. As can be seen in Figure 4.4 an increase in the formed complex can be observed, meaning that even lower temperatures is more favorable for the extraction process. Hence, further experimentation should be done to quantify the increase of extraction efficiency at these lower temperatures. Additionally, it will assess whether the gain in extraction efficiency justifies the additional energy costs associated with operating at lower temperatures.

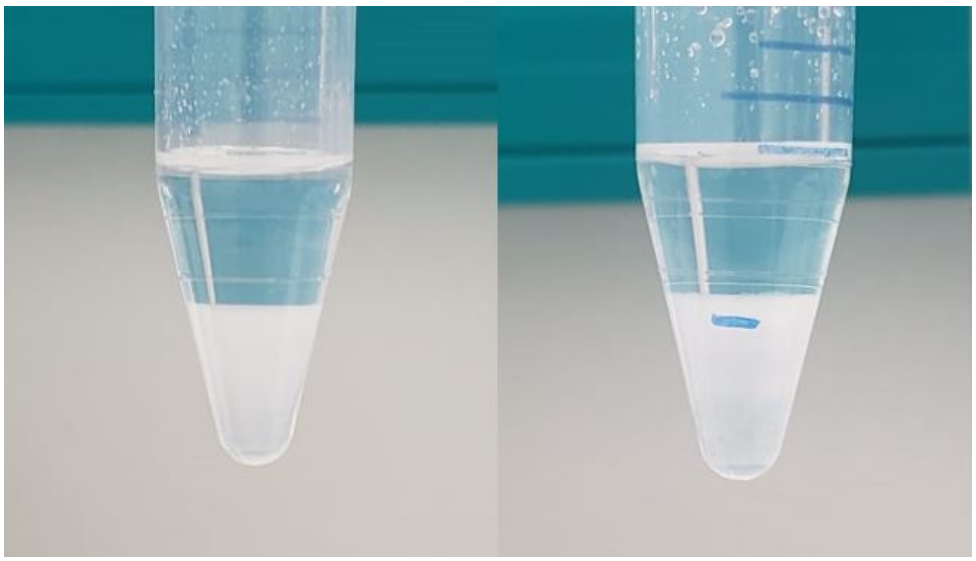

Figure 4.4: Difference in the amount of formed complex, before (left) and after (right) the experiment in ice bath, with a marked reference point for comparison. This figure shows that the amount of formed complex increases for even lower temperature (0 °C). Further analysis should be done to quantify the increase of extraction efficiency at these lower temperatures.

4.1.3. Effect of Time

This section presents and analyzes the outcomes of varying the extraction time on the extraction yield. The experimental results for different extraction times (5, 15, and 30 minutes) for 8:1 mole ratio are depicted in Figure 4.5, revealing that the extraction yield remains relatively unaffected within this range. This suggests that the complex formation kinetics occur rapidly. It should be noted that the extraction time specifically refers to the period during which the vials are agitated, while the settling time, fixed at 30 minutes for all experiments, is necessary for accurate sampling but not considered within the extraction time.

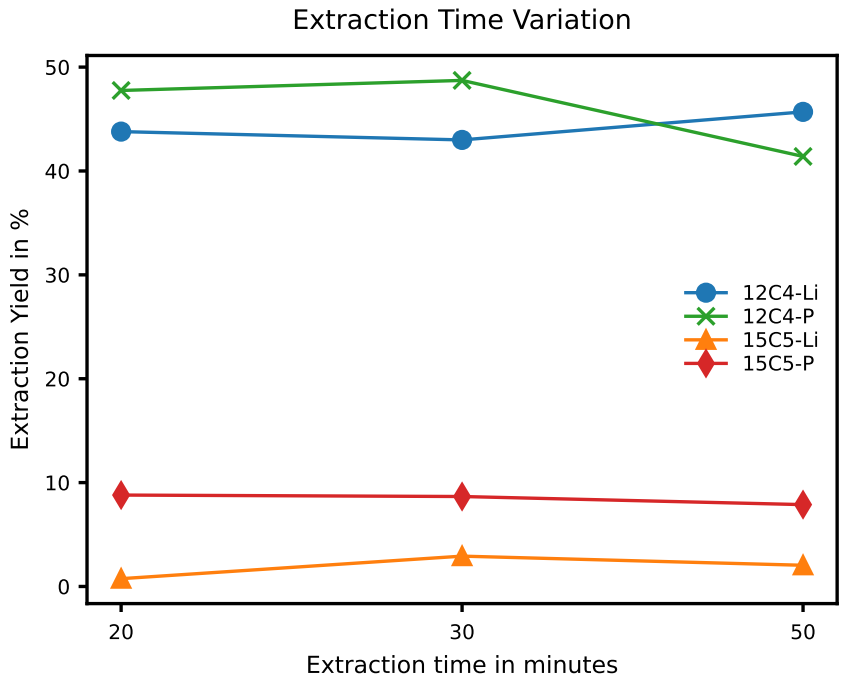

Figure 4.5: Effect of Extraction Time on Extraction Yield: The graph presents the experimental outcomes for different extraction times at a fixed mole ratio of 8:1 for both 12C4 and 15C5 crown ethers. The extraction yield remains relatively unaffected within this range (5 min to 30 min), meaning that the complex formation kinetics occur rapidly.

4.1.4. Extraction Yield based on Mass

Lithium Salt

In some of the experiments, an alternative approach is employed to calculate the extraction yield based on mass, which serves as an additional validation step to corroborate the results and gain more insight into the mass balance within the extraction process. This approach is applied to one set of 12C4 with mole ratios of 2:1, 4:1, 6:1, 8:1, and 20:1

Using the 2:1 mole ratio of 12C4 as a calculation example, the initial mass of Li and P is determined using equation 4.1. To obtain the final mass of Li and P that remained in the mixture after the extraction process, the mass of the remaining solution is carefully measured, following the specific procedures outlined in section 3.1.4. The recorded mass of the remaining mixture is 2.51 g. Subsequently, the final mass of Li and P in the remaining solution is computed by multiplying their respective concentrations obtained from ICP-OES (4.212 mg/g and 13.739 mg/g, respectively) with the mass of the remaining mixture, as shown in equation 4.5.

$$m_{f,\texttt{Li or P}} = m_{f,\mathrm{m}} \times C_{f,\texttt{Li or P}} \tag{4.5}$$

$$m_{f,\texttt{Li}} = 2.51\,\mathrm{g} \times 4.212\,\mathrm{mg/g} = 10.57\,\mathrm{mg}$$

$$m_{f,\texttt{P}} = 2.51\,\mathrm{g} \times 13.739\,\mathrm{mg/g} = 34.48\,\mathrm{mg}$$

Finally, the extraction yield, based on mass, is determined using equation 4.6.

$$\eta_{\texttt{c.e.}} = \frac{m_{i,\text{Li or P}} - m_{f,\text{Li or P}}}{m_{i,\text{Li or P}}} \times 100\% \tag{4.6}$$

$$\eta_{\texttt{12C4,Li}} = \frac{18\,\text{mg} - 10.57\,\text{mg}}{18\,\text{mg}} \times 100\% = 41.3\,\%$$

$$\eta_{\texttt{12C4,P}} = \frac{62.88\,\text{mg} - 34.48\,\text{mg}}{62.88\,\text{mg}} \times 100\% = 45.2\,\%$$

The extraction yield for each mole ratio is shown in Table 4.1. Figure 4.6 depicts the extraction yield based on concentration and mass, with only the data for lithium presented to avoid cluttering the figures. Remarkably, the extraction yield based on mass consistently shows higher values than the yield based solely on concentration. The reason behind this disparity lies in the fact that the extraction yield solely based on concentration neglects the variation in initial and final mass of the mixture. Hence, by accounting for the change in mass of the mixture, a more accurate determination of the extraction yield can be achieved.

Table 4.1: Calculated Extraction Yield Based on Mass: The table displays the 12C4 extraction yield results for each mole ratio (MR), determined through mass-based calculations. This table shows the final mass of the mixture ($m_{f,\texttt{m}}$), the initial ($m_{i,\texttt{P}}$) and final mass of Phosphorus in the mixture ($m_{f,\texttt{P}}$), the initial ($m_{i,\texttt{Li}}$) and final mass of lithium in the mixture ($m_{f,\texttt{Li}}$), and the extraction yield of Phosphorus ($\eta_{\texttt{12C4,P}}$) and Lithium ($\eta_{\texttt{12C4,Li}}$).

MR	$m_{f,\texttt{m}}$ (g)	$m_{i,\texttt{P}}$ (mg)	$m_{f,\texttt{P}}$ (mg)	$\eta_{\texttt{12C4,P}}$	$m_{i,\texttt{Li}}$ (mg)	$m_{f,\texttt{Li}}$ (mg)	$\eta_{\texttt{12C4,Li}}$
2:1	2.51	62.88	34.48	45.2%	18.00	10.57	41.3%
4:1	3.01	63.13	26.24	58.4%	18.07	8.00	55.8%
6:1	3.8	62.88	22.32	64.5%	18.00	7.05	60.9%
8:1	3.36	46.90	23.09	50.8%	13.43	7.27	45.9%
20:1	1.66	12.93	5.61	56.6%	3.70	1.33	64%

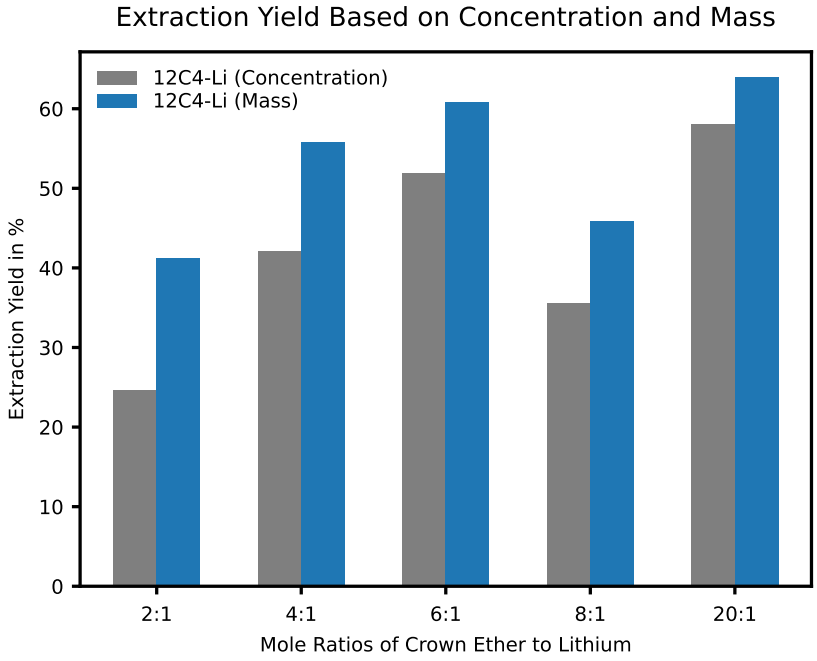

Figure 4.6: Comparison of Extraction Yield for 12C4: The figure illustrates the extraction yield results based on concentration (blue) and mass (orange) for different mole ratios of 12C4. The mass-based approach consistently yields higher values than the concentration-based approach, because it takes the difference between initial and final mixture's mass, caused by complex formation, into account.

Nevertheless, it is important to acknowledge that there is a portion of mass that could not be accurately accounted for when determining the final mass of the mixture. The suction power of the vacuum pump could lead to a small amount of fluid being unintentionally sucked into the vacuum pump instead of falling down into the flask. This is possible because the outlet of the Buchner funnel is at the same height as the inlet of the vacuum pump, as depicted in Figure 4.7. Hence, it is crucial to carefully assess the setup to prevent such occurrences and ensure the accuracy and reliability of the measurement process.

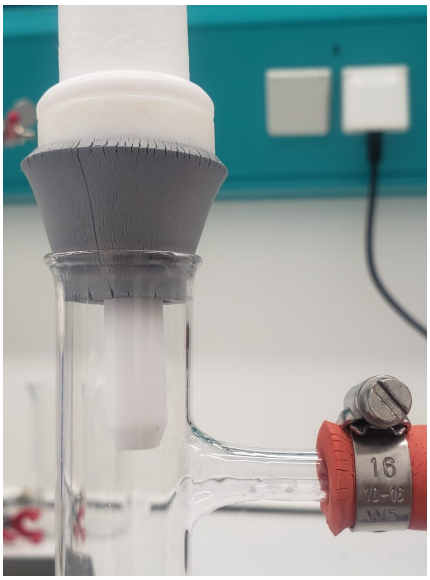

Figure 4.7: Fluid Loss in the Process: This figure demonstrates a critical aspect of the vacuum filtration setup, revealing the potential for fluid loss during the extraction process due to the positioning of the outlet of the Buchner funnel at the same level as the inlet of the vacuum pump.

Assuming that 100 % of this unaccounted mass should be considered part of the remaining mixture, the adjusted mass of the remaining mixture is calculated and the results are presented in Table 4.2.

Table 4.2: Adjusted Mass of final Mixture: This table presents the calculated adjusted mass of the final mixture, considering the unaccounted mass as an integral part of the mixture.

Mole Ratio	Final Mixture (g)	Unaccounted Mass (g)	Adjusted Final Mixture (g)
2:1	2.51	0.2	2.71
4:1	3.01	0.26	3.27
6:1	3.80	0.15	3.95
8:1	3.36	0.01	3.37
20:1	1.66	0.16	1.82

Consequently, based on the adjusted mass calculation, the revised extraction yield is calculated and is illustrated in Table 4.3. The observed results make it evident that incorporating the change in mass during the calculations results in a higher efficiency compared to solely relying on concentration-based calculations. This approach allows for a more precise determination of the extraction yield, enhancing the accuracy and reliability of the results obtained for the extraction process.

Table 4.3: Revised Extraction Yield Calculation: This table presents the 12C4 extraction yield for Phosphorus ($\eta_{\texttt{12C4,P}}$) and Lithium ($\eta_{\texttt{12C4,Li}}$), based on the adjusted mass calculation, offering a more precise assessment of the extraction process and its outcomes. This table shows the mole ratio (MR), the final mass of the mixture ($m_{f,\texttt{m}}$), the initial ($m_{i,\texttt{P}}$) and final mass of Phosphorus in the mixture ($m_{f,\texttt{P}}$), and the initial ($m_{i,\texttt{Li}}$) and final mass of lithium in the mixture ($m_{f,\texttt{Li}}$).

MR	$m_{f,\texttt{m}}$ (g)	$m_{i,\texttt{P}}$ (mg)	$m_{f,\texttt{P}}$ (mg)	$\eta_{\texttt{12C4,P}}$	$m_{i,\texttt{Li}}$ (mg)	$m_{f,\texttt{Li}}$ (mg)	$\eta_{\texttt{12C4,Li}}$
2:1	2.71	62.88	37.23	40.8%	18.00	11.41	36.6%
4:1	3.27	63.13	28.50	54.8%	18.07	8.69	51.9%
6:1	3.95	62.88	23.20	63.1%	18.00	7.32	59.3%
8:1	3.37	46.90	23.16	50.6%	13.43	7.29	45.7%
20:1	1.82	12.93	6.15	52.5%	3.70	1.46	60.5%

Crown Ethers

In order to gain deeper insights into the extraction process, the effective utilization of crown ether is also assessed. It considers the actual mass of crown ether that is actively involved in the extraction process and compares it to the total initial mass of crown ether added. This analysis is performed for one set of 12C4 (with mole ratios of 2:1, 4:1, 6:1, 8:1, and 20:1) and one set of 15C5 (with mole ratios of 6:1, 8:1, 10:1, 12:1, and 20:1). Through Gas Chromatography (GC), the concentration of crown ether in the final mixture is determined (0.189 g/g) for the 2:1 mole ratio of 12C4. The mass of crown ether in the final mixture ($m_{f,\texttt{c.e.}}$) is obtained using equation 4.7, where $m_{af,\text{m}}$ is the adjusted mass of the final mixture.

$$m_{f,\texttt{c.e.}} = m_{af,\text{m}} \times C_{f,\texttt{c.e.}} \tag{4.7}$$

$$m_{f,\texttt{12C4}} = 2.71\,\text{g} \times 0.189\,\text{g/g} = 0.5122\,\text{g}$$

The effective crown ether utilization (ECU) is calculated using equation 4.8, where $m_{i,\texttt{c.e.}}$ denotes the initial mass of crown ether which is 0.74 g in this case.

$$ECU = \frac{m_{i,\texttt{c.e.}} - m_{f,\texttt{c.e.}}}{m_{i,\texttt{c.e.}}} \times 100\% \tag{4.8}$$

$$ECU = \frac{0.74\,\text{g} - 0.5122\,\text{g}}{0.74\,\text{g}} \times 100\% = 30.8\,\%$$

This is done for every case and the results for 12C4 and 15C5 are shown in Table 4.4 and 4.5, respectively, along with the lithium extraction yield (η_{Li}) for each case.

Table 4.4: Crown Ether Utilization: This table shows the effective crown ether utilization (ECU), and lithium extraction yield (η_{Li}) for different mole ratios of 12C4 (MR), along with the adjusted mass of the final mixture ($m_{af,\text{m}}$), and initial ($m_{i,\texttt{c.e.}}$) and final mass of 12C4 ($m_{f,\texttt{c.e.}}$) in the mixture.

MR	$m_{af,\text{m}}$ (g)	$m_{i,\texttt{c.e.}}$ (g)	$m_{f,\texttt{c.e.}}$ (g)	ECU	η_{Li}
2:1	2.71	0.74	0.51	30.8%	36.6%
4:1	3.27	1.45	1.05	27.8%	51.9%
6:1	3.95	2.19	1.91	12.7%	59.3%
8:1	3.37	2.15	1.35	37%	45.7%
20:1	1.82	1.42	1.27	10.7%	60.5%

Table 4.5: Crown Ether Utilization: This table shows the effective crown ether utilization (ECU), and lithium extraction yield (η_{Li}) for different mole ratios of 15C5 (MR), along with the adjusted mass of the final mixture ($m_{af,\mathrm{m}}$), and initial ($m_{i,\mathtt{c.e.}}$) and final mass of 15C5 ($m_{f,\mathtt{c.e.}}$) in the mixture.

MR	$m_{af,\mathrm{m}}$ (g)	$m_{i,\mathtt{c.e.}}$ (g)	$m_{f,\mathtt{c.e.}}$ (g)	ECU	η_{Li}
6:1	2.4	1.35	1.31	3.1%	7.2%
8:1	2.77	1.74	1.68	3.7%	8.9%
10:1	3.13	2.17	2.04	6.1%	13.9%
12:1	2.85	2.10	1.97	6.2%	21.1%
20:1	2.05	1.72	1.62	5.8%	8%

The results reveal that, even at the lowest mole ratios for 12C4, a maximum of 31 % of the crown ether binds to the lithium salt and forms a complex, leaving 69 % of the added crown ether unused. This indicates that a significant portion of the crown ether remains in the mixture and unused for this particular set of experiments. For 15C5, the results are even less favorable, with only 3.1 % of the crown ether binding to the lithium to form a complex. This further supports the assertion that 12C4 is a superior choice compared to 15C5. The need for a substantial amount of 15C5, while only a small fraction of the added crown ether forms the desired complex with lithium, highlights the ineffectiveness of this particular crown ether. These results are based on limited data, and more comprehensive experiments are needed to verify the reliability of these findings. Further investigations will provide a deeper understanding of the extraction process and enable more accurate assessments of the crown ether effectiveness.

4.1.5. Complex

SEM and EDX

To investigate the structural characteristics of the formed complex, scanning electron microscopy (SEM) is employed. The SEM images for the 12C4-$LiPF_6$ and 15C5-$LiPF_6$ complexes are depicted in Figure 4.8a and Figure 4.8b, respectively. Notably, the crystals of both complexes exhibit a rectangular shape. Further analysis shows that there is a size difference between the crystals of these two compounds. The average width of the crystals of the 12C4-$LiPF_6$ complex (5 µm) are smaller when compared to the crystals of the 15C5-$LiPF_6$ complex (10 µm). While the presence of lithium cannot be discerned through EDX analysis, the supplementary data presented in Appendix C demonstrates that the examined complex contains carbon and oxygen from the crown ether, along with phosphorus and fluorine elements originating from $LiPF_6$.

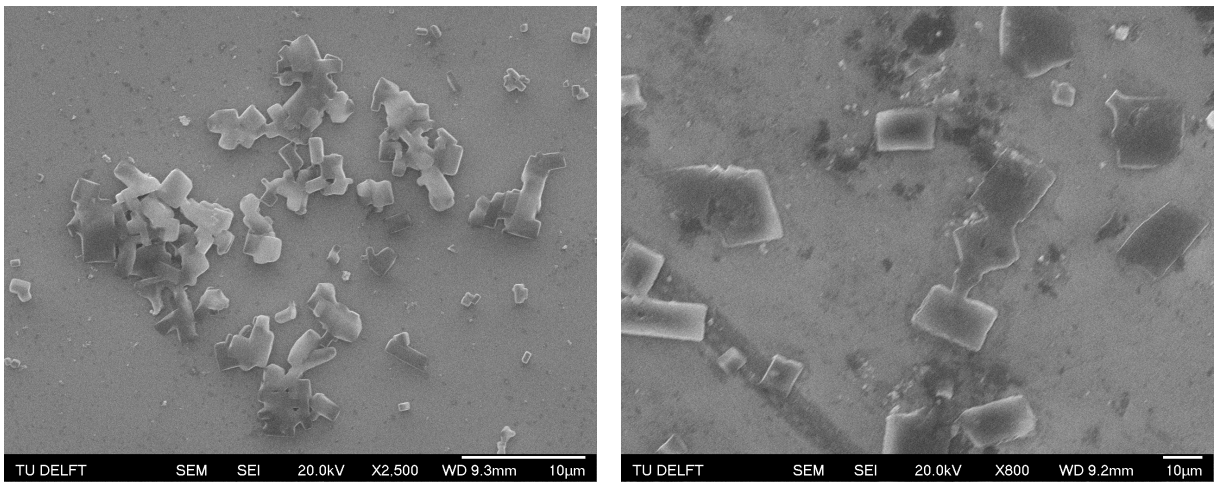

(a) SEM image for the 12C4-$LiPF_6$ complex.

(b) SEM image for the 15C5-$LiPF_6$ complex.

Figure 4.8: SEM images for 12C4 and 15C5 complexes. The images show that the complexes have a rectangular crystal structure and that the crystals of the 12C4 complex are smaller compared to those of the 15C5 complex.

XPS

Given the limitations of EDX in detecting lithium, a thorough XPS analysis of the complexes is conducted to validate and confirm their elemental composition. The XPS data set initially comprises a survey spectrum, which is an initial, standard-resolution, broad scan of the entire energy range of emitted photoelectrons. The survey scan provides an overview of the elemental composition present on the surface of two samples of interest, namely 12C4-$LiPF_6$ complex and 15C5-$LiPF_6$ complex. As can be seen in Figure 4.9, the survey scan detects peaks corresponding to different elements present in the samples, which in this case are fluorine, oxygen, carbon, phosphorus and lithium. Note that the peak intensities in the two complexes cannot be directly compared due to variations in the mass of the samples loaded into the XPS. Specifically, a greater amount of 12C4-$LiPF_6$ complex is used for the analysis, resulting in higher peak intensities for the 12C4-$LiPF_6$ complex. While the survey scan offers valuable information about the overall elemental composition, it does not provide detailed information about the chemical states of the elements. Therefore, high-resolution scans and curve fitting techniques are employed on the specific peaks of interest, to analyse their chemical states (Appendix D).

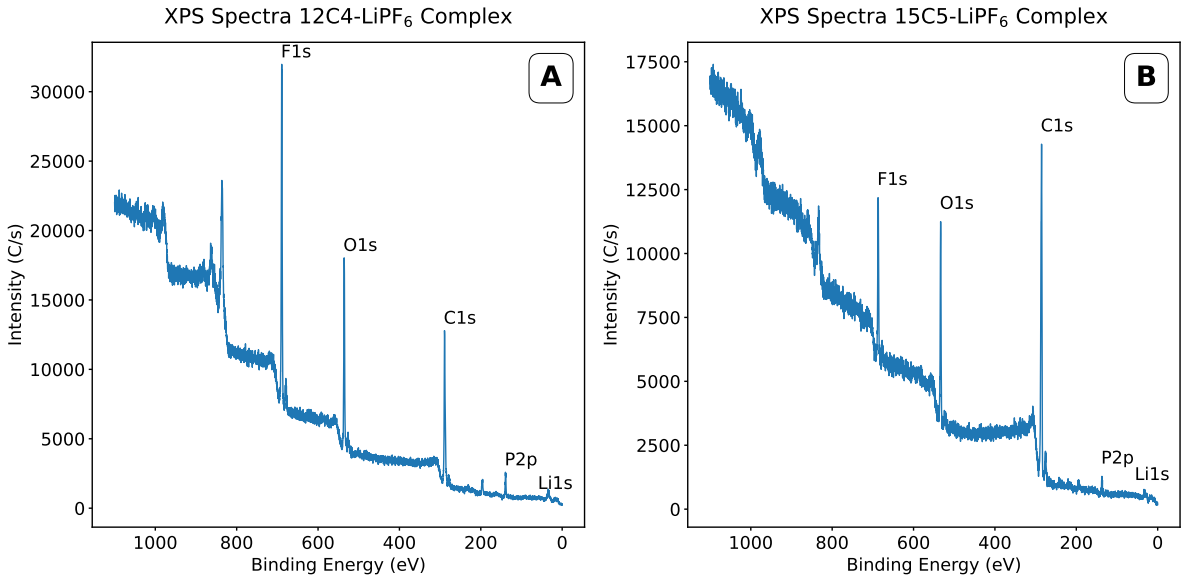

Figure 4.9: Survey spectrum of (A) 12C4-$LiPF_6$ complex and (B) 15C5-$LiPF_6$ complex with detected peaks for Fluorine (F1s), Oxygen (O1s), Carbon (C1s), Phosphorus (P2p) and Lithium (Li1s).

The atomic concentrations of the different elements are presented in Table 4.6. While XPS is highly effective at identifying elements and their chemical context, it has limitations when it comes to accurately determining absolute elemental concentrations. Hence, the presented values serve as approximations.

Table 4.6: Atomic concentration (in percentage) of the elements present in the 12C4-$LiPF_6$ and 15C5-$LiPF_6$ complexes. The substantially higher carbon concentration can be primarily attributed to the sensitivity of XPS to minute traces of carbon contaminants present in the analysis environment.

Complex:	12C4-$LiPF_6$	15C5-$LiPF_6$
Carbon	39.7 %	70.6 %
Oxygen	21.5 %	12.1 %
Lithium	9.5 %	7.4 %
Fluorine	25.1 %	7.3 %
Phosphorus	4.3 %	2.7 %

An initial observation of the data highlights a remarkable contrast in carbon concentration compared to the levels of other elements. XPS exhibits a heightened sensitivity to ambient carbon. As a consequence, the substantially higher carbon concentration can be primarily attributed to the inherent sensitivity of XPS to minute traces of carbon contaminants present in the analysis environment. This is confirmed with high resolution scans of the carbon peak presented in Figure D.1 in Appendix D. Observing the contrast in the concentrations of lithium and phosphorus, it can be inferred that the lithium salt underwent decomposition into throughout the extraction process. Extraction of intact $LiPF_6$ would have resulted in more comparable phosphorus and lithium levels. The presence of lithium metal in the complex, which is confirmed with high resolution scan of the lithium peak, can also be a reason for this difference. This high-resolution scan is provided in Figure D.3 in Appendix D.

The arrangement of the donor atoms in the crown ether, the size of the cavity and the stoichiometry of the crown ether to metal ion can affect the interaction's strength and, consequently, the stability of the complex [48]. This interplay is illustrated in Figure 4.10. As outlined in Table 4.6, the relative proportion of oxygen to lithium does not indicate a substantial likelihood of a sandwich-type complex formation in either of these compounds. This suggests that both complexes are more likely to assume a single complex structure. The experimental findings emphasize that modifying the cavity size to more precisely accommodate the lithium ion exerts a more pronounced impact than increasing the donor atom count. Therefore, despite 12C4 having fewer donor atoms in comparison to 15C5, its compact cavity dimensions allow for a stronger interaction with lithium, enhancing its stability and making it a more suitable candidate for the extraction process.

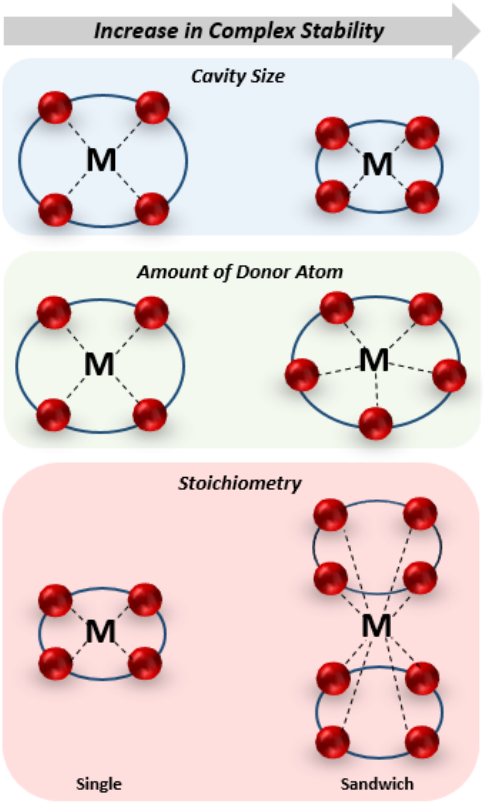

Figure 4.10: Crown ether-metal ion complexes. Factors such as Cavity size, amount of donor atom and the stoichiometry are factors that affects the stability of the complex. "M" stands metal-ion, the red dot represents oxygen and the interaction between crown ether and metal ion is denoted by the dashed lines.

Crown Ether Recovery

In order to complete the recycling process, it is important to find a way to separate the lithium from the crown ether. Conventionally, this process involves the use of acids, which unfortunately compromise the integrity of the crown ether, rendering it non-recoverable. Hence, an innovative alternative must be explored to achieve lithium extraction without compromising the integrity of the crown ether. One potential alternative that needs investigation involves the use of CO_2 as an extraction medium. At low pressures, there will be a gaseous CO_2 phase and a solid phase containing the crown ether and the lithium salt. When the pressure is increased beyond the critical point of CO_2 (>74 bar and 31 °C), a top liquid phase will emerge. Under these conditions, the complex is expected to dissolve in the CO_2 to facilitate extraction. According to literature [15, 27], super critical CO_2 can extract the electrolyte solvent leaving the lithium behind. By applying a similar concept, it can be investigated whether CO_2 can selectively extract the crown ether while leaving the lithium salt behind. Subsequent reduction in pressure enables the separation of the extracted crown ether from CO_2, allowing for its reuse in subsequent extraction processes. This can be investigated, in a future study, using the high pressure setup described in Section 3.2.2.

4.2. Modeling Results

This section presents the findings obtained from the modeling exercise. The main objective of these simulations is to determine the suitable operating conditions, such as temperature and pressure, for conducting the extraction of the organic solvent in the electrolyte solution using sub or supercritical CO_2. To achieve this, the phase equilibrium between CO_2 and the solvent components is investigated. The phase equilibrium $P-xy$ diagrams for the CO_2 and DEC, and CO_2 and DMC mixtures are determined at various temperatures. The diagrams are visually presented in figures 4.11, and 4.12 respectively, showcasing the relationship between pressure (P) and mole fraction of CO_2 in the liquid- and vapor phase for each respective mixture. Appendix A shows the P-xy diagrams along with the experimental data.

To achieve successful solvent component extraction, it is crucial to transfer them to the vapor phase. Analyzing the Pxy-diagram of CO_2 and DMC reveals that the vapor phase predominantly consists of CO_2 (with a mole fraction above 0.9), while DMC's presence remains limited (max 0.1 mole fraction). The vapor composition is predominantly influenced by temperature, with higher temperatures leading to decreased mole fraction of CO_2 in the vapor phase, thereby favoring the extraction of DMC. On the other hand, pressure has a relatively minor impact on vapor composition, as indicated by the steep vapor line. Therefore, adopting higher temperatures proves more favorable for the extraction process, with the only limitation being $LiPF_6$ decomposition, which occurs around 333 K (60 °C). In the case of CO_2 and DEC, temperature has a lesser impact on vapor composition, remaining relatively consistent regardless of temperature. However, at higher pressures (above 80 bar), a slight decrease in CO_2 mole fraction in the vapor phase is observed for temperature above 320 K (47 °C), indicating better extraction at elevated pressures.

Based on the Pxy-Diagram of the CO_2 and DMC, and CO_2 and DEC mixtures, a range for the operating conditions in the extraction process can be suggested. It is important to note that although the CO_2 and EC mixture is not modeled, due to limited experimental data, the insights from the other two mixtures can still guide the recommended conditions. Considering these insights, the recommended operating conditions for the extraction process involve a pressure range of 80 to 100 bar and a maximum temperature up to 323 K (50 °C). These conditions serve as a solid starting point for conducting the experiments and provide a foundation for further optimization. As the experiments progress and more data is gathered, adjustments and refinements to these parameters can be made to enhance the overall efficiency and effectiveness of the extraction process.

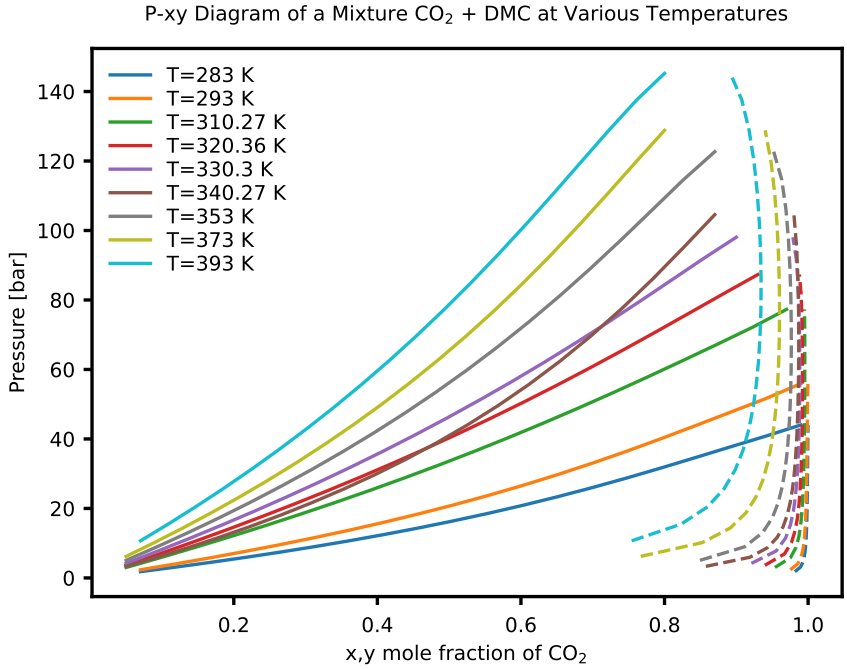

Figure 4.11: $P - xy$ diagram for the binary mixture of CO_2 and DMC. In this diagram, the y-axis represents pressure (P), the x-axis represents the mole fraction of CO_2 (x,y), the solid line represents the composition of the liquid phase, and the dotted line represents the composition of the vapor phase. The vapor composition is predominantly influenced by temperature, with higher temperatures leading to decreased mole fraction of CO_2 in the vapor phase, thereby favoring the extraction of DMC.

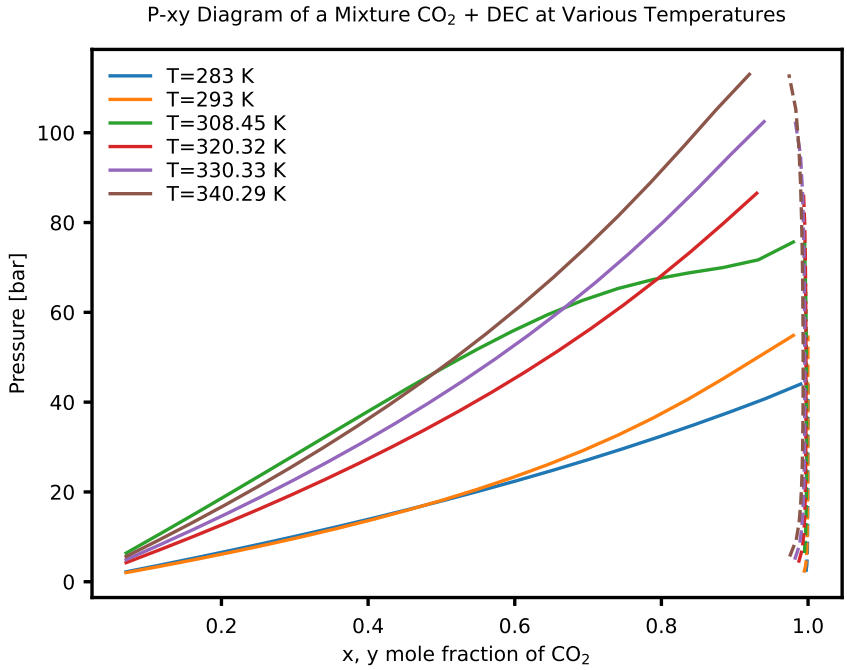

Figure 4.12: $P - xy$ diagram for the binary mixture of CO_2 and DEC. In this diagram, the y-axis represents pressure (P), the x-axis represents the mole fraction of CO_2 (x,y), the solid line represents the composition of the liquid phase, and the dotted line represents the composition of the vapor phase. The influence of temperature on the vapor composition vapor composition is negligible. However, at higher pressures, a slight decrease in CO_2 mole fraction in the vapor phase is observed for temperature above 320 K (47 °C), indicating better extraction at elevated pressures.

5

Conclusion and Recommendations

This chapter provides the conclusive outcomes of this study by addressing the research questions. The findings are discussed, and prospects for further investigations are suggested.

5.1. Conclusion

Limited amount of research is focused on recycling the electrolyte, particularly the lithium salt. In traditional recycling processes, the common approach for handling the aged organic electrolyte involves removing the aged electrolytes through calcination or evaporation during pretreatment steps of the recycling process. The lithium salts are left in the active materials and are recovered along with other metal components using a hydrometallurgical method. This method typically reclaims lithium in the final phase, resulting in a low lithium recovery efficiency, due to its low concentration in the leaching solution.

Due to their high selectivity in metal ion extraction, crown ethers are among the preferred choices for lithium ion extraction. This study delves into the extraction and recycling of lithium salt ($LiPF_6$) from spent LIB electrolytes, employing 12C4 and 15C5 as the crown ethers of interest. While both crown ethers achieve comparable maximum extraction yields, a pivotal distinction emerges in the required mole ratio for reaching these yields. Notably, 12C4 accomplishes this feat at a modest 6:1 mole ratio, whereas 15C5 demands a significantly higher 20:1 mole ratio. The experimental outcomes for 15C5 exhibit a higher degree of uncertainty, thereby complicating precise extraction yield determination and hinting at potential instability within the 15C5-$LiPF_6$ complex. Despite 12C4 having fewer donor atoms in comparison to 15C5, its compact cavity dimensions allow for a stronger interaction with lithium, enhancing its stability and making it a more suitable candidate for the extraction process.

Regarding the quantification of extraction yield, there are two calculation methods: concentration-based and mass-based. Interestingly, the mass-based approach consistently yields higher values than its concentration-based counterpart. This discrepancy stems from the concentration-based method's inability to account for variations between initial and final mixture mass caused by complex formation and precipitation. Ultimately, this study highlights the efficacy of crown ethers, with 12C4 achieving 60 % maximum mass-based extraction yield at a 6:1 mole ratio, emphasizing their potential in lithium extraction from LIB electrolytes. However, even at the lowest mole ratios tested for 12C4, a maximum of 31 % of the crown ether forms a complex with the lithium salt, leaving a substantial 69 % of the initially added crown ether unused.

Concerning the extraction parameters, it is apparent that a decrease in the mole ratio corresponds to a decrease in the extraction yield, while an increase in the mole ratio results in a higher extraction efficiency. Notably, the extraction yield appears to reach a plateau at approximately a mole ratio of 6:1 for 12C4 and 12:1 for 15C5. Both 12C4 and 15C5 exhibit extraction yields

that are notably influenced by temperature variations. As temperatures rise, there is a decrease in extraction yield, indicating the exothermic nature of the complex formation process. This indicates the preference for lower temperatures in promoting complex formation. Examining the impact of different extraction durations (5 min to 30 min), it becomes evident that the extraction yield remains relatively stable within this range. Meaning that the complex formation kinetics occur rapidly.

SEM analysis reveals that the crystals of both complexes exhibit a rectangular morphology, with a noticeable disparity in size between the crystals of these two compounds. The average width of the crystals in the 12C4-$LiPF_6$ complex (5 µm) is comparatively smaller than those within the 15C5-$LiPF_6$ complex (10 µm). Verification by XPS confirms the presence of fluorine, oxygen, carbon, phosphorus, and lithium within the complex. Notably, the difference between lithium and phosphorus concentrations within the complex alludes to a plausible occurrence of $LiPF_6$ degradation during the extraction process. Moreover, XPS analysis indicates that both complexes are more inclined to adopt a singular complex structure as opposed to a sandwich-type configuration.

The simulations performed to establish optimal extraction conditions for the organic solvent in the electrolyte solution using CO_2 indicate that the recommended operating parameters for the extraction process involves maintaining pressures within the range of 80 bar to 100 bar, along with a maximum temperature of 50 °C. These conditions serve as a solid starting point for conducting the experiments and provide a foundation for further optimization.

5.2. Recommendations

$LiPF_6$ is prone to hydrolysis upon contact with moisture or water, leading to the degradation of $LiPF_6$ and potential adverse impacts on the environment and health of individuals. Although not a focus of this study, this aspect warrants considerable attention when developing a new process for recycling LIB electrolytes. Thus, more comprehensive research is needed to understand the conditions and strategies to mitigate $LiPF_6$ degradation effectively.

To optimize the recycling of LIBs, exploring whether the same extraction method investigated in this study can be extended to recycle the cathode material is a valuable avenue for future investigation. Successful implementation could lead to improvements in the current hydrometallurgical recycling process, reducing the reliance on acidic leaching procedures.

Preliminary findings indicate the possibility of extracting more $LiPF_6$ by lowering the temperature below room temperature. However, quantifying this potential increase requires further analysis. Therefore, a thorough investigation is recommended to determine the practical significance of this extraction yield enhancement.

During the separation of the mixture from the complex, a design flaw in the equipment led to unintended mass loss. Should the same equipment be used in future research, careful attention should be given to the vacuum pump's suction power to prevent inadvertent suction of the mixture into the pump rather than its proper collection in the flask. Alternatively, exploring alternative equipment could circumvent this issue.

To fully realize a holistic recycling process, devising a method to separate lithium from the crown ether while preserving the crown ether's structural integrity is a crucial task. This necessitates further exploration of innovative separation techniques to enable crown ether reuse in subsequent extraction processes. A promising avenue for investigation is the potential use of CO_2 for this separation process.

A

Phase Equilibrium Experimental Data

A.1. Carbon Dioxide and DMC

This section presents the phase equilibrium experimental data of CO_2 + Dimethyl Carbonate (DMC) mixture. The experimental data was retrieved from [46].

Table A.1: Phase equilibrium of CO_2 and DMC at a temperature of (a) 283 K and (b) 293 K.

(a)

Pressure [MPa]	xCO_2	yCO_2
0.66	0.2765	0.9898
1.38	0.4429	0.991
2.03	0.5573	0.9902
2.64	0.6791	0.9899
3.17	0.7974	0.9854

(b)

Pressure [MPa]	xCO_2	yCO_2
0.73	0.2401	0.9965
1.52	0.3921	0.9942
2.21	0.4865	0.9922
3.16	0.6275	0.9767
4.19	0.8035	0.9658

Table A.2: Phase equilibrium of CO_2 and DMC at a temperature of (a) 310.27 K and (b) 320.36 K.

(a)

Pressure [MPa]	xCO_2	yCO_2
0.863	0.1431	0.9525
1.897	0.3019	0.9818
2.556	0.3919	0.9885
3.19	0.4809	0.9879
3.718	0.5473	0.9907
4.38	0.6273	0.9917
5.547	0.7648	0.993
6.714	0.8867	0.9931
7.246	0.929	0.9934

(b)

Pressure [MPa]	xCO_2	yCO_2
0.827	0.114	0.9388
1.664	0.225	0.9699
2.553	0.3356	0.9778
3.219	0.4144	0.985
4.25	0.5269	0.9881
5.757	0.682	0.9885
7.084	0.8162	0.9888
7.697	0.8597	0.9879
8.14	0.895	0.9866

Table A.3: Phase equilibrium of CO_2 and DMC at a temperature of (a) 330.3 K and (b) 340.27 K.

(a)

Pressure [MPa]	xCO_2	yCO_2
1.237	0.1477	0.9587
2.509	0.2914	0.9755
3.438	0.3876	0.9812
4.299	0.4707	0.9828
5.218	0.5565	0.9842
6.136	0.6397	0.9844
7.403	0.749	0.9829
8.53	0.8307	0.9813
9.256	0.8954	0.9741

(b)

Pressure [MPa]	xCO_2	yCO_2
1.019	0.1076	0.9276
2.403	0.245	0.9645
3.684	0.3616	0.9741
4.866	0.4667	0.9773
5.852	0.5445	0.9786
7.082	0.6412	0.9787
8.269	0.7353	0.9776
9.413	0.8141	0.9727
9.996	0.8569	0.963

Table A.4: Phase equilibrium of CO_2 and DMC at a temperature of (a) 353 K and (b) 373 K.

(a)

Pressure [MPa]	xCO_2	yCO_2
3.98	0.381	0.9831
5.12	0.4656	0.9811
6.52	0.5549	0.9797
8.45	0.6563	0.9748
10.51	0.7577	0.9481
11.87	0.8332	0.9059

(b)

Pressure [MPa]	xCO_2	yCO_2
4.46	0.389	0.9782
5.48	0.4598	0.976
6.62	0.5226	0.9762
7.67	0.5763	0.9688
8.84	0.6195	0.9651
9.94	0.6538	0.96
11.13	0.6929	0.9504

Table A.5: Phase equilibrium of CO_2 and DMC at 393 K.

Pressure [MPa]	xCO_2	yCO_2
5.57	0.4143	0.9559
6.57	0.4699	0.96
8.07	0.5245	0.9526
9.56	0.5787	0.9491
11.06	0.6287	0.9294
12.57	0.6878	0.9137
13.75	0.7459	0.8935

A.2. Peng Robinson and Exp. Data - DMC

The graphs in this section shows the P-xy diagram of CO_2 and DMC, modelled with the Peng-Robinson (PR) equation of state, at various temperatures, along with the experimental data provided in section A.1.

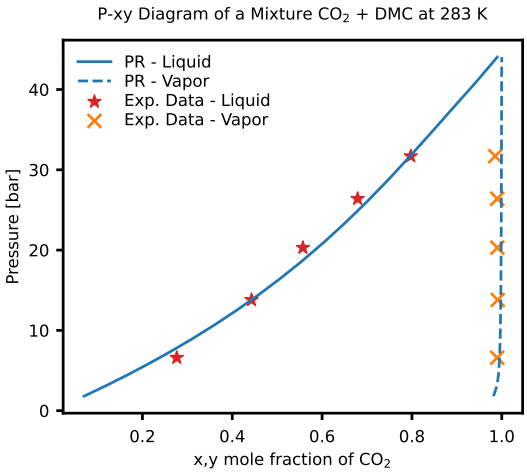

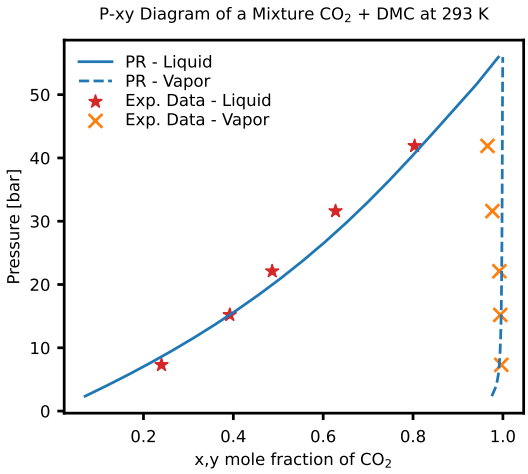

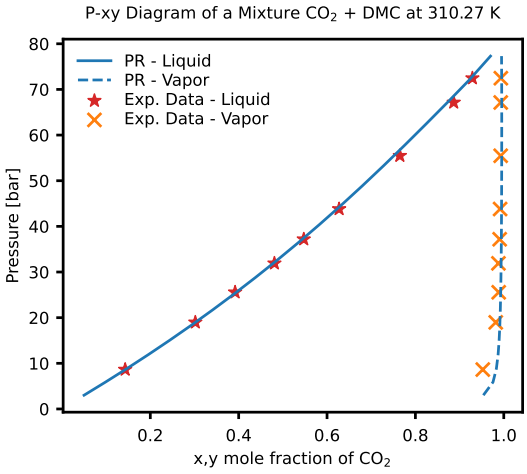

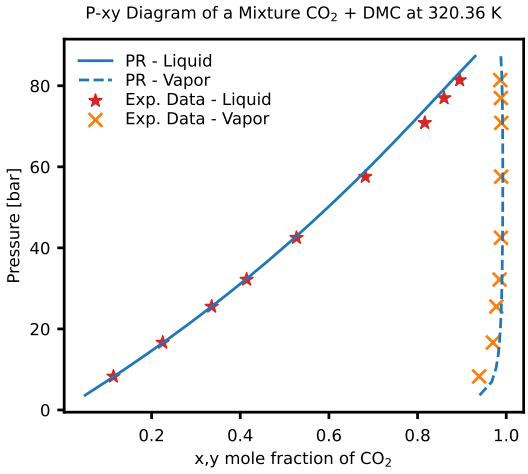

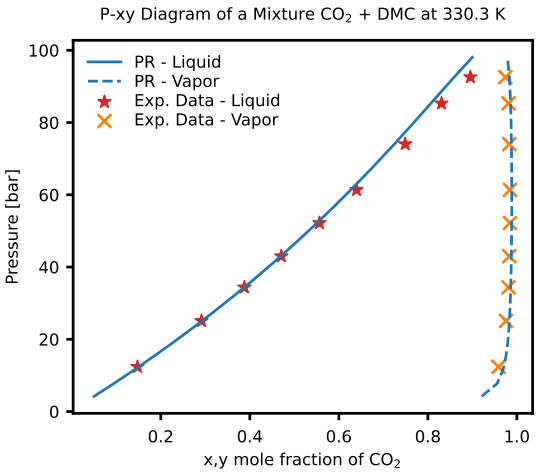
P-xy Diagram of a Mixture CO_2 + DMC at 330.3 K
PR - Liquid
PR - Vapor
Exp. Data - Liquid
Exp. Data - Vapor
Pressure [bar]
x,y mole fraction of CO_2

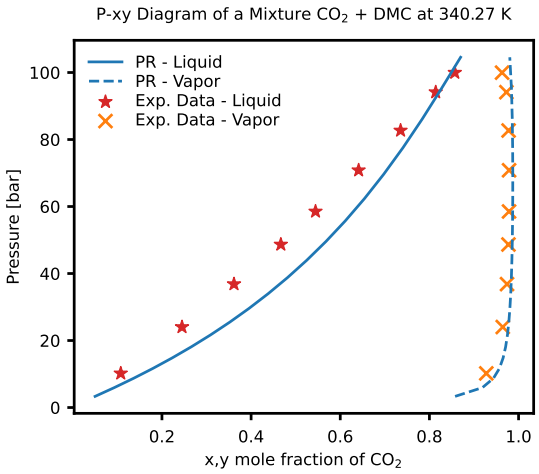
P-xy Diagram of a Mixture CO_2 + DMC at 340.27 K
PR - Liquid
PR - Vapor
Exp. Data - Liquid
Exp. Data - Vapor
Pressure [bar]
x,y mole fraction of CO_2

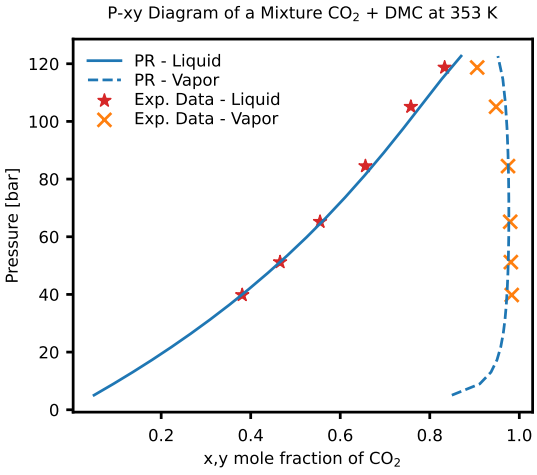
P-xy Diagram of a Mixture CO_2 + DMC at 353 K
PR - Liquid
PR - Vapor
Exp. Data - Liquid
Exp. Data - Vapor
Pressure [bar]
x,y mole fraction of CO_2

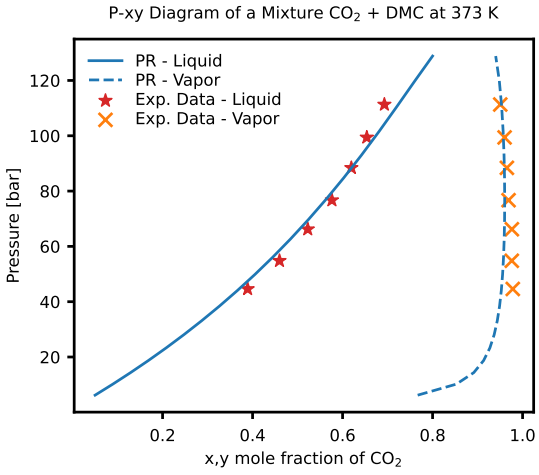
P-xy Diagram of a Mixture CO_2 + DMC at 373 K
PR - Liquid
PR - Vapor
Exp. Data - Liquid
Exp. Data - Vapor
Pressure [bar]
x,y mole fraction of CO_2

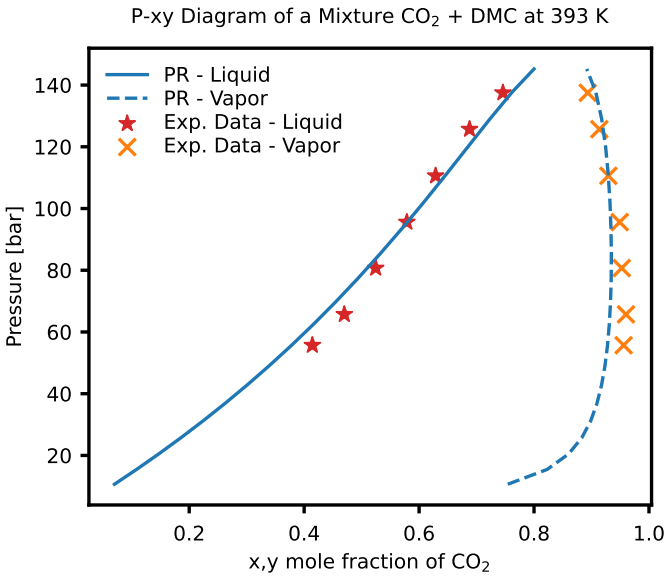
P-xy Diagram of a Mixture CO_2 + DMC at 393 K
PR - Liquid
PR - Vapor
Exp. Data - Liquid
Exp. Data - Vapor
Pressure [bar]
x,y mole fraction of CO_2

A.3. Carbon Dioxide and DEC

Table A.6: Phase equilibrium of CO_2 and DEC at a temperature of (a) 283 K and (b) 293 K.

(a)

Pressure [MPa]	xCO_2	yCO_2
0.58	0.2341	0.9786
1.2	0.3618	0.9778
1.8	0.5006	0.9767
2.37	0.6252	0.9745
3.05	0.723	0.9613

(b)

Pressure [MPa]	xCO_2	yCO_2
0.83	0.2665	0.9942
1.26	0.3759	0.9888
2.24	0.5636	0.988
3.13	0.7047	0.9888
3.87	0.8237	0.98

Table A.7: Phase equilibrium of CO_2 and DEC at a temperature of (a) 308.45 K and (b) 320.32 K.

(a)

Pressure [MPa]	xCO_2	yCO_2
4.72	0.5	0.9947
5.06	0.53	0.9948
5.5	0.585	0.995
5.8	0.625	0.9955
6.07	0.682	0.9958
6.5	0.73	0.9968
6.75	0.8	0.9973
6.94	0.84	0.9968
7.14	0.892	0.9961

(b)

Pressure [MPa]	xCO_2	yCO_2
0.715	0.1194	0.9743
1.902	0.2961	0.9894
2.66	0.3903	0.9923
3.351	0.4706	0.9941
4.441	0.5835	0.9949
6.079	0.737	0.9953
7.365	0.846	0.9945
8.411	0.9426	0.9906

Table A.8: Phase equilibrium of CO_2 and DEC at a temperature of (a) 330.33 K and (b) 340.29 K.

(a)

Pressure [MPa]	xCO_2	yCO_2
0.746	0.1095	0.9689
1.715	0.2367	0.9854
2.434	0.3204	0.9906
3.458	0.4301	0.9922
4.61	0.5374	0.993
6.069	0.6554	0.9936
7.175	0.7438	0.9932
8.33	0.8227	0.9916

(b)

Pressure [MPa]	xCO_2	yCO_2
1.183	0.149	0.9762
2.147	0.2566	0.9848
3.228	0.3625	0.9885
4.058	0.4357	0.99
5.557	0.5587	0.991
6.747	0.6439	0.991
7.761	0.7138	0.9903
9.008	0.796	0.9878

A.4. Peng Robinson and Exp. Data - DEC

The graphs in this section shows the P-xy diagram of CO_2 and DEC, modelled with the Peng-Robinson (PR) equation of state, at various temperatures, along with the experimental data provided in section A.3

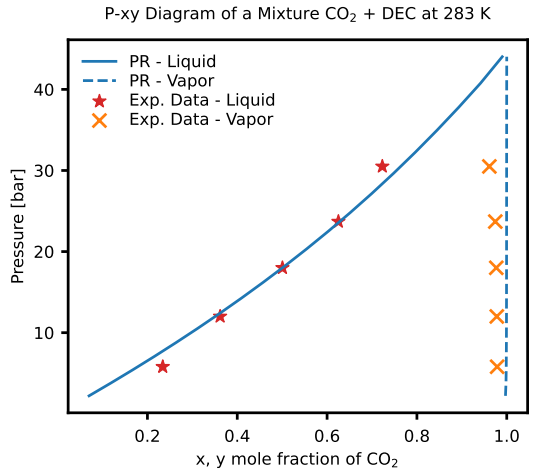
P-xy Diagram of a Mixture CO_2 + DEC at 283 K
PR - Liquid
PR - Vapor
Exp. Data - Liquid
Exp. Data - Vapor
Pressure [bar]
x, y mole fraction of CO_2

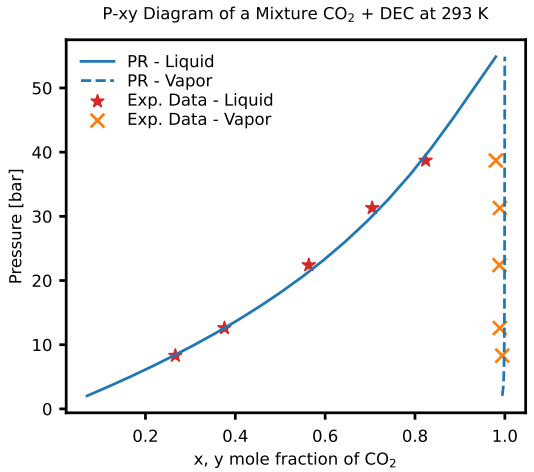
P-xy Diagram of a Mixture CO_2 + DEC at 293 K
PR - Liquid
PR - Vapor
Exp. Data - Liquid
Exp. Data - Vapor
Pressure [bar]
x, y mole fraction of CO_2

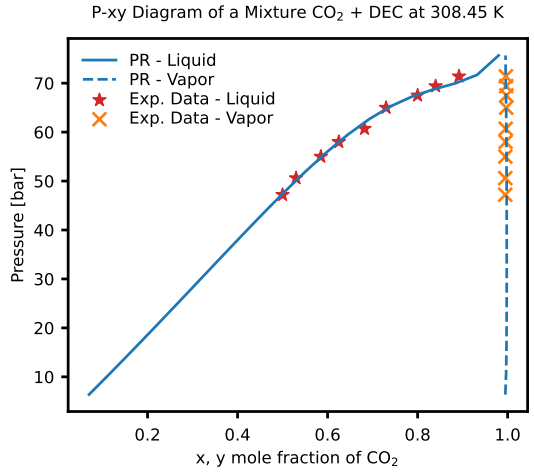
P-xy Diagram of a Mixture CO_2 + DEC at 308.45 K
PR - Liquid
PR - Vapor
Exp. Data - Liquid
Exp. Data - Vapor
Pressure [bar]
x, y mole fraction of CO_2

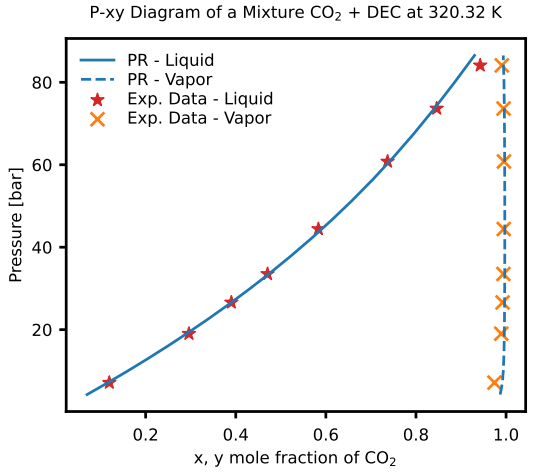
P-xy Diagram of a Mixture CO_2 + DEC at 320.32 K
PR - Liquid
PR - Vapor
Exp. Data - Liquid
Exp. Data - Vapor
Pressure [bar]
x, y mole fraction of CO_2

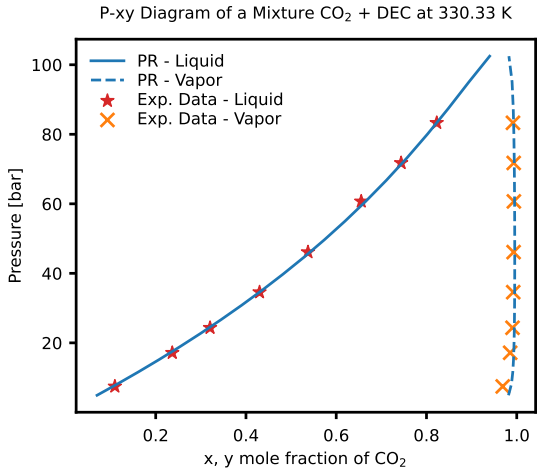
P-xy Diagram of a Mixture CO_2 + DEC at 330.33 K
PR - Liquid
PR - Vapor
Exp. Data - Liquid
Exp. Data - Vapor
Pressure [bar]
x, y mole fraction of CO_2

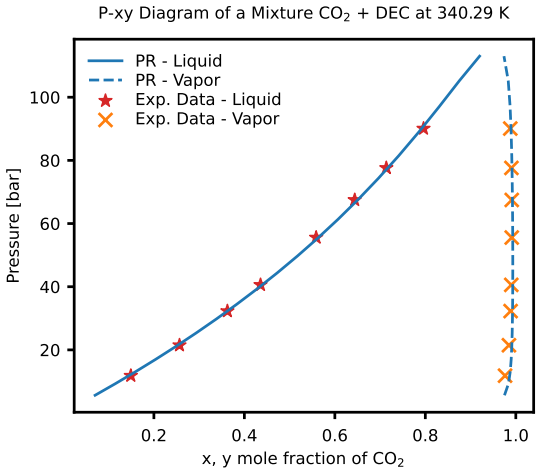
P-xy Diagram of a Mixture CO_2 + DEC at 340.29 K
PR - Liquid
PR - Vapor
Exp. Data - Liquid
Exp. Data - Vapor
Pressure [bar]
x, y mole fraction of CO_2

B

Extraction Efficiency - Ratio

Table B.1: Extraction Yield and Uncertainty for 12C4

(a) Extraction yield results of 12C4 for four distinct experimental runs conducted at various mole ratios.

	1st run		**2nd run**		**3rd run**		**4th run**	
Mole Ratio	Li	P	Li	P	Li	P	Li	P
2	27.03%	30.50%	28.37%	30.50%	31.34%	33.76%	24.66%	29.64%
4	43.30%	45.66%	44.93%	48.70%	47.16%	49.72%	42.08%	45.60%
6	48.45%	50.10%	49.04%	52.28%	50.50%	52.86%	51.91%	56.37%
8	49.90%	51.49%	47.56%	50.15%	45.69%	48.98%	35.57%	41.40%
20	42.05%	45.96%	49.52%	52.52%	46.16%	47.94%	58.09%	49.58%

(b) Mean extraction yield of 12C4 and associated uncertainties for different mole ratios based on the four experimental runs.

	Mean		**Std.dev**		**Std.Error**		**U(95%)**	
Mole Ratio	Li	P	Li	P	Li	P	Li	P
2	27.85%	31.10%	2.79%	1.82%	1.39%	0.91%	2.79%	1.82%
4	44.37%	47.42%	2.20%	2.11%	1.10%	1.05%	2.20%	2.11%
6	49.97%	52.90%	1.55%	2.60%	0.77%	1.30%	1.55%	2.60%
8	44.68%	48.01%	6.31%	4.52%	3.15%	2.26%	6.31%	4.52%
20	48.95%	49.00%	6.81%	2.77%	3.41%	1.39%	6.81%	2.77%

Table B.2: Extraction Yield and Uncertainty for 15C5

(a) Extraction yield results of 15C5 for four distinct experimental runs conducted at various mole ratios.

	1st run		2nd run		3rd run		4th run	
Mole Ratio	**Li**	**P**	**Li**	**P**	**Li**	**P**	**Li**	**P**
2	-1.06%	0.19%	-0.89%	2.71%	0.70%	5.84%	7.52%	6.32%
4	1.27%	4.70%	8.29%	14.41%	10.63%	15.92%	6.97%	7.42%
6	10.65%	12.74%	28.82%	33.21%	22.97%	27.79%	7.52%	8.03%
8	20.26%	23.13%	31.65%	35.27%	31.88%	36.17%	6.39%	7.60%
10	29.25%	31.90%	35.59%	39.19%	62.30%	64.21%	15.13%	16.52%
12	42.08%	43.41%	46.21%	49.46%	59.96%	61.98%	19.20%	22.40%
20	63.80%	65.54%	62.28%	64.13%	61.98%	63.20%	26.25%	28.91%

(b) Mean extraction yield of 15C5 and associated uncertainties for different mole ratios based on the four experimental runs.

	Mean		Std.dev		Std.Error		U(95%)	
Mole Ratio	**Li**	**P**	**Li**	**P**	**Li**	**P**	**Li**	**P**
2	1.57%	3.76%	2.87%	2.02%	1.43%	4.04%	2.87%	4.04%
4	6.79%	10.61%	3.98%	5.41%	1.99%	2.70%	3.98%	5.41%
6	17.49%	20.44%	10.08%	11.98%	5.04%	5.99%	10.08%	11.98%
8	22.54%	25.54%	12.06%	13.36%	6.03%	6.68%	12.06%	13.36%
10	35.57%	37.95%	19.77%	19.89%	9.88%	9.95%	19.77%	19.89%
12	41.86%	44.31%	16.93%	16.53%	8.47%	8.27%	16.93%	16.53%
20	53.58%	55.45%	18.23%	17.71%	9.12%	8.86%	18.23%	17.71%

C

EDX Elemental Mapping

Figure C.1 and C.2 illustrate the elemental mapping of the 12C4-$LiPF_6$ and 15C5-$LiPF_6$ complex.

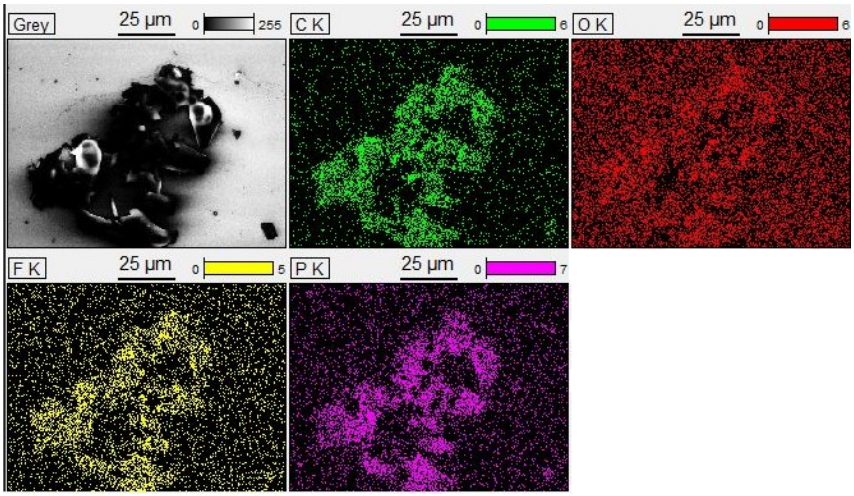

Figure C.1: Energy-Dispersive X-ray Spectroscopy (EDX) Elemental Mapping: Color-coded representation of 12C4-$LiPF_6$ complex showcasing the spatial distribution of major elements. Carbon is depicted in green, oxygen in red, fluorine in yellow, and phosphorus in purple.

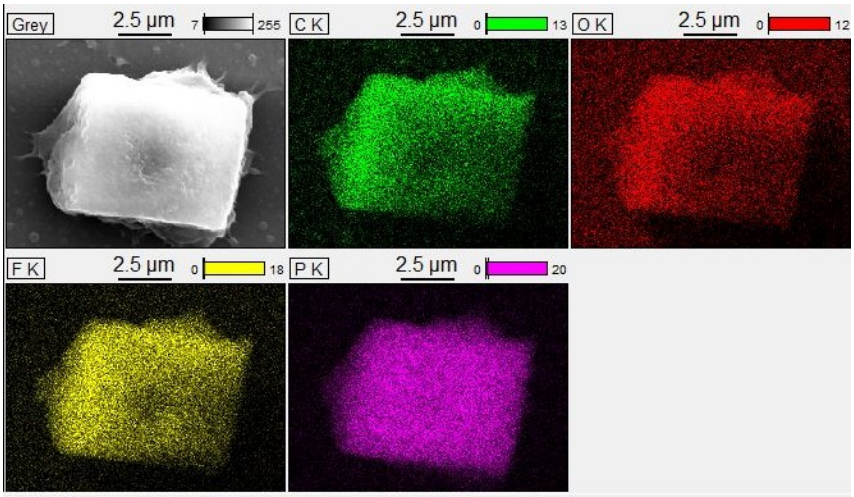

Figure C.2: Energy-Dispersive X-ray Spectroscopy (EDX) Elemental Mapping: Color-coded representation of 15C5-$LiPF_6$ complex showcasing the spatial distribution of major elements. Carbon is depicted in green, oxygen in red, fluorine in yellow, and phosphorus in purple.

The atomic concentrations of the elements are presented in Table C.1. The accuracy of the oxygen concentration measurement in the samples is compromised due to the presence of a silica (SiO_2) substrate used for the EDX analysis. It is important to acknowledge that standard EDX techniques encounter challenges in accurately detecting elements with low atomic numbers like lithium. When subjected to X-ray analysis, lithium doesn't exhibit pronounced X-ray fluorescence, leading to its diminished detectability in EDX spectra. The lower energy X-rays used for analysis are often inadequate to excite lithium atoms effectively, resulting in weak or indiscernible signals. As a result, quantifying the concentration of lithium in a sample through EDX becomes less accurate, and any readings obtained might carry a higher degree of uncertainty.

Table C.1: Elemental Composition Table: Atomic concentrations of carbon, oxygen, fluorine, and phosphorus in 12C4-$LiPF_6$ and 15C5-$LiPF_6$ complex, determined by Energy-Dispersive X-ray Spectroscopy (EDX).

Complex:	12C4-$LiPF_6$	15C5-$LiPF_6$
Carbon	26.04 %	34.42 %
Oxygen	44.79 %	24.51 %
Fluorine	27.02 %	35.81 %
Phosphorus	2.15 %	5.27 %

D

XPS High-Resolution Scan and Analysis

A single peak observed in an XPS survey spectrum often represents a superposition of multiple overlapping sub-peaks from different chemical states. These overlapping sub-peaks arise due to variations in bonding environments, oxidation states, or coordination of an element. For example, in a peak corresponding to a specific element, such as oxygen, the de-convolution might reveal sub-peaks related to oxygen atoms bonded to different elements (e.g., carbon, hydrogen, or metals) or in different oxidation states (e.g., $O_2{}^-$ and OH^-). By using high-resolution scans and curve fitting, the subtle variations in binding energy within a peak, which correspond to different chemical states of an element can be discern. To determine which binding energy corresponds to which chemical state, reference data and established knowledge is used. This is done for all the elements present in the complexes.

Carbon Figure D.1 illustrates the high resolution scan of carbon for the two complexes. The fitted carbon XPS spectra reveals 4 sub-peaks. The peak with the higher binding energy (286.2 eV for 12C4 and 287.3 eV for 15C5) corresponds to C−O from the crown ethers. The peak at 284.8 eV for 12C4 and 285.1 eV for 15C5 comes from adventitious carbon (AdC), which is a thin layer of carbonaceous material commonly present on surfaces of samples exposed to air [49]. The peak at 283 eV for 12C4 and 283.3 eV for 15C5 is most likely of the C−C bonding in the crown ether. The peak observed at 281.2 eV for 12C4 and 281.9 eV for 15C5 is most probably due to C−F bonding. If there are exclusively C−F bonds, the binding energy will be higher, around 288 eV [50]. However, the presence of F bonds with P leads to a decrease in the binding energy between C and F.

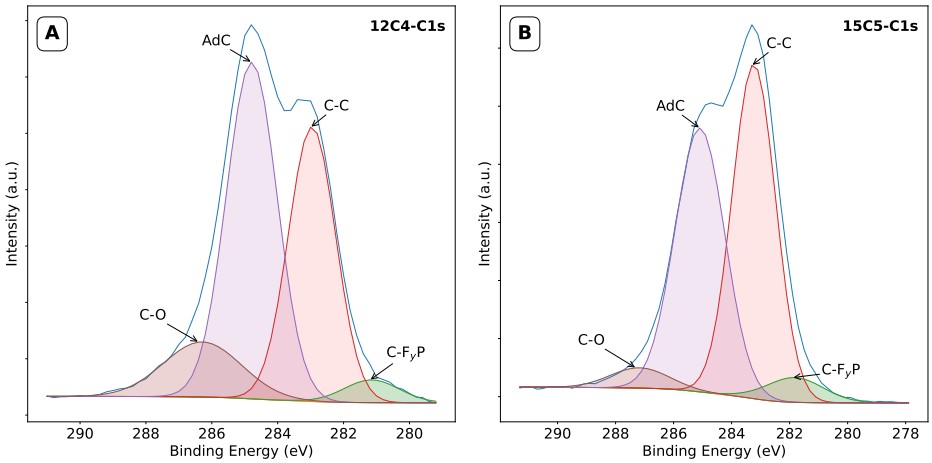

Figure D.1: Chemical State Analysis of C 1s Using High-Resolution XPS: Comparative Fitted Spectra for 12C4 and 15C5 Complexes. Figure A illustrates the fitted spectra for the 12C4 complex, while Figure B depicts the fitted spectra for the 15C5 complex. The spectra exhibit sub-peaks for C−O, adventitious carbon (AdC), C−C, and C−F$_y$P with the convoluted peak (indicated in blue) capturing intricate chemical information.

Oxygen The high resolution scan of oxygen for the two complexes is shown in Figure D.2, and it reveals three sub-peaks. The high peak at 531.4 eV for 12C4 and 531.7 eV for 15C5 can be assigned to C−O. The peak at 533 eV for 12C4 and 534.7 eV for 15C5 corresponds to Li$_x$PF$_y$O$_z$, which is a possible oxygen-containing decomposition compound from $LiPF_6$ [51]. The spectra of oxygen for both complexes exhibit remarkable resemblance. The peak at 530 eV for 12C4 and 528.7 eV for 15C5 corresponds to the bond between lithium and oxygen Li_2O [52].

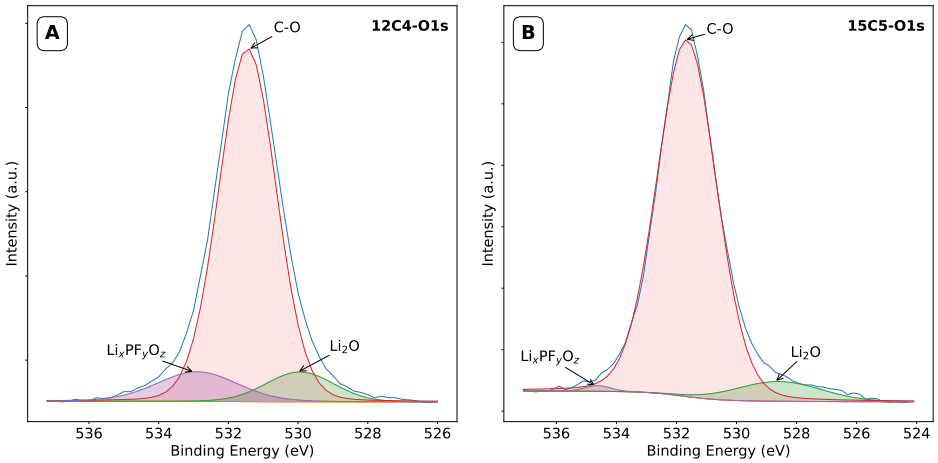

Figure D.2: Chemical State Analysis of O 1s Using High-Resolution XPS: Comparative Fitted Spectra for 12C4 and 15C5 Complexes. Fitted oxygen spectra for the 12C4 complex are featured in Figure A, while the corresponding fitted spectra for the 15C5 complex are presented in Figure B. Notably, each spectrum reveals the presence of three distinct sub-peaks corresponding to Li$_x$PF$_y$O$_z$, C−O, Li_2O with the convoluted peak highlighted in blue.

Lithium The fitted lithium XPS spectra, shown in Figure D.3, reveals two sub peaks. The sub-peak at 54.2 eV for 12C4 and 53.9 eV for 15C5 is attributed to Li_2O. The sub-peak at 51 eV for 12C4 and 50.7 eV for 15C5 corresponds to Li^o [53]. While peak positions remain relatively unchanged, the shapes of the peaks differ significantly. Notably, the sub-peak for Li^o is substantially larger for the 15C5-$LiPF_6$ complex compared to the 12C4-$LiPF_6$ complex.

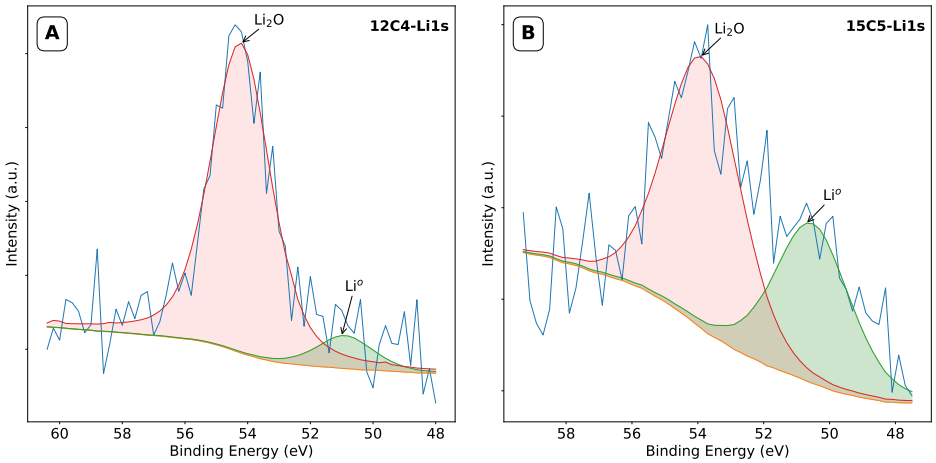

Figure D.3: Comparative Analysis of Lithium Chemical States Using High-Resolution XPS: Fitted Spectra for 12C4 and 15C5 Complexes. Fitted spectra for the 12C4 complex are featured in Figure A, while the corresponding fitted spectra for the 15C5 complex are presented in Figure B. Notably, each spectrum reveals the presence of two distinctive sub-peaks, which corresponds to the lithium-oxygen bond (Li_2O) and lithium metal (Li^o).

Fluorine Figure D.4 shows the results of the high resolution scan for fluorine. The fitted fluorine XPS spectra shows sub-peak related to C−F bond at 686.6 eV for 12C4-$LiPF_6$ complex and 685.3 eV for 15C5-$LiPF_6$ complex [54]. The sub-peaks at 685 eV for 12C4-$LiPF_6$ complex and 685.3 eV for 15C5-$LiPF_6$ complex are assigned to the P−F bond in $LiPF_6$. The sub-peak at 683.6 eV for 12C4 and 683.5 eV for 15C5 corresponds to $Li_xPF_yO_z$, which is a possible oxygen-containing decomposition compound from $LiPF_6$ [55]. The spectra of the two complexes are similar. The positions of the peaks remain relatively consistent, while the sub-peak 683.6 eV exhibits greater magnitude for the 12C4-$LiPF_6$ complex compared to the 15C5-$LiPF_6$ complex.

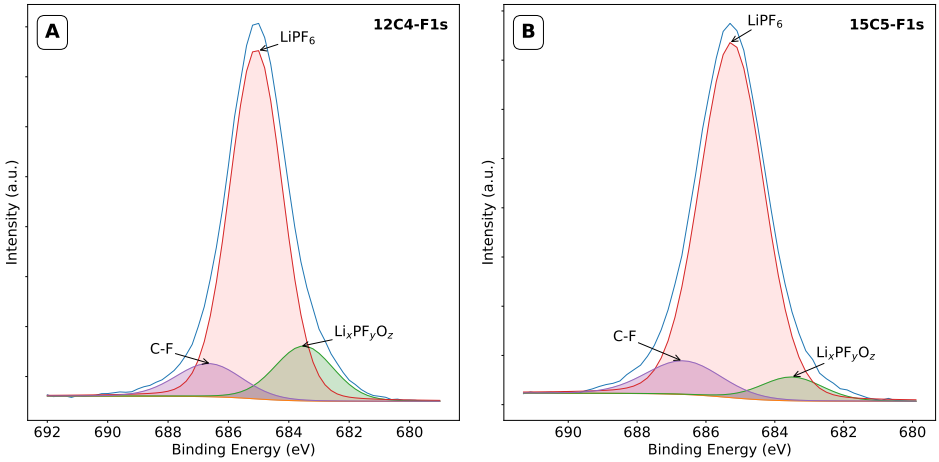

Figure D.4: Comparative Analysis of Fluorine Chemical States Using High-Resolution XPS: Fitted Spectra for 12C4 and 15C5 Complexes. The fitted spectra for the 12C4 complex is displayed in Figure A, while the corresponding fitted spectra for the 15C5 complex is showcased in Figure B. Notably, each spectrum unveils the presence of three distinct sub-peaks, which corresponds to C−F, P−F bond in $LiPF_6$, and $Li_xPF_yO_z$.

Phosphorus Figure D.5 illustrate the high resolution scan for Phosphorus. The fitted phosphorus XPS spectra shows sub-peak related to P−F bond in $LiPF_6$ at 135 eV for 12C4-$LiPF_6$ complex and 135.1 eV for 15C5-$LiPF_6$ complex [55]. The sub-peak at 132.4 eV for 12C4-$LiPF_6$ complex and 132.5 eV for 15C5-$LiPF_6$ complex corresponds to the decomposition product $Li_xPF_yO_z$. The spectra of the two complexes revealed minimal difference between the complexes,

with nearly identical peak positions.

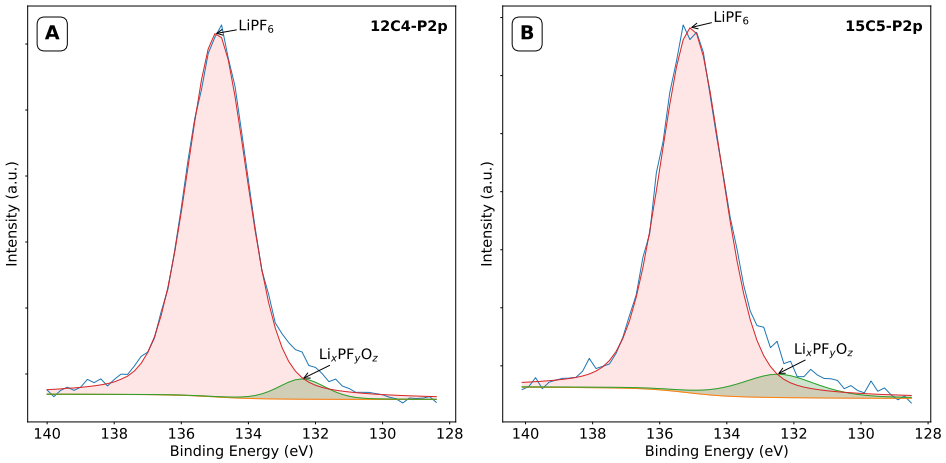

Figure D.5: Comparative Analysis of Phosphorus Chemical States Using High-Resolution XPS: Fitted Spectra for 12C4 and 15C5 Complexes. The fitted spectra for the 12C4 complex are illustrated in Figure A, while the corresponding fitted spectra for the 15C5 complex are presented in Figure B. This figure highlights the high-resolution XPS spectra providing detailed insights into the chemical states of phosphorus (P) within the 12C4 and 15C5 complexes. The sub-peaks in this figure corresponds to P−F bond in $LiPF_6$, and the decomposition product $Li_xPF_yO_z$.

Bibliography

[1] Gavin Harper et al. "Recycling lithium-ion batteries from electric vehicles". In: *Nature* 575.7781 (Nov. 2019), pp. 75–86. ISSN: 14764687. DOI: 10.1038/s41586-019-1682-5.

[2] Haruka Pinegar and York R. Smith. "Recycling of End-of-Life Lithium-Ion Batteries, Part II: Laboratory-Scale Research Developments in Mechanical, Thermal, and Leaching Treatments". In: *Journal of Sustainable Metallurgy* 6.1 (Mar. 2020), pp. 142–160. ISSN: 21993831. DOI: 10.1007/s40831-020-00265-8.

[3] G. P. Nayaka et al. "Dissolution of cathode active material of spent Li-ion batteries using tartaric acid and ascorbic acid mixture to recover Co". In: *Hydrometallurgy* 161 (May 2016), pp. 54–57. ISSN: 0304-386X. DOI: 10.1016/J.HYDROMET.2016.01.026.

[4] C. M. Costa et al. "Recycling and environmental issues of lithium-ion batteries: Advances, challenges and opportunities". In: *Energy Storage Materials* 37 (May 2021), pp. 433–465. ISSN: 24058297. DOI: 10.1016/j.ensm.2021.02.032.

[5] Ruihan Zhang et al. "Organic Electrolytes Recycling From Spent Lithium-Ion Batteries". In: *Global Challenges* 6.12 (Dec. 2022). ISSN: 20566646. DOI: 10.1002/gch2.202200050.

[6] Sascha Nowak and Martin Winter. *The role of sub- and supercritical CO2 as "processing solvent" for the recycling and sample preparation of lithium ion battery electrolytes*. Mar. 2017. DOI: 10.3390/molecules22030403.

[7] Martin Grützke et al. "Extraction of lithium-ion battery electrolytes with liquid and supercritical carbon dioxide and additional solvents". In: *RSC Advances* 5.54 (2015), pp. 43209–43217. ISSN: 20462069. DOI: 10.1039/c5ra04451k.

[8] Robert C. Massé et al. "Energy storage through intercalation reactions: Electrodes for rechargeable batteries". In: *National Science Review* 4.1 (Jan. 2017), pp. 26–53. ISSN: 2053714X. DOI: 10.1093/nsr/nww093.

[9] Lisa Brückner, Julia Frank, and Tobias Elwert. *Industrial recycling of lithium-ion batteries—A critical review of metallurgical process routes*. Tech. rep. 8. Aug. 2020, pp. 1–29. DOI: 10.3390/met10081107.

[10] Laurence Kavanagh et al. "Global lithium sources-industrial use and future in the electric vehicle industry: A review". In: *Resources* 7.3 (2018). ISSN: 20799276. DOI: 10.3390/resources7030057.

[11] Jiakai Zhang and Gisele Azimi. "Recycling of lithium, cobalt, nickel, and manganese from end-of-life lithium-ion battery of an electric vehicle using supercritical carbon dioxide". In: *Resources, Conservation and Recycling* 187 (Dec. 2022). ISSN: 18790658. DOI: 10.1016/j.resconrec.2022.106628.

[12] Bin Huang et al. "Recycling of lithium-ion batteries: Recent advances and perspectives". In: *Journal of Power Sources* 399 (Sept. 2018), pp. 274–286. ISSN: 03787753. DOI: 10.1016/j.jpowsour.2018.07.116.

[13] Haruka Pinegar and York R. Smith. "Recycling of End-of-Life Lithium Ion Batteries, Part I: Commercial Processes". In: *Journal of Sustainable Metallurgy* 5.3 (Sept. 2019), pp. 402–416. ISSN: 21993831. DOI: 10.1007/s40831-019-00235-9.

[14] Alexandre Chagnes and Beata Pospiech. "A brief review on hydrometallurgical technologies for recycling spent lithium-ion batteries". In: *Journal of Chemical Technology and Biotechnology* 88.7 (July 2013), pp. 1191–1199. ISSN: 02682575. DOI: 10.1002/jctb.4053.

[15] Yuanlong Liu et al. "Supercritical CO2 extraction of organic carbonate-based electrolytes of lithium-ion batteries". In: *RSC Advances* 4.97 (2014), pp. 54525–54531. ISSN: 20462069. DOI: 10.1039/c4ra10530c.

[16] Weiguang Lv et al. "A Critical Review and Analysis on the Recycling of Spent Lithium-Ion Batteries". In: *ACS Sustainable Chemistry and Engineering* 6.2 (Feb. 2018), pp. 1504–1521. ISSN: 21680485. DOI: 10.1021/acssuschemeng.7b03811.

[17] Chunwei Liu et al. "Recycling of spent lithium-ion batteries in view of lithium recovery: A critical review". In: *Journal of Cleaner Production* 228 (Aug. 2019), pp. 801–813. ISSN: 0959-6526. DOI: 10.1016/J.JCLEPRO.2019.04.304.

[18] Hyuntae Bae and Youngsik Kim. "Technologies of lithium recycling from waste lithium ion batteries: A review". In: *Materials Advances* 2.10 (May 2021), pp. 3234–3250. ISSN: 26335409. DOI: 10.1039/d1ma00216c.

[19] European Commission. *Green Deal: Sustainable batteries for a circular and climate neutral economy*. https://ec.europa.eu/commission/presscorner/detail/en/ip_20_2312. Accessed on 10-02-2023. Dec. 2020.

[20] Liu Yun et al. "Metallurgical and mechanical methods for recycling of lithium-ion battery pack for electric vehicles". In: *Resources, Conservation and Recycling* 136 (Sept. 2018), pp. 198–208. ISSN: 18790658. DOI: 10.1016/j.resconrec.2018.04.025.

[21] Yue Sun et al. "A novel approach for the selective extraction of Li+ from the leaching solution of spent lithium-ion batteries using benzo-15-crown-5 ether as extractant". In: *Separation and Purification Technology* 237 (Apr. 2020), p. 116325. ISSN: 1383-5866. DOI: 10.1016/J.SEPPUR.2019.116325.

[22] Faiza Arshad et al. "A Comprehensive Review of the Advancement in Recycling the Anode and Electrolyte from Spent Lithium Ion Batteries". In: *ACS Sustainable Chemistry and Engineering* 8.36 (Sept. 2020), pp. 13527–13554. ISSN: 21680485. DOI: 10.1021/acssuschemeng.0c04940.

[23] Yuanlong Liu et al. "Analysis on extraction behaviour of lithium-ion battery electrolyte solvents in supercritical CO2 by gas chromatography". In: *International Journal of Electrochemical Science* 11.9 (2016), pp. 7594–7604. ISSN: 14523981. DOI: 10.20964/2016.09.03.

[24] Michael Schmidt et al. *Process for Recycling Negative Electrode Materials from Spent Lithium Batteries (US Patent)*. 2003.

[25] Bruna Aparecida Souza Machado et al. "Supercritical Fluid Extraction Using CO2: Main Applications and Future Perspectives". In: *Separation Science and Technology (Philadelphia)* 48.18 (Dec. 2013), pp. 2741–2760. ISSN: 01496395. DOI: 10.1080/01496395.2013.811422.

[26] Steven Sloop. *System and method for removing an electrolyte from an energy storage and/or conversion device using a super critical fluid*. Tech. rep. 2003.

[27] Martin Grützke et al. "Supercritical carbon dioxide extraction of lithium-ion battery electrolytes". In: *The Journal of Supercritical Fluids* 94 (Oct. 2014), pp. 216–222. ISSN: 0896-8446. DOI: 10.1016/J.SUPFLU.2014.07.014.

[28] Michael Jonathan Lain. "Recycling of Galvanic Cells (US Patent)". In: *US Patent* US 6447669 B1 (Sept. 2002).

[29] X. Zhang et al. "Diagnostic Characterization of High Power Lithium-Ion Batteries for Use in Hybrid Electric Vehicles". In: *Journal of The Electrochemical Society* 148.5 (2001), A463. ISSN: 00134651. DOI: 10.1149/1.1362541.

[30] S.E. Sloop et al. "Chemical reactivity of PF5 and LiPF6 in ethylene carbonate/dimethyl carbonate solutions". In: *Electrochemical and Solid-State Letters* 4.4 (Apr. 2001). ISSN: 10990062. DOI: 10.1149/1.1353158.

[31] Merck Life Science N.V. *Lithium Hexafluorophosphate*. Tech. rep. 2023. URL: https://www.sigmaaldrich.com/NL/en/sds/aldrich/450227.

[32] Sergej Rothermel et al. "Graphite Recycling from Spent Lithium-Ion Batteries". In: *ChemSusChem* 9.24 (Dec. 2016), pp. 3473–3484. ISSN: 1864564X. DOI: 10.1002/cssc.201601062.

[33] Aimin Li et al. "Practical applications of supramolecular extraction with macrocycles". In: *Chemistry Letters* 49.10 (Oct. 2020), pp. 1125–1135. ISSN: 13480715. DOI: 10.1246/CL.200409.

[34] Jonathan P. Gluckman, Garret Kraft, and Glen Southard. *Lithium Extraction with Crown Ethers (WO2020131964A1)*. 2020.

[35] Jonathan W Steed, David R Turner, and Karl J Wallace. *Core Concepts in Supramolecular Chemistry and Nanochemistry*. John Wiley & Sons, 2007. ISBN: 978-0-470-85866-0.

[36] Arna Pálsdóttir, Christopher A. Alabi, and Jefferson W. Tester. "Characterization of 14-Crown-4 Ethers for the Extraction of Lithium from Natural Brines: Synthesis, Solubility Measurements in Supercritical Carbon Dioxide, and Thermodynamic Modeling". In: *Industrial and Engineering Chemistry Research* 60.21 (June 2021), pp. 7926–7934. ISSN: 15205045. DOI: 10.1021/acs.iecr.1c00346.

[37] T. Georgi-Maschler et al. "Development of a recycling process for Li-ion batteries". In: *Journal of Power Sources* 207 (June 2012), pp. 173–182. ISSN: 0378-7753. DOI: 10.1016/J.JPOWSOUR.2012.01.152.

[38] Edwin Weber and Fritz Vögtle. "Crown-type compounds - An introductory overview". In: *Host Guest Complex Chemistry I*. Berlin, Heidelberg: Springer Berlin Heidelberg, 1981, pp. 1–41. ISBN: 978-3-540-38706-0.

[39] Ayaulym Belgibayeva et al. "Lithium-ion batteries for low-temperature applications: Limiting factors and solutions". In: *Journal of Power Sources* 557 (Feb. 2023). ISSN: 03787753. DOI: 10.1016/j.jpowsour.2022.232550.

[40] Juris Meija et al. *Atomic weights of the elements 2013 (IUPAC Technical Report)*. Tech. rep. 3. Mar. 2016, pp. 265–291. DOI: 10.1515/pac-2015-0305.

[41] Zhigang Lei, Chengna Dai, and Biaohua Chen. "Extractive distillation". In: *Special Distillation Processes* (Jan. 2022), pp. 65–154. DOI: 10.1016/B978-0-12-820507-5.00003-8.

[42] Jianbo Wang et al. "Leaching Study of Spent Li-ion Batteries". In: *Procedia Environmental Sciences* 16 (2012), pp. 443–450. ISSN: 18780296. DOI: 10.1016/j.proenv.2012.10.061.

[43] Kai He et al. "A green process for exfoliating electrode materials and simultaneously extracting electrolyte from spent lithium-ion batteries". In: *Journal of Hazardous Materials* 375 (Aug. 2019), pp. 43–51. ISSN: 0304-3894. DOI: 10.1016/J.JHAZMAT.2019.03.120.

[44] Ángel Martín et al. "Teaching advanced equations of state in applied thermodynamics courses using open source programs". In: *Education for Chemical Engineers* 6.4 (Dec. 2011). ISSN: 17497728. DOI: 10.1016/j.ece.2011.08.003.

[45] T. Y. Kwak and G. A. Mansoori. "Van der waals mixing rules for cubic equations of state. Applications for supercritical fluid extraction modelling". In: *Chemical Engineering Science* 41.5 (Jan. 1986), pp. 1303–1309. ISSN: 0009-2509. DOI: 10.1016/0009-2509(86)87103-2.

[46] Aspen Technology. *Aspen Plus (Version 12)*. Computer software. Bedford, MA: Aspen Technology, Inc. URL: https://www.aspentech.com/en/products/engineering/aspen-plus.

[47] Carl L. Yaws and Prasad K. Narasimhan. "Critical properties and acentric factor—Organic compounds". In: *Thermophysical Properties of Chemicals and Hydrocarbons* (Jan. 2009), pp. 1–95. DOI: 10.1016/B978-081551596-8.50006-7.

[48] Iklima Oral and Volker Abetz. "Improved alkali metal ion capturing utilizing crown ether-based diblock copolymers in a sandwich-type complexation". In: *Soft Matter* 18.5 (Feb. 2022), pp. 934–937. ISSN: 17446848. DOI: 10.1039/d1sm01815a.

[49] Mark C. Biesinger. "Accessing the robustness of adventitious carbon for charge referencing (correction) purposes in XPS analysis: Insights from a multi-user facility data review". In: *Applied Surface Science* 597 (Sept. 2022). ISSN: 01694332. DOI: 10.1016/j.apsusc.2022.153681.

[50] G. Cunge et al. "New chamber walls conditioning and cleaning strategies to improve the stability of plasma processes". In: *Plasma Sources Science and Technology* 14.3 (Aug. 2005), pp. 599–609. ISSN: 09630252. DOI: 10.1088/0963-0252/14/3/025.

[51] David Ensling et al. "A comparative XPS surface study of Li2FeSiO4/C cycled with LiTFSI- and LiPF6-based electrolytes". In: *Journal of Materials Chemistry* 19.1 (2009), pp. 82–88. ISSN: 09599428. DOI: 10.1039/b813099j.

[52] J. P. Tonks et al. "Corrosion studies of LiH thin films". In: *Journal of Nuclear Materials* 484 (Feb. 2017), pp. 228–235. ISSN: 00223115. DOI: 10.1016/j.jnucmat.2016.12.008.

[53] Min A. Lee et al. "Stable Li Metal-Electrolyte Interface Enabled by SEI Improvement and Cation Shield Functionality of the Azamacrocyclic Ligand in Carbonate Electrolytes". In: *ACS Applied Materials and Interfaces* 14.31 (Aug. 2022), pp. 35645–35653. ISSN: 19448252. DOI: 10.1021/acsami.2c07932.

[54] Jin Zhao et al. "Introducing Crown Ether as a Functional Additive for High-Performance Dendrite-free Li Metal Batteries". In: *ACS Applied Energy Materials* 4.8 (Aug. 2021), pp. 7829–7838. ISSN: 25740962. DOI: 10.1021/acsaem.1c01174.

[55] Liping Zheng et al. "Li[(FSO2)(n-C4F9SO2)N] versus LiPF6 for graphite/LiCoO2 lithium-ion cells at both room and elevated temperatures: A comprehensive understanding with chemical, electrochemical and XPS analysis". In: *Electrochimica Acta* 196 (Apr. 2016), pp. 169–188. ISSN: 00134686. DOI: 10.1016/j.electacta.2016.02.152.